Imperial College
London

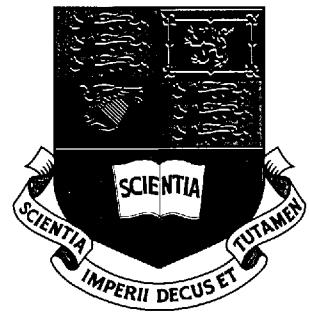

AN INVESTIGATION OF FUNCTIONAL MRI ACTIVATION REPRODUCIBILITY

By

NADIA MULLA-ALI

A THESIS SUBMITTED TO THE UNIVERSITY OF LONDON

FOR THE DEGREE OF DOCTOR OF PHILOSOPHY

BIOENGINEERING DEPARTMENT

IMPERIAL COLLEGE LONDON

NOVEMBER 2006

Abstract

Functional MRI has been used as a tool to detect and quantify change in volumetric data sets. It is an important non-invasive functional neuroimaging method which has been developing rapidly. Functional images of the brain are commonly analysed by using some form of statistical parametric mapping.

The motivation of this work is to investigate the reliability and reproducibility of activation detection, and to validate the analysis of standard fMRI data analysis techniques. The reproducibility of activation has been studied under the effects of registration, choice of a hemodynamic response function (HRF) and under different experimental protocols. A set of tools has been developed to enable independent evaluation of the presence of activation patterns engaged in repetitive tasks. This was utilized to investigate, briefly, the effect of the realignment process and, extensively, the effect of the choice of HRF signal on the activation. Comparisons are made between data analyzed using the accepted 'gold standard' technique of SPM and our alternative method, and the results are presented and qualitatively evaluated. ROC curves were produced to provide a graphical illustration of the results.

Declaration

The work presented in this thesis was carried out between October 2001 and August 2005 in the Department of Bioengineering at Imperial College London under the supervision of Dr. Anil A. Bharath and Dr. Donald McRobbie. The material herein is original and has not been submitted for a degree or diploma at any other university.

Acknowledgements

First, I would like to thank my supervisors, Dr. Anil Bharath and Dr. Donald McRobbie, for their support and guidance over the last four years. Their continuous encouragement, trust and confidence in my work have been invaluable.

I would also like to thank Annie Papadaki for her help in supplying the data used in this study and making sure it is in the correct format. I am also grateful to Oliver Krause for his excellent IT support and to Saleh Basalamah, Jeffery Ng and Melvin Lim for their constant help in the programming aspect of my research as well as their friendship.

I would like to thank the Kuwaiti Government and the Kuwaiti Cultural Office for their financial and moral support.

Finally, I would like to thank my family for their constant support, love and encouragement.

Table of Contents

1. **INTRODUCTION** **19**

2. **PRINCIPLES OF FUNCTIONAL MRI** **23**

2.1 INTRODUCTION 23

2.2 CONTRAST IN FUNCTIONAL MRI IMAGING 24

2.3 BOLD MECHANISM 25

2.3.1 Biophysics of BOLD fMRI *25*
2.3.2 The Physiological Basis of BOLD fMRI *28*
2.3.3 Hemodynamic Response Function *32*
2.3.4 Linearity *35*
2.3.5 Modelling Neurological Response *37*
2.3.6 Field strength influence on BOLD signal *38*
2.3.7 Activation Detection *38*
2.4 Echo-planar Imaging (EPI) *39*

2.5 NOISE INDUCING FACTORS IN FMRI 44

2.6 SUMMARY 51

3. **IMAGE REGISTRATION REVIEW** **52**

3.1 INTRODUCTION 52

3.2 APPLICATIONS OF IMAGE REGISTRATION 53

3.3 CLASSIFICATION OF REGISTRATION TECHNIQUES 54

3.4 STEPS OF REGISTRATION 59

3.5 MISREGISTRATION 71

3.6 VALIDATION OF MOTION CORRECTION 74

3.7 SUMMARY 75

4. **STATISTICAL PROCEDURES FOR FMRI** **76**

4.1 INTRODUCTION 76
4.2 GENERAL LINEAR MODEL (GLM) 80
4.3 THE T-TEST 82
4.4 SPM 85
4.4.1 Limitations of SPM *88*
4.4.2 SPM99 vs. SPM2 *88*
4.5 REPRODUCIBILITY OF FMRI 96
4.6 SUMMARY 97

5. METHODS 98

5.1 INTRODUCTION 98
5.2 EXPERIMENTAL DESIGN AND DATA ACQUISITION 99
5.2.1 Summary of Data *99*
5.3 DATA ANALYSIS METHODS 102
5.3.1 SPM99 and SPM2 *103*
5.3.2 Automated Image Registration (AIR) *106*
5.3.3 Correlation Method *107*
5.4 METHODS OF ANALYSIS USING HISTOGRAMS 109
5.5 HRF DECONVOLUTION 110
5.6 SUMMARY 114

6. REGISTRATION AND REPRODUCIBILITY 115

6.1 INTRODUCTION 115
6.2 STANDARD MEASURES OF REPRODUCIBILITY 116
6.2.1 SPM RESULTS 116
6.2.2 CORRELATION METHOD RESULT 119
6.3 SIMULATED DATA RESULTS 123
6.4 COMPARISON OF REALIGNED DATA USING SPM99, SPM2 AND AIR 126
6.5 COMPARISON OF REALIGNED VERSUS NON REALIGNED DATA IN SPM2 129
6.6 COMPARISON OF REPRODUCIBILITY USING FWER AND FDR IN SPM2 131
6.7 NORMALITY TESTS 134
6.8 SUMMARY 138

7. **HRF AND REPRODUCIBILITY** **141**

7.1 INTRODUCTION 141
7.2 PHASE SHIFT 141
7.3 EMPIRICAL HRF EXTRACTION 145
7.4 COMPARISONS OF HRFS 163
7.5 CLINICAL APPLICATION 187
7.6 SUMMARY 205

8. **CONCLUSIONS AND FUTURE WORK** **208**

9. **APPENDIX A** **220**

MATLAB SCRIPTS 220
*Matlab script to load data in *.img format* *220*
Matlab script to calculate the amplitudes of the activation *221*
Matlab script for connected component labelling of the clusters *221*
Matlab script to find activation in the data loaded *223*
Matlab script to visualize regions of activation *224*
Matlab script to plot histograms of subclusters *225*
Matlab script to plot ROC curves after the calculation of the false positive and the false negative of activation *229*
Matlab script to calculate the mean signal and the standard deviation for a group of signals *234*
Matlab script to create simulated data *236*
Matlab script to find the mutual active areas between two sets of data *241*

10. **APPENDIX B** **244**

RESULTS 244

11. **APPENDIX C** **257**

SPM PARAMETERS 257

List of Figures

2.1 Alterations in Blood Oxygenation..... 27

2.2 Hemodynamic response function (HRF) – Standard HRF extracted from SPM99..... 33

2.3 Link between stimulation and BOLD response..... 35

2.4 K-space in EPI..... 39

3.1 Image registration..... 53

3.2 Translation..... 59

3.3 Rotation..... 60

3.4 Scaling..... 61

3.5 Rescaling (aspect ratio)..... 62

3.6 Shear. 62

3.7 Projective..... 63

3.8 Non-linear warps..... 64

3.9 Interpolation..... 68

5.1 On-Off (boxcar Function)..... 100

5.2 Boxcar function convolved with HRF..... 105

5.3 Initial function used to initialise the candidate HRF.....111

6.1 SPM99 Results with a *p*-value of 0.001..... 117

6.2 SPM activation superimposed on glass brain with a *p*-value of 0.001 118

6.3 correlation method results with a *p*-value of 0.001. Slices 1-10 are displayed from top left to bottom right..... 119

6.4 Activation in slice 8 using the correlation method..... 120

6.5 Intensity at each voxel across time at one point in space... 121

6.6 Signal amplitude at each voxel across the volumes..... 121

6.7 SPM99 results with a *p*-value of 0.001..... 124

6.8 SPM2 results with a *p*-value of 0.001..... 125

6.9 correlation method results with a *p*-value of 0.001.....126

6.10 Analysis of data set 1 using SPM2 with a *p*-value of 0.001..... 131

6.11 Analysis of data set 1 in SPM2 using FWER with a *p*-value of 0.05..... 132

6.12 Analysis of data set 1 in SPM2 using FDR with a *p*-value of 0.05..... 133

6.13 Generated Histograms..... 135

7.1 plot of SPM2 results of number of active voxels versus the phase shift.....143

7.2 plot of correlation method results of number of active voxels versus the phase shift.....144

7.3 plot of correlation method results of the similarity measure versus the phase shift.....144

7.4 HRF signal used in SPM..... 146

7.5 HRF signal of collapsed average signal at maximum activation..... 147

7.6 HRF signal of the collapsed average 3D signal at Maximum activation..... 147

7.7 HRF signal extracted from all active areas for week 16..... 151

7.8 HRF signal extracted from all active areas for week 17..... 152

7.9 HRF signal extracted from all active areas for week 19..... 152

7.10 HRF signal extracted from all active areas for week 20..... 152

7.11 HRF signal extracted from all active areas for week 22..... 153

7.12 HRF signal extracted from all active areas for week 29..... 153

7.13 HRF signal extracted from all active areas for week 30..... 153

7.14 HRF signal extracted from all active areas for week 33..... 154

7.15 HRF signal extracted from all active areas for week 34..... 154

7.16 HRF signal extracted from all active areas for week 36..... 154

7.17 HRF signal extracted from all active areas for week 37..... 155

7.18 HRF signal extracted from all active areas for week 38..... 155

7.19 HRF signal extracted from all active areas for week 39..... 155

7.20 HRF signal extracted from all active areas for week 42..... 156

7.21 Mean signal and standard deviation of the finger tapping smoothed HRFs..... 156

7.22 HRF signal at active voxel in subject 1 (100% contrast)..... 160

7.23 HRF signal at active voxel in subject 2 (100% contrast)..... 160

7.24 HRF signal at active voxel in subject 3 (100% contrast)..... 160

7.25 HRF signal at active voxel in subject 4 (100% contrast)..... 161

7.26 HRF signal at active voxel in subject 5 (100% contrast)..... 161

7.27 Mean and standard deviation of the visual 100% contrast smoothed HRFs..... 162

7.28 Mean and standard deviation of the visual 10% contrast smoothed HRFs..... 163

7.29 Unsmoothed mean extracted HRF..... 167

7.30 Unsmoothed mean extracted HRF convolved with the boxcar signal..... 167

7.31 Interpolated smoothed mean HRF..... 168

7.32 SPM HRF signal..... 168

7.33 SPM HRF signal convolved with the boxcar signal..... 168

7.34 activation superimposed on brain and plot at maximum activation..... 169

7.35 activation superimposed on brain and plot at maximum activation..... 170

7.36 Unsmoothed mean extracted HRF..... 171

7.37 Unsmoothed mean extracted HRF convolved with the boxcar signal..... 171

7.38 SPM HRF signal..... 171

7.39 SPM HRF signal convolved with the boxcar signal..... 172

7.40 activation superimposed on brain and plot at maximum activation..... 173

7.41 activation superimposed on brain and plot at maximum activation..... 173

7.42 ROC curve for the realigned week 17..... 178

7.43 ROC curve for the realigned week 19..... 178

7.44 ROC curve for the realigned week 29..... 179

7.45 ROC curve for the realigned 10% contrast subject 1..... 180

7.46 ROC curve for the realigned 10% contrast subject 2..... 180

7.47 ROC curve for the realigned 10% contrast subject 3..... 181

7.48 ROC curve for the realigned 10% contrast subject 4..... 181

7.49 ROC curve for the realigned 10% contrast subject 5..... 182

7.50 ROC curve for the realigned week 17 run1..... 183

7.51 ROC curve for the realigned week 17 run2..... 183

7.52 ROC curve for the realigned week 17 run3..... 184

7.53 ROC curve for the realigned week 17 run4..... 184

7.54 ROC curve for the realigned week 17 run5..... 185

7.55 Mean of False Positives vs. the Threshold..... 186

7.56 Variance of False Positives from the mean..... 186

7.57 SPM2 results for the right finger tapping activation using correlation method..... 188

7.58 The correlation method results for the right finger tapping activation using the SPM activation signal (patient 1)..... 188

7.59 HRF signal extracted from the maximum activation (patient 1 – right hand)..... 189

7.60 HRF signal extracted from the maximum activation (patient 2 – right hand)..... 189

7.61 HRF signal extracted from the maximum activation (patient 3 – right hand)..... 190

7.62 HRF signal extracted from the maximum activation (patient 4 – right hand)..... 190

7.63 HRF signal extracted from the maximum activation (patient 5 – right hand)..... 191

7.64 The mean of the HRF signals extracted from the maximum activation across patients (right hand)..... 191

7.65 The mean HRF signal convolved with the boxcar signal (right hand)..... 192

7.66 The correlation method results for the right finger tapping activation using the mean extracted activation signal for patient 1..... 192

7.67 The correlation method results for the right finger tapping activation using the mean extracted activation signal for patient 2 193

7.68 The correlation method results for the right finger tapping activation using the mean extracted activation signal for patient 3 193

7.69 The correlation method results for the right finger tapping activation using the mean extracted activation signal for patient 4 194

7.70 The correlation method results for the right finger tapping activation using the mean extracted activation signal for patient 5 194

7.71 ROC curve for the realigned right finger tapping 195

7.72 SPM2 results for the left finger tapping activation (patient 1 – left hand) 196

7.73 The correlation method results for the left finger tapping activation using the SPM activation signal (patient 1 – left hand) 197

7.74 HRF signal extracted from the maximum activation (patient 1 – left hand) 197

7.75 HRF signal extracted from the maximum activation (patient 2 – left hand) 198

7.76 HRF signal extracted from the maximum activation (patient 3 – left hand) 198

7.77 HRF signal extracted from the maximum activation (patient 4 – left hand) 199

7.78 HRF signal extracted from the maximum activation (patient 5 – left hand) 199

7.79 The mean of the HRF signals extracted from the maximum activation across patients (left hand) 200

7.80 The mean HRF signal convolved with the boxcar signal (left hand) 200

7.81 The correlation method results for the left finger tapping activation using the mean extracted activation signal (patient 1)..... 201

7.82 The correlation method results for the left finger tapping activation using the mean extracted activation signal (patient 2)..... 201

7.83 The correlation method results for the left finger tapping activation using the mean extracted activation signal (patient 3)..... 202

7.84 The correlation method results for the left finger tapping activation using the mean extracted activation signal (patient 4)..... 202

7.85 The correlation method results for the left finger tapping activation using the mean extracted activation signal (patient 5)..... 203

7.86 ROC curve for the realigned right finger tapping..... 204

List of Tables

3.1 Type-I and Type-II errors..... 73

4.1 Table of summary adapted from Nichols [1]..... 95

5.1 Pre-processing steps in SPM99..... 104

5.2 Pre-processing steps in SPM2..... 106

6.1 Percentage of activation results for the finger tapping data (Data Set 1) with *p*-value of 0.001..... 122

6.2 Percentage of activation results for the four subject visual data (Data Set 2) with *p*-value of 0.001..... 122

6.3 Similarity measure comparison between SPM99, SPM2 and AIR..... 127

6.4 Mean and range value of similarity measure at active areas..... 128

6.5 Similarity measure comparison between realigned and non realigned data..... 130

6.6 Mean and range value of signal distribution normality in active areas..... 136

6.7 Mean value of signal distribution normality at active and non-active areas..... 137

7.1 Effect of phase shift on activation in SPM2 and the correlation method..... 142

7.2 Summary of ratio of energies for each subset for finger tapping data..... 151

7.3 Summary of ratio of energies for each subset for visual data..... 159

7.4 Comparison of the mean and the SPM HRF signals for the finger tapping data set.....163

7.5 Comparison between the individual's HRF signals and the mean HRF signals for the finger tapping data set..... 164

7.6 Comparison of the mean 100%, 10% and SPM HRF signals for the visual data set.....165

7.7 Comparison of the individual 100% and mean HRF signals for the visual data set.....165

7.8 Comparison of the mean 100% visual, 10% visual and finger tapping HRF signals..... 166

7.9 Scheme for comparing results of different methods of activation detection.....174

7.10 Finger tapping results..... 175

7.11 Visual data 100% contrast results..... 175

7.12 Realigned finger tapping results..... 175

7.13 The Realigned visual data 100% contrast results..... 175

7.14 Summary of the similarity measure results for each patient using the SPM HRF and the mean extracted HRF signals (right hand). 195

7.15 Summary of the similarity measure results for each patient using the SPM HRF and the mean extracted HRF signals (left hand).....203

List of Acronyms

fMRI:	Functional Magnetic Resonance Imaging.
RF pulse:	Radio Frequency pulse.
TE:	Echo Time. It is the time from the application of the RF pulse to the peak of the signal induced in the coil.
TR:	Repetition Time. It is the time from the application of one RF pulse until the next RF pulse.
T_1:	Spin-Lattice Relaxation Time. It is the time of the recovery of the magnetisation aligned along the main field.
T_2:	Spin-Spin Relaxation Time. It is the time of the decay of the signal in the transverse plane.
T_2^* Relaxation:	The combined T_2 and magnetic field inhomogeneity.
BOLD fMRI:	Blood Oxygenation Level Dependent fMRI.
CBF:	Cerebral Blood Flow.
CBV:	Cerebral Blood Volume.
$CMRo_2$:	Cerebral Metabolic Rate of Oxygen Consumption.
ATP:	Adenosine Triphosphate.
Glycolysis:	The metabolism of glucose.
LFP:	Local field potentials.
MUA:	Multi-Unit Activity.

EPI:	Echo Planar Imaging.
HRF:	Hemodynamic Response Function.
SPM:	Statistical Parametric Mapping.
S/N:	Signal to noise ratio.
CSF:	Cerebral Fluid.
FLAIR:	Fluid Attenuated Inversion Recovery.
Pixel:	Picture element.
Voxel:	Volume element, a three dimensional pixel.
CC:	Correlation Coefficient.
RIU:	Ratio Image Uniformity.
ROC:	Receiver Operating Characteristic.
GLM:	General Linear Model.
RFT:	Random Field Theory.
FWHM:	Full Width at Half the Maximum.
EC:	Euler Characteristic.
ANOVA:	Analysis of Variance.
ANCOVA:	Analysis of Covariance.
Resel:	Resolution Element.
FWER:	Family-wise Error Rate.
FDR:	False Discovery Rate.
AC:	Anterior Commisure.

Chapter 1

Introduction

Medical images are increasingly being used within healthcare for diagnosis, treatment planning, guidance during treatment procedures and monitoring disease progression. Medical images are captured by a variety of techniques, one of which is magnetic resonance imaging (MRI). Although the primary clinical usage for MRI remains anatomical imaging, it has been shown to be useful in the detection of brain activity via the relatively indirect coupling of neural activity to cerebral blood flow and subsequently to magnetic resonance signal intensity [2]. The goal of a broad class of techniques known as "*functional neuroimaging*" is to map the activity of the living brain in space and time. This requires the acquisition of multiple volumes of data from subjects at different times. fMRI is an important non-invasive functional neuroimaging method which has been developing rapidly. It has many advantages over other methods which include: the signal comes directly from functionally induced changes, speed, good spatial resolution (1-2 mm), good delineation of the spatial extent on an

activated area, little known risk and accurate matching to anatomical structures [3]. Data is acquired while the subject is engaged in a set of cognitive tasks designed to isolate specific brain functions. fMRI offers a powerful tool for mapping brain activation and for exploring the neural basis of human cognition, perception, and behaviour. Some of its clinical applications include [3]: neurological studies (epilepsy, Dementia, and Stroke), emotional studies (Affective Disorders, Externally Elicited Affect, and Pain), psychiatry, pediatrics, pharmacology, and surgical planning. Chapter 2 presents some basic concepts concerning functional MRI in terms of contrast, BOLD mechanism, biophysics and physiology, hemodynamic response function, the linearity issue, EPI and noise in fMRI.

A fundamental step in the analysis of fMRI time-series of the brain is the correction for subject motion. This is necessary because the signal changes due to the hemodynamic response to neural activity can be small compared to signal changes that can result from subject motion, especially when the subject movement is correlated with the task. This will lead to uncertainty in deciding whether the changes in intensity are due to brain activity or subject movement. Subject head movement in the scanner cannot be completely eliminated, so motion correction needs to be performed as a preprocessing step on the image data. This requires the aligning of images as closely as possible prior to performing any statistical tests. The first step in the subject motion correction is image registration.

Chapter 3 discusses the applications of image registration, the classification of registration techniques, registration steps, causes of misregistration and validation of the motion correction.

Functional images of the brain are commonly compared using some form of "*statistical parametric mapping*". There are several public domain algorithms currently available for the analysis of fMRI data using a technique known as statistical parametric mapping, some of which are: Automated Image Registration (AIR), Analysis of Functional NeuroImages (AFNI), Statistical Parametric mapping (SPM) and the pyramid method of Thevenaz, Ruttimann and Unser (TRU), Independent Component Analysis (ICA) and BrainTools [4]. A widely used and freely distributed software package is SPM, which is designed to analyse functional neuroimaging data. SPM is a widely used algorithm package written in *Matlab*. It was developed originally in 1991 by K. Friston and was made available freely to the functional imaging community. Its main goal is to produce a statistically meaningful comparison between groups of images. A method has been developed to analyze fMRI data independently from SPM, and thus can be used as a comparative tool. Chapter 4 presents the statistical procedures for fMRI discussing the basic concepts of the general linear model, the *t* test and a detailed description of SPM99 and its comparison to SPM2.

Chapter 5 describes the methods utilized in the investigation, chapter 6 and 7 describe the results obtained with detailed discussion of these results. Finally, Chapter 8 presents a conclusion of this work and suggests future directions for work.

Chapter 2

Principles of Functional MRI

2.1 Introduction

Functional magnetic resonance imaging (fMRI) has greatly increased our ability to study localized brain activity in humans by taking advantage of the coupling between neuronal activity and hemodynamics (the local control of blood flow and oxygenation) in the brain.

fMRI is a tomographic technology used in medical imaging that enables a non-invasive study of the function of the brain by measuring hemodynamic changes related to alterations in neural activity. Its main advantage over other imaging techniques is the absence of ionising radiation, which allows for repeated measurements to be made, allowing for the study of the reproducibility of activation images [5].

2.2 Contrast in Functional MRI Imaging

The apparent structure of what we see in the image (contrast) depends on how it is acquired. MR images are produced using radio frequency (RF) pulses and gradient fields in the presence of the main magnetic field of the scanner. By the choice of their timings (TE and TR), it is possible to highlight various characteristics of the tissue being imaged [5-8].

Body tissues have different proton density (PD), depending on the number of hydrogen atoms in the tissues. The PD determines the strength of the net magnetisation vector, which affects the overall signal strength. When the body is placed in a scanner, the induced magnetisation will initially be aligned with the main field of the scanner. The presence of the RF pulse will cause the magnetisation to be knocked out of alignment into the transverse plane (perpendicular to the main field). After the RF pulse, the magnetisation will return to its equilibrium position via two relaxation processes: spin-lattice relaxation (T_1) which controls the recovery of the magnetisation aligned along the main field, and spin-spin relaxation (T_2) which controls the decay of the signal in the transverse plane. Field variations randomly alter the frequency of the proton's precession, disturbing the phase coherence and speeding the transverse relaxation. The combined T_2 and magnetic field inhomogeneity is known as T_2^* relaxation. In the brain, the extent of the inhomogeneities depends on the physiological state, which in turn is dependent on the neural activity.

Therefore, measurement of the T_2^* parameter is an indirect measurement of the neural activity [6;8].

Until the late 1980's, the T_2^* relaxation was considered to be a nuisance. But, once it was realised that the presence of a paramagnetic substance in the bloodstream (deoxyhemoglobin) could act as a vascular marker, T_2^* started being used in MRI and the technique was applied eventually to functional activation studies to detect changes in brain activation via the relatively indirect coupling of the neural activity to cerebral blood flow and subsequently to magnetic resonance signal intensity [2;9].

2.3 BOLD Mechanism

Changes in the T_2^* parameter are connected to the neural activities via changes in the oxygenation of venous blood, or what is known as the BOLD contrast mechanism [5;6].

2.3.1 Biophysics of BOLD fMRI

In 1990, the effects of changes in the relative concentration of oxygenated and deoxygenated blood on T_2^* were first reported [10]. It was noted that cortical blood vessels become more visible as blood oxygen was lowered and hence, the term BOLD (Blood Oxygenation Level Dependent) fMRI. BOLD does not provide a direct measurement of quantitative flow but it is

related to the regional changes in brain activity in areas close to the observed signal. It is a technique that relies on variation in the MRI signal due to the physical process of changing proportions of deoxyhemoglobin in the blood. It does not require injection of a contrast agent, but does require a rigid active/inactive model to produce data sets during known functional activity/inactivity [11]. Images are obtained while the subject is engaged in a set of tasks to isolate specific brain functions. The nature of the activity field is then roughly thought to be as follows. Increase in the neural activity will induce an increase in the regional blood flow, which will in turn cause vasodilation of the venules and veins and thus an increase in the venous oxygenated blood (Fig. 2.1). This will overcompensate for the consumption of oxygen in the area leading to a decrease in the concentration of the deoxyhemoglobin in the blood. Deoxyhemoglobin is paramagnetic and has a different magnetic susceptibility relative to the surrounding tissue [12;13]. Its presence alters the local magnetic susceptibility, creating magnetic field distortions within and around the blood vessels, which in turn produce a slight alteration in the local MR signal [14]. Therefore, the decrease in the deoxyhemoglobin concentration relative to the oxyhemoglobin in the blood will lead to a reduction in the local field inhomogeneity, an increase in T2* and a slower decay of the MR signal, thus resulting in increased MR signal intensity [15;16].

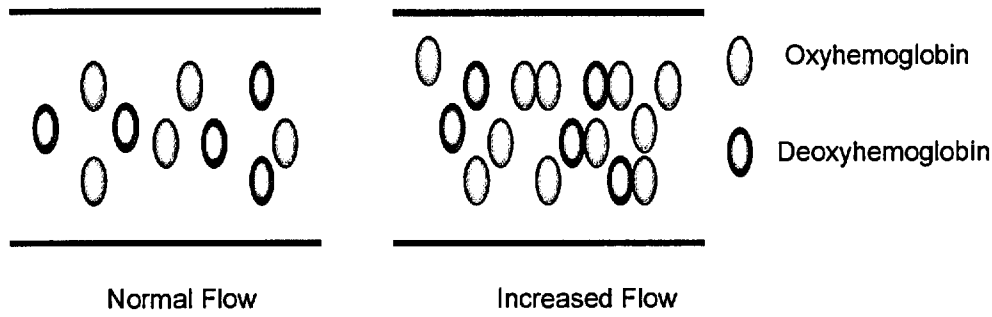

Fig. 2.1 Alterations in Blood Oxygenation.

As we mentioned previously, the intensity of the signal depends on the change in the oxy/deoxyhemoglobin ratio in the blood. If the local oxygen consumption remained constant, the deoxyhemoglobin concentration would not change. The BOLD contrast is determined by the supply (cerebral blood flow (CBF) and cerebral blood volume (CBV)) and demand (cerebral metabolic rate of oxygen consumption ($CMRo_2$)), as well as the baseline physiological state. The interaction between the neural activity and the physiological variables (CBF, CBV, $CMRo_2$) involves a number of factors including the cell types and circuitry driven during activation, and the processes that couple energy demand to its supply to the brain [6].

There are contradictory results regarding the effect of the baseline state on the BOLD response. Some researchers have noted that the baseline CBF has a strong effect on the magnitude of the BOLD response, where an increase in the baseline CBF will cause a decrease in the BOLD response

[14]. Others have observed that an increase in the global blood flow resulted in a noted earlier response with higher amplitude and narrower width [17]. The relative changes in the CBF and $CMRo_2$ determine the level of oxygenation of the blood, where an increase in the neural activity will cause CBF to increase much more than $CMRo_2$ and therefore, cause a decrease in the local oxygen extraction. The CBV determines the total amount of blood (and thus the total deoxyhemoglobin in the voxel) [10;14;18].

2.3.2 The Physiological Basis of BOLD fMRI

It is known that the fMRI signal is triggered by the metabolic demands of increased neuronal activity. The interpretation of task-induced functional imaging of the brain is dependent on understanding the relationship between observed hemodynamic responses and the underlying neural changes. Simultaneous fMRI and electrophysiological recordings have confirmed that the BOLD contrast mechanism reflects aspects of the neural responses elicited by a stimulus [6]. The exact relationship between the neural activity and the BOLD contrast mechanism is unclear and is still under analysis [6;13;19-22].

It is widely believed that increased blood flow follows directly from increased synaptic activity, where the propagation of action potentials along

the axon of the neuron due to the inflow of Na^+, will result in the release of neurotransmitters known as Glutamate (dominant excitatory neurotransmitter of the brain). Glial cells known as astrocytes, are present in the extracellular space, and are connected to the synapses of the neurons and the brain's vasculature (capillaries). The release of glutamate from the synaptic cleft triggers the astrocytes to uptake the glutamate and glucose from the blood. A process known as "glycolysis" occurs in the astrocytes, where glucose is consumed and converted to pyruvate, which is then converted into lactate and energy is released. This energy is then used to convert glutamate to glutamine (neurotransmitter recycling). Lactate is consumed by the neurons through oxidative phosphorylation to produce pyruvate and energy (ATP). Glutamine is subsequently released by astrocytes and taken up by the neuronal terminals, and the energy is used to reconvert the glutamine back to glutamate. Most of the energy is consumed by the neurons, and a small amount is consumed by the astrocytes to clear glutamate from the extracellular space [3;6;13;23].

The enhancement of the BOLD contrast is due to an increase in the cerebral blood flow (CBF) that overcompensates for the decrease in oxygen, delivering an oversupply of oxygenated blood. The reason of the mismatch between the supply and the consumption of blood oxygen is still unclear. Two main viewpoints attempt to explain the mismatch:

Glucose Supply:

It is widely believed that an increase in the synaptic activity will cause an increase in the blood flow. This is due to two observations that noted an increase in the blood flow due to an increase in glucose consumption, and a link between glucose metabolism and synaptic activity. This view explains the mismatch between the blood flow and the oxygen consumption, as blood flow provides the level of glucose required regardless of the blood oxygenation [6].

Oxygen Supply:

The other view is that the blood flow provides the oxygen levels required by the neurons. This view attributes the mismatch to the inefficient extraction of oxygen at higher flow rates, which is supported by observations noting an increase in oxygen consumption with neuronal activity and that most of the energy in the brain is used by the neurons, which rely on oxidative metabolism of lactate, and only a small amount is used for the neurotransmitters recycling by the astrocytes, which rely on non-oxidative glycolysis. However, due to contradictory observations, this hypothesis still remains uncertain [6;13].

There has been some controversy in regards to whether the oxygenation level is related to the intracellular neural activity (Sub-threshold activity

represented by Local Field Potential LFP) or if it is related to the extracellular neural activity (Supra-threshold firing (spiking) rate).

Local field potentials (LFP) represent slow electrical signals and sub-threshold activity including synaptic potentials, afterpotentials of somatodendritic spikes and voltage-gated membrane oscillations. Therefore, it reflects the input signal and the local processing mediated by the sub-threshold signals of interneurons but does not reflect the action potentials carried by the principal (output) neurons. On the other hand, Multi-Unit Activity (MUA) measures regional neuronal spiking and reflects the action potential carried by the output neurons. The magnitude of the MUA is determined by the local cell size and therefore, its magnitude varies considerably across brain sites [6].

Recent studies have concluded that increases in the BOLD signal is correlated most clearly with the local field potential rather than the neuronal firing rate [6;7;18]. Other studies have confirmed this by noting that the HRF reflects the neuronal input (LFP) to the relevant area of the brain rather than the signals transmitted by the action potentials to other regions of the brain (spiking activity). This may be a cause of false activation, depending on whether the output is correlated with the input or whether the input plays a primarily modulatory role [6]. In general, the LFP is believed to be often (but not always) correlated with the output spiking activity [13].

Further studies are required to determine if spikes (MUA) are not a key variable in the BOLD response [6;18]. Studies also concluded that the BOLD signal does not correlate perfectly with action potentials, but rather measures a mix of continuous membrane potentials and action potentials [6].

2.3.3 Hemodynamic Response Function

The activation-induced fMRI signal change has a magnitude and time delay determined by a transfer function for the response which is referred to as the hemodynamic response function (HRF). It depends on a combination of changes in cerebral blood flow (CBF), cerebral metabolic rate of oxygen ($CMRO_2$), cerebral blood volume (CBV) and also on the baseline physiological state [14]. The HRF is the theoretical signal that BOLD fMRI would measure in response to a single, very short stimulus of unit intensity [24]. It is not well understood and there is still ongoing research to determine a precise and robust estimation of the HRF, since it has the potential to give an insight into the underlying dynamics of brain activation and the relationships between active areas [14;24-28].

Fig. 2.2 represents the time course of a typical hemodynamic response function for a neural event that lasts a second. HRF is composed of three stages: after stimulus onset, the BOLD signal exhibits an initial dip due to

the rapid increase in local deoxyhemoglobin (due to initial period of oxygen consumption). The signal increase is delayed by 2-3 s followed by a ramp of 6-9 s to a peak value (due to the oversupply of oxygenated blood). The signal eventually returns to the baseline with an evident undershooting (due to the diminishing of the oversupply of oxygenated blood) [6;13;27;29;30].

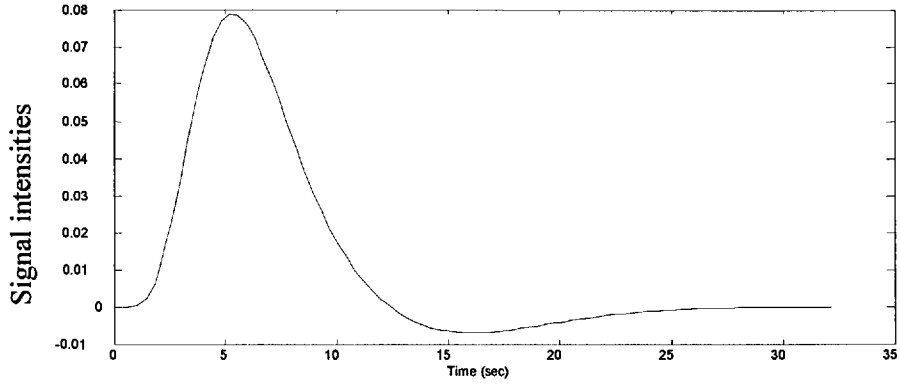

Fig. 2.2 Hemodynamic response function (HRF) – Standard HRF extracted from SPM99.

Initial dip:

A small transient decrease in the BOLD signal lasting 1-2 s before the standard BOLD signal increase has been observed in some areas of the brain. Most of the empirical evidence for the initial dip comes from optical imaging studies as well as some reports of it using BOLD fMRI and magnetic resonance spectroscopy [13;20]. This initial dip has been interpreted as reflecting local deoxygenation of blood in the capillaries

preceding the inflow and volume effects that take place and the onset of activation. The initial dip is a highly controversial topic, as studies have not always been able to find it in the responses measured [7;13;14;20].

Variability:

Heterogeneity in the timing, amplitude and shape of the HRF signal was found across regions, tasks, subjects and sessions. This reflects the variability of the underlying neural activity, but might include some other factors including partial volume imaging of veins, slice timing differences, global magnetic susceptibilities, hematocrit concentrations, caffeine, alcohol, or lipid ingestion [6;22;24;24;28;31-33]. Some of the variations noted include an initial dip, a slow ramp and an overshoot at the end of the stimulus [14]. Further research is required to investigate the variability in the temporal behaviour of the BOLD response, especially addressing the within-subject variability across session. Understanding the within-subject variability across sessions is essential for better interpretation of the results from the between subjects. It could also be used for learning and habituation effects on the subject's performance as well as the aging and recovery effect on subjects [30]. Further research is needed to characterise the extent of the variability and examine how these observed variations affect the statistical results of BOLD fMRI studies [32].

2.3.4 Linearity

An important step in characterising the relationship between the neural activity and the measured fMRI signal is by assessing the linearity of the measured BOLD signal in response to neural stimulation. The general understanding of the relationship between the input stimulation and the output BOLD response is shown below in Fig. 2.3.

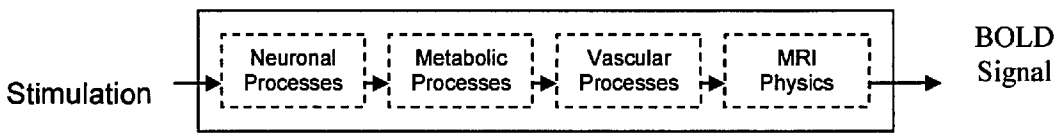

Fig. 2.3 Link between stimulation and BOLD response.

In general, the relationship between stimulus energy and the BOLD response is nonlinear. Nonlinearity is an important issue in the design of experiments and in the analysis of fMRI data [34]. The nonlinearity could be due to the relationship between neural signal and the stimulus energy, or due to the relationship between the neural signal and the BOLD response [6;17;34]. Recent studies have shown that the relationship between the BOLD response and the neural activity is varying spatially, where there is a linear relationship at high contrasts but nonlinear relationship at low contrasts [13]. Logothetis et al [6] confirmed this, where a linear relationship was observed at higher contrasts. Further investigations are required to study the nature of the nonlinearity in the low-contrast regions. Their study

also concluded that the neuronal synaptic activity responses are nonlinearly related to the stimulus properties [6;31;31].

Other studies have also found a temporal nonlinearity, where the addition of a shift and an added response over-predicted the true response. This nonlinearity was more evident when using a stimulus that is less than 4 s to predict the response of a stimulus that is longer than 6 s. There is some suggestion that this might be due to failure in the design of the experiments, and not to failure of the temporal linear summation itself. This is due to the observation that the experiments were completed in the primary sensory and motor cortical areas, where short-duration stimuli are expected to give disproportionately large neuronal responses, which according to the linear transform model, should in turn evoke disproportionately large fMRI responses. Therefore, further investigation is required to study the effects of the response transients, adaptation and attention on the temporal summation of the fMRI responses [13;14;35-38].

Nonlinearity has also been reported as a refractory period, where two identical stimuli close together in time produced a net response that is less than twice the integrated response of a single stimulus [14]. Recent research regarding the refractory effect concluded that it reflects the adaptation of local stimulus-specific neuronal or neurovascular (local vasculature that directly supports a functional region) populations, so that

they will be present for stimuli that evoke similar neuronal activity but absent for stimuli that evoke different neuronal activity [39].

As mentioned earlier, the main goal of neuroimaging studies is to depict the neuronal activity associated with the performance of a particular task. Nonlinearities could either be eliminated (or minimised) or incorporated into the analysis. The failure to model the nonlinear effects in the data analysis may reduce the statistical significance or may introduce biased or incorrect results. Addressing the nonlinear effects in fMRI data is still an active area of research. In most of this work, however, we rely on the linear model of approximation of BOLD signal.

2.3.5 Modelling Neurological Response

A large series of images is acquired rapidly while the subject performs a task that oscillates the brain activity between two or more states (On-Off). Several hundred volumetric scans of the brain are collected in a single session while the subject is performing the task [7]. If the task variations evoke a large enough change in the metabolic demand (blood flow and oxygenation) in certain areas in the brain, then the image intensity in that region will modulate over time about its mean intensity value. These changes are around $\pm$5% at best [13;25;29;40].

2.3.6 Field strength influence on BOLD signal

Changes in the image intensity due to changes in the neural activity are dependent on the magnetic field strength. Some studies have investigated the relationship between the BOLD signal and the static field strength of the MRI scanner and found that there is a linear increase in the BOLD signal change in relation to the field strength for blood vessels that are of greater radius than about 8 μm and a quadratic increase for vessels that are smaller than that [7]. Other studies have also confirmed this, where they showed that BOLD signal increases with field strength and that the gain in the SNR offered by the high field imaging translates to a decrease in the minimum number of cycles needed in fMRI experiments [41].

2.3.7 Activation Detection

It is possible to identify areas of activation in the brain by correlating the signal time course at each voxel with the known time course of the task (model) [7]. The model is designed to mimic the paradigm or stimulation protocol. The model is a convolution of the rectangular waveform (On-Off) with a suitable hemodynamic response function [29]. Note, this is a linear model for activation, but the non-linear relationship discussed earlier implies that there is not a linear relation between the strength of the activation and the amplitude of the signal.

2.4 Echo-planar Imaging (EPI)

Echo-planar imaging was conceived in 1977 by Sir Peter Mansfield. It is a commonly used technique for fMRI studies of the human brain. It is the fastest practical imaging method available which can acquire a slice in less than 100ms and thus the entire brain can be imaged in few seconds [42]. It is a method that can form a complete image from a single RF pulse (single shot). The k-space in the EPI is formed by collecting raw data lines (K_x) using a single slice-selective RF pulse and by using a continuous phase encode gradient (nonblipped) during the oscillating readout gradient, which are then sampled in the presence of a rapidly switched (oscillating) magnetic field gradient, resulting in an irregular zigzag path through the k-space, and this is known as nonblipped EPI. The same process can be done by using (blipped) brief pulse of the phase encoding gradient (K_y) at each readout gradient reversal to move to the next line in the phase encode direction resulting in a regular path through the k-space (Fig. 2.4), and this is known as blipped EPI [5;8;29].

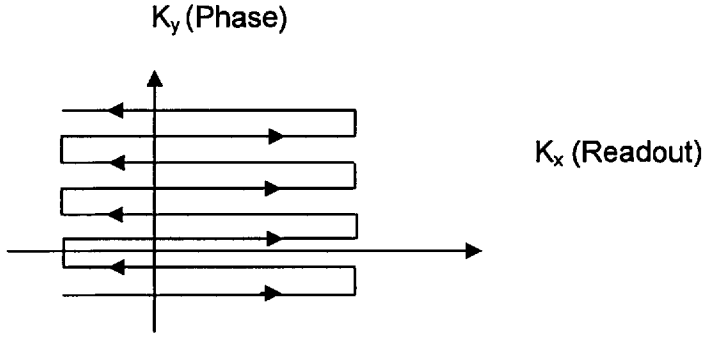

Fig. 2.4 K-space in EPI.

Both the k-space matrix and the real space matrix have the same size, but the pixels do not correspond to each other directly. Data in the middle of k-space will contain information about the signal to noise ratio (S/N) and the contrast, whereas data around the outside will contain information about the resolution. 3D volumes (images) are reconstructed from multiple 2D slices in the k-space using a Fourier Transform [8].

This rapid data acquisition technique has enabled the development of real-time MRI. Changes in the blood oxygenation in response to brain function result in a rapid alteration of the MR signal, which can be measured using EPI.

Artifacts:

The imaging speed in EPI is a result of very rapid sampling, which requires very high amplitude field gradient. This will cause the bandwidth to be very high along the readout axis (K_x) and relatively low along the phase encoding axis (K_y). This leads to artifacts like: shape distortion and chemical shifts. The alternating sign of successive k-space acquisitions (gradient echoes) may lead to image ghosts [8;9;22;29;43].

Another major limitation of EPI is the relatively low spatial resolution. This problem is more apparent at high magnetic fields with increasingly shorter $T2^*$ relaxation times. The maximum switching rate of the magnetic field

gradients used for the echo generation is restricted to avoid peripheral nerve stimulation [29]. The spatial resolution can be increased by increasing the gradient amplitude and/or the gradient duration, which may subsequently lead to safety problems and a decrease in the image bandwidth causing shape distortion [43].

Other artifacts related to the EPI imaging technique are similar to those experienced by other MR imaging techniques, which are sensitive to motion, displacement of internal tissues, blood flow in discrete vessels etc. [40].

Several modifications have been made to the basic EPI sequence to compensate for these artifacts like segmented EPI, introduction of phase correction, spiral scanning etc. [5;29].

Thus, the EPI technique involves a degree of compromise between sensitivity to hydraulic flow (flow not associated with change in the oxyhemoglobin / deoxyhemoglobin ratio) and sensitivity to the BOLD effect [40].

There is a wide variety of sequence and sequence parameters of EPI that are used to obtain an image with a range of contrast behaviors. Two main classes are: spin echo imaging and gradient echo sequences.

Spin Echo (SE) sequence:

Spin-echo sequences are the most common implementation of EPI in clinical imaging. In the SE sequence, the spatial encoding module is preceded by a 90° excitation pulse and a 180° echo forming pulse, resulting in the formation of a Hahn echo during the readout period [43].

It is an attractive alternative to a gradient echo sequence due to its ease of implementation, signal retention in areas with large magnetic susceptibility gradients (which eliminates non-specific contributions from extravascular BOLD signal changes in the vicinity of large venous vessels) and improved localization of neural activity. But the imaging time is too slow for most fMRI [44;45].

The signal intensity from a voxel for a spin echo sequence can be written in terms of echo time (TE), repetition time (TR), longitudinal relaxation time (T_1), transverse relaxation time (T_2), proton density (ρ) and constant of proportionality K_{SE} as shown below: [3;43].

$$SI = K_{SE}\rho\,(1- e^{-TR/T1})\, e^{-TE/T2} \quad \text{for TR>>TE} \qquad (2.1)$$

Images obtained using the SE sequence show relatively little sensitivity to local field homogeneities and behave similar to conventional MR images. The difference is that in the SE sequence, the TR is effectively infinite and

the images can be obtained with little or no T_1 contrast. This is an advantage in T_2-weighted studies, where the simultaneous manifestation of T1 and T2 contrasts tend to cause an overall reduction in the image contrast [3;43].

Gradient Echo (GE) sequence:

Gradient-echo sequences remain the most widely used fMRI method. In the GE sequence, the 180° echo forming pulse is omitted and the signal is focused solely by the gradients, hence the name of the sequence [43].

GE sequences are sensitive to both large vessels and small capillaries [45]. They have a faster imaging time (several seconds to a minute) compared to spin echo. The main reason for using the GE sequences is that the contrast includes a T_2^* component as opposed to the T_2 component, which is the dominant mechanism in BOLD functional imaging [43].

The signal intensity from a voxel for a gradient echo sequence can be written in terms of echo time (TE), repetition time (TR), longitudinal relaxation time (T_1), transverse relaxation time including both inhomogeneous (time reversible) and homogeneous (time irreversible) broadening contributions (T_2^*), proton density (ρ) and constant of proportionality K_{GE} as shown below [3;43]:

$$SI = K_{GE}\rho\, e^{-TE/T2^*}\sin(\alpha)\,\frac{1-2e^{(-TR-TE/2)/T1}}{1+\cos(\alpha)e^{-TR/T1}} \qquad (2.2)$$

The signal is optimized (for any combination of TR and T_1) when the flip angle (α) is adjusted to the Ernst angle, which is shown below:

$$\alpha = \cos^{-1}(e^{-TR/T1}) \qquad (2.3)$$

When TR is chosen to be shorter than T_1, the Ernst angle will be less than 90° resulting in less disturbance from the magnetic equilibrium and therefore shorter relaxation recovery time [3;43].

2.5 Noise Inducing Factors in fMRI

The change in signal intensity due to brain activity is small in general and, in particular, smaller than the noise and the baseline signal intensity [24]. This will lead to confusion in whether the activation detected is due to brain activity or noise. There are several factors, other than brain activity, that contribute to image intensity changes in fMRI. These factors can be divided into two sections:

A. Factors that affect the concentration of the paramagnetic deoxyhemoglobin in the blood:

1. Research found that fMRI signals reflect the collective activity of a very large number of neurons; changes in the fMRI responses may be due to either large changes in the firing rates in a small subpopulation of neurons or small changes in the firing rates in a much larger subpopulation of neurons [13;21].

2. The BOLD contrast change is due to the deoxyhemoglobin-related susceptibility effects, which alter the microscopic magnetic field gradients in (water molecules in the blood) and around (surrounding tissues) the vessels. Therefore, the BOLD contrast is composed of both an intravascular and extravascular component. Their contribution to the BOLD contrast depend on the static magnetic field strength, the echo time of the imaging sequence and the nature of the MRI signal. This could cause detection of activation at areas of some distance from the site of neuronal activity [7;14;29].

3. Vasomotion: Local changes in blood flow at rest: due to vasomotion where the arteries experience arrhythmic dilation and contraction of the blood vessels [46].

4. Pharmacological modulations and pathological alterations: Some drugs can have a vasodilatory (i.e. acetazolamide) or vasoconstrictory (i.e. aminophylline) effects and therefore a change in the BOLD signal strength. Also some diseases affect the speed of vasomotor reaction to functional activation (i.e. cerebrovascular disease) [29].

5. Physiological noise: the heart cycle causes periodic blood flow which is confined mainly to vessels [9].

B. Factors that affect the signal intensity other than the concentration of the paramagnetic deoxyhemoglobin in the blood:

1. Vessels: Signal intensity is dependent on the position of the nuclear spin within the vessel and its proximity to an adjacent vessel with a different magnetic susceptibility. It is also dependent on shape, size of the vessel and the orientation of the vessel relative to the main magnetic field [3;11;30].

2. Susceptibility differences: due to the differences in magnetic susceptibility between brain tissue and air-filled spaces [29].

3. Comparative studies of the brain are also influenced by the scanning hardware, procedures, experimental designs, analysis tools, and post-processing strategies [30].

4. Subject movement: It is the major source of noise in fMRI, especially if it is correlated with the stimulus [29;47]. There are two main types of motion:
   a. Between acquisition [4;48]: attempts were made to limit head movement using facial masks, but it is not practical especially when used in patient studies and also found not to eliminate the problem completely.
   b. During acquisition: during the filling of the k-space for a single slice. It is not likely to be a significant issue when using EPI, due to its speed of acquisition.

5. Spin excitation history effect [10;49;50]: Changes in the observed signal are a function of both the current position and the spin excitation history (past positions). The spin excitation history is determined by the history of past movements. A displacement (motion) during the experiment can modify the intensity of the subsequently scanned volumes, even if those volumes are not displaced themselves. The spin excitation history effect will be evident

if the excited spins in the acquisition volume do not have enough time to return to equilibrium before the next excitation pulse occurs.

6. Respiratory effects: due to small field shifts induced in the brain caused by gross magnetic susceptibility change as the lungs in the chest cavity expand and contract. Field shifts will induce a field gradient across the brain, which will cause fluctuations in the signal intensity due to dephasing of the signal [3;51;52].

7. Cardiac motion: contractions of the heart within the chest cavity will cause a pulsatile motion that can extend throughout the entire brain and can induce fluctuations in magnetic susceptibility. Cardiac gating can be used in conventional MRI to correct for the cardiac effects, and Gradient Moment Nulling may be used in peripheral imaging [3;9;51;52].

8. Cerebrospinal fluid (CSF): this flows throughout the brain and the spinal cord and is driven by the cardiac pulsations of the brain with a rhythmic modulation superimposed by breathing. It is a potential source for signal fluctuation

especially at regions in and around the ventricles. It can be corrected for using Inversion Nulling or FLAIR (FLuid Attenuated Inversion Recovery) [3;46;53].

9. Interpolation scheme used to resample realigned images can lead to motion-correlated residual intensity errors. It is possible that these may lead to false activations appearing [10;12;49;50].

10. Inhomogeneity of the static magnetic field (B_o) and the field of the RF electromagnetic radiation [24;46;54]. There are many reasons causing these inhomogeneities including magnetic field gradient switching faults, chemical shift of the Larmor frequency, tissue magnetic susceptibility and ferromagnetic materials [55]. Dynamic Shimming may be used to minimize B_o inhomogeneities using small DC current offsets in the gradient coil adjusted with the subject in place.

11. Thermal noise: temperature instability of the electronics of the scanner receiver subsystem, A/D system and elsewhere [8;51;52].

12. HRF variability: variability of the HRF signal between subjects, tasks and regions in the brain will affect the ability to detect regions of activation [48].

13. Eye motion: causing ghosting effects by increasing the variance in regions in the phase-encode direction [3;47].

14. External sources: Mechanical vibration due to the lack of stability of the site supporting the magnet [3;24].

Thus, the fMRI time series can be viewed as a mixture of signal and noise and can be divided into three main components [51]:

1. Correlated signal: conforms to changes in neural activity (low frequency).

2. Correlated noise: physiological noise from cardiac and respiratory cycles and motion correlated signal noise (low frequency).

3. Aliasing: it is present when high frequency physiological pulsations are critically sampled at a lower frequency than their own. Over a prolonged period of scanning, this would create an artefactual signal of low frequency [56-58].

4. Uncorrelated noise: thermal noise (high frequency).

It is crucial to know the exact amount of influence these factors have on the measured fMRI signal for a further understanding of the neurovascular coupling and the accurate interpretation and statistical analysis of these measurements [30].

The main problem with ensuring a valid signal from a BOLD analysis is in controlling the effects of motion, which can be considerable during the length of the experiment and can correlate directly with the task performed which will then lead to false activation.

2.6 Summary

Some basic fMRI concepts were presented in this chapter, in terms of contrast, BOLD mechanism, biophysics and physiology of BOLD fMRI, hemodynamic response function, the linearity issue, EPI and noise in affecting fMRI. In the next chapter, we will consider the registration process. This is used to register volumetric data sets to a reference volume to reduce noise due to subject motion in between volumetric data sets acquisitions.

Chapter 3

Image Registration Review

3.1 Introduction

Changes in the MR signal intensity that result from the subject stimulation are typically small compared to the baseline signal intensity and noise level. Therefore, the data can be easily corrupted by small involuntary movements of the subject between volume acquisitions, particularly where there is a large spatial variation in image intensity: at tissue boundaries, at the edge of the brain or near major vessels [59]. Movement of the subject's head is a fundamental problem in fMRI studies, especially when it is correlated with the task and it has been found to cause signals which mimic true activation (false activation). Realignment of fMRI time series is considered a prerequisite preprocessing step in the analysis of functional activation studies [4;11;12]. Several public domain algorithms are currently available for motion detection in fMRI. Registration involves the spatial alignment of images (which have a common underlying anatomy, acquired

at different times, from different view points, and/or by different sensors) by transforming one volume with respect to the other as shown in Fig. 3.1. This involves estimating a mapping between the two volumetric data sets. One assumed to remain stationary (the target), whereas the other (the source) is transformed to match the target. This requires a mapping from each voxel position in the target to a corresponding position in the source. The source is then resampled at the new positions [60].

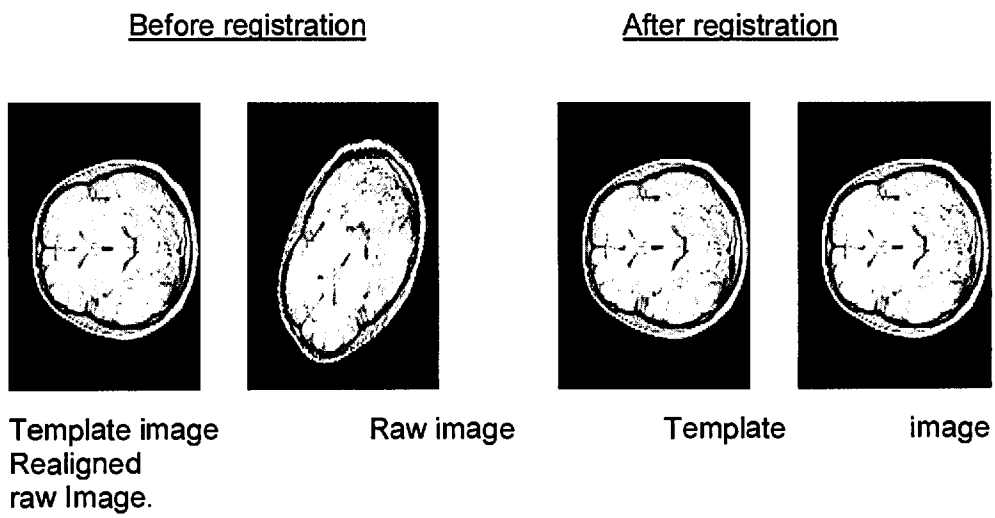

Fig. 3.1 Image registration

3.2 Applications of Image Registration

Image registration has a vast range of applications. Images acquired using different modalities usually provide complementary information. Image registration is required in the integration (or fusion) of data from these

images [61-63]. It is also used for integrating information from data sets obtained with the same modality at different times for the purpose of quantitative comparison [64]. Some of its applications in medicine include pathology detection (detecting abnormal brain structures), analyzing brain data (comparing brain function between individuals and groups), measuring anatomical differences (quantification of local and global shape changes), population-based atlases (creating a probabilistic brain atlas that encodes patterns of anatomic variation in human populations and detecting structural differences that do not belong to a specific group) and measuring brain changes (temporal single subject monitoring) [65]. It also has applications in remote sensing (environmental monitoring, weather forecasting) and in computer vision (quality control) [66].

3.3 Classification of Registration Techniques

Registration techniques may be classified according to the criteria formulated by van den Elsen [62]:

1. *Dimension of data to be registered* [62;67]: Registration can be performed in any dimension, whether all dimensions are spatial or that time is an added dimension:

    a. 2D/2D: registration of two image slices.

b. 2D/3D: registration of spatial data to projective data (and vice versa). An example is the registration of pre-operative CT image to an intra-operative x-ray image.

c. 3D/3D: registration of two volumetric datasets.

All of the above may include time as extra dimension (2D becomes 3D and 3D becomes 4D).

2. *Modalities* [67;67-69] :Images are divided into two main types:

I. Functional: showing information on the metabolism of the underlying anatomy (i.e. SPECT, PET, fMRI, etc).

II. Anatomical: showing information about the topography or the structure (i.e. x-ray, CT, MRI, etc).

Therefore, image-type related registration can be divided as follows:

a. Intra-modality: registration of images from the same source.

b. Inter-modality: registration of images that come from different technologies (i.e. MRI and CT). An example is the registration required in radiotherapy treatment, when a CT image is needed to compute the radiation dose and an MR image is used for delineation of tumour tissue.

c. Modality to model: registration of one image to a model.

d. Patient to modality: registration of one image to the patient him/herself. It appears in intra-operative and radiotherapy applications.

3. *Degree of user interaction* [67]: registration methods have varying degrees of user interaction:

a. Interactive: requires human interaction.
b. Semi-automatic: transformations are determined by the computer while the user determines the image properties required for registration and decides when to start and stop the registration.
c. Automatic: does not require human interaction.

4. *Subject* [67;67]:

a. Single subject (intra-subject): where registration is between different images for the same subject, (i.e. in case of progression of disease study).
b. Multi-subjects (inter-subject): registration between images of different subjects, (i.e. in case of group disease related study).
c. Single subject and Atlas. Appears mostly in 3D/3D MR applications.

5. *Matching features (nature of registration algorithms)* [62;64;67;67;69;70].

a. Extrinsic (prospective): based on artificial (foreign) objects introduced into the imaged space. It can be invasive (i.e. screw-mounted markers) or non-invasive (i.e. stereotactic frame).
b. Intrinsic (retrospective): based on image information generated by the subject:
    I. Landmark (homologous) based: Where a set of identified points representing the same feature in the different images is directly compared to each other.
    II. Segmentation based: a set of identified surfaces, contours or volumes are extracted and deformed to fit the original image.
    III. Voxel based: operate on the grey values (intensity) of each voxel in the image to perform the registration.
c. Non-image based: the calibration of the image coordinate systems of two scanners, assuming that the patient remains stationary between acquisition and that the scanners are in the same physical location. (i.e. Ultrasound systems).

6. *Nature of transformation:*

This refers to the transformations needed to align the images. The transformations are divided into four major classes: rigid-body, affine, projective and curved. Rigid-body, affine and projective transformations are known as linear transformations because they map straight lines to straight

lines. They are most commonly used where the image scaling factors are unknown or suspected to be incorrect (MR images with geometric distortions). Curved transformations are known as nonlinear transformations because they map straight lines onto curves. Generally, local transformations are nonlinear, where subsections of the image have their own transformation defined [71].

7. *Domain of the transformation:*

   a. Global: when change in any one of the matching parameters influences the transformation of the image as a whole.
   b. Local: change influences only part of the image.

8. *Optimization procedure (parameter determination):* [62;67;70]

   a. Direct: straightforward calculation from the data upon the assumption that the problem of finding the best match is simple. Used in small point sets.
   b. Search-oriented: starts from one or more initial guesses and tries to find the optimal transformation.

9. *Object:* the part of the body that images have been acquired of and subsequently conducted a registration on [70].

10. *Tightness of feature coupling:* transformation between two images can be interpolating or approximating. Interpolating transformations map the images precisely, while approximating transformations distribute the matching error over all the features and have a zero mean (i.e. least-squares fit) [62;72].

3.4 Steps of Registration

Registration can be separated into the following steps:

1. Transformation: This captures the fundamental mapping of any image registration technique. It is the mapping of points from image or volumetric data to new locations in another. There are different types of transformations which can be classified as follows [60;62;63;67-69;73;74]:

a. Rigid-body: It preserves relative lengths and all angles (7 degrees of freedom (DOF)). The relative distance between two points in the first image is preserved when these two points are mapped onto the second image. Rigid body is composed of a combination of:

i. Translation: 3D shifting (3 DOF), as shown in Fig. 3.2.

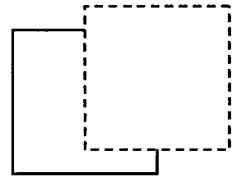

Fig. 3.2 Translation.

In matrix terms, it is represented as follows:

$$\begin{bmatrix} y1 \\ y2 \\ y3 \\ 1 \end{bmatrix} = \begin{bmatrix} 1 & 0 & 0 & q1 \\ 0 & 1 & 0 & q2 \\ 0 & 0 & 1 & q3 \\ 0 & 0 & 0 & 1 \end{bmatrix} \begin{bmatrix} x1 \\ x2 \\ x3 \\ 1 \end{bmatrix} \tag{3.1}$$

Where y_i represent the output (or image A), x_i represent the input (or image B), and q_i represent the translation parameters in the x, y and z direction.

ii. Rotation: 3D rotation around x, y and z axes (3 DOF) as shown in Fig. 3.3.

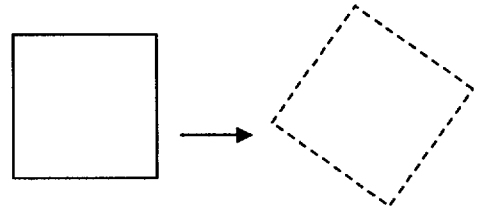

Fig.3.3 Rotation.

In matrix terms, it is represented as follows. The matrix format for the rotation around the x axis (pitch):

$$\begin{bmatrix} y1 \\ y2 \\ y3 \\ 1 \end{bmatrix} = \begin{bmatrix} 1 & 0 & 0 & 0 \\ 0 & \cos(q1) & \sin(q1) & 0 \\ 0 & -\sin(q1) & \cos(q1) & 0 \\ 0 & 0 & 0 & 1 \end{bmatrix} \begin{bmatrix} x1 \\ x2 \\ x3 \\ 1 \end{bmatrix} \tag{3.2}$$

The matrix format for the rotation around the y axis (roll):

$$\begin{bmatrix} y1 \\ y2 \\ y3 \\ 1 \end{bmatrix} = \begin{bmatrix} \cos(q_2) & 0 & \sin(q_2) & 0 \\ 0 & 1 & 0 & 0 \\ -\sin(q_2) & 0 & \cos(q_2) & 0 \\ 0 & 0 & 0 & 1 \end{bmatrix} \begin{bmatrix} x1 \\ x2 \\ x3 \\ 1 \end{bmatrix} \quad (3.3)$$

The matrix format for the rotation around the *z* axis (yaw):

$$\begin{bmatrix} y1 \\ y2 \\ y3 \\ 1 \end{bmatrix} = \begin{bmatrix} \cos(q_3) & \sin(q_3) & 0 & 0 \\ -\sin(q_3) & \cos(q_3) & 0 & 0 \\ 0 & 0 & 1 & 0 \\ 0 & 0 & 0 & 1 \end{bmatrix} \begin{bmatrix} x1 \\ x2 \\ x3 \\ 1 \end{bmatrix} \quad (3.4)$$

Where y_i represent the output (or image A), x_i represent the input (or image B), and q_i represent the angles in radians around the *x*, *y* and *z* direction. The order in which the operations are performed are important.

iii. Scaling: zooming in the x, y and z direction (1 DOF). It preserves angles and relative lengths as shown in Fig. 3.4.

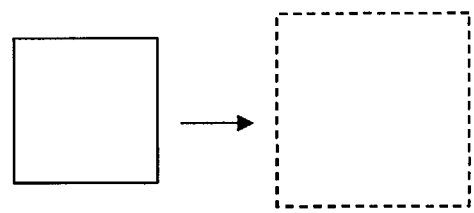

Fig. 3.4 Scaling.

(Sometimes, scaling is categorized separately).

In matrix terms, it is represented as follows:

$$\begin{bmatrix} y1 \\ y2 \\ y3 \\ 1 \end{bmatrix} = \begin{bmatrix} q1 & 0 & 0 & 0 \\ 0 & q2 & 0 & 0 \\ 0 & 0 & q3 & 0 \\ 0 & 0 & 0 & 1 \end{bmatrix} \begin{bmatrix} x1 \\ x2 \\ x3 \\ 1 \end{bmatrix} \tag{3.5}$$

Where y_i represent the output (or image A), x_i represent the input (or image B), and q_i represent the scaling parameters along the x, y and z axes.

b. Affine (first order polynomial) transformation: It preserves straight lines and parallelism between lines (12 DOF):

i. Translation: 3D shifting (3 DOF).

ii. Rotation: 3D rotation (3 DOF).

iii. Rescaling (aspect ratio): independent scaling in the x, y and z direction (3 DOF) as shown in Fig. 3.5.

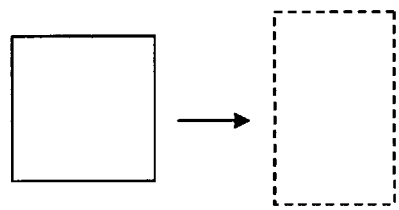

Fig. 3.5 Rescaling (aspect ratio).

iv. Shear (skew): (3 DOF) does not preserve angles and lengths as shown in Fig. 3.6.

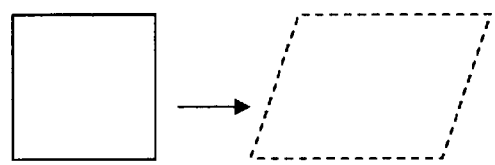

Fig. 3.6 Shear.

In matrix terms, it is represented as follows:

$$\begin{bmatrix} y1 \\ y2 \\ y3 \\ 1 \end{bmatrix} = \begin{bmatrix} 1 & q_1 & q_2 & 0 \\ 0 & 1 & q_3 & 0 \\ 0 & 0 & 1 & 0 \\ 0 & 0 & 0 & 1 \end{bmatrix} \begin{bmatrix} x1 \\ x2 \\ x3 \\ 1 \end{bmatrix} \tag{3.6}$$

Where y_i represent the output (or image A), x_i represent the input (or image B), and q_i represent the shearing parameters along the x, y and z axes.

c. Projective and perspective: preserves straight lines, but not parallelism as shown in Fig. 3.7 (projective: 2D/2D, perspective: 3D/2D).

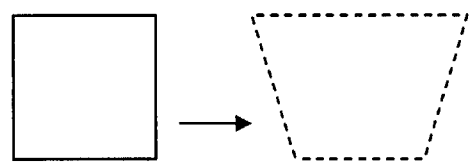

Fig. 3.7 Projective.

d. Non-linear warps (higher order polynomial, spline, curved or elastic): it preserves the topology of an image. This is the most general transformation which allows local deformation in the image, where each voxel can have 3 DOF leading to very large DOF for a typical volumetric data set. The bilinear transformation is the simplest polynomial transformation [75].

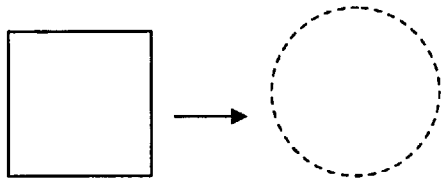

Fig. 3.8 Non-linear warps.

From above we can see that rigid transformations are a subset of affine, which is in turn a subset of projective and perspective, which are subsets of non-linear transformations. Therefore, rigid transformations are curved transformations with zero elasticity.

The type of transformation used to register images depends on the cause of the misalignment, which may or may not account for the variations between the images.

2. *Similarity measure:* This is a function which quantifies the similarity between two images using either the features derived from the data or the data themselves [49;60;67;68;72]. The choice of the similarity measure may highly influence the procedure robustness and accuracy. Some of these are listed below:

a. Correlation Methods:

I. Normalized Correlation coefficient (CC): based on the correlation over the set of all voxel pairs calculated. This

method is used when slight rotation and scaling is present [66;67;75].

II. Sequential similarity detection algorithm: by calculating the accumulated sum of absolute differences of the image intensity values and applying a threshold. It is a computationally simpler distance measure than the CC. It is less accurate than the CC but it is faster [66].

b. Ratio Image Uniformity (RIU) (Woods Function): based on the derived ratio image calculated from the two images. It maximizes the uniformity of this ratio, which is quantified as the normalized standard deviation of the voxels in the ratio image. It has recently been widely used for serial MR registration and is available in the AIR registration package from UCLA [63].

c. Mutual Information (MI): it is a measure of the dependency between two data sets and it's based on the entropy of the individual images and the joint entropy, which is defined by the correspondence between voxels. The MI methods have appeared recently and represent the leading technique in multimodal registration [49;66;67;75].

d. Least-squares: it is the sum of the squared difference of pixel intensities between the images. It is one of the simplest voxel similarity measures and is the optimum measure when two images only differ by Gaussian noise. It is widely used for serial MR registration [49;62-64;73;75].

e. Moments matching: by comparing the principal axes which can be derived from the moments of inertia of the objects. This method is used in registration problems that require no high accuracy because of the automatic and very fast nature of its use and easy implementation. It is used in the realignment of scintigraphic cardiac studies and as a coarse pre-registration in various other registration areas. [62;64;67;75].

f. Fourier methods: used when images are corrupted by frequency-dependent noise, if an acceleration of the computational speed is needed or if the images were acquired under varying conditions. It computes the cross-power spectrum of the images and looks for the location of the peak in its inverse [62;66;67;73].

g. Number of sign changes in the pointwise subtraction of the two images. Used when the images are dissimilar [73].

3. *Optimization:* The objective of optimisation is to determine a set of parameters for which some function is minimized (or maximized) by searching through the possible transformations [76]. It utilizes an iterative approach, in which an initial estimate of the transformation is gradually refined by trial and error. In each iteration, the current estimate of the transformation is used to calculate a similarity measure. The optimization algorithm then makes another (hopefully better) estimate of the transformation, evaluates the similarity measure again, and continues until the algorithm converges, at which point no transformation can be found that results in a better value of the similarity measure [63]. There are several mathematical optimization methods available.

To speed up the optimization process, a multi-resolution (pyramid) and multi-scale optimization methods are frequently used, where fast, but coarse techniques (low resolution image) are followed by an accurate, yet slow one (high resolution image) [67].

4. *Resampling:* where each image is resampled according to the spatial transformation estimated using an interpolation scheme [60]. This involves the extraction and interpolation of gray levels from pixel locations in the original distorted image and their relocation to the approximate matrix coordinate in the rectified (corrected) image as shown in Fig. 3.9. Interpolation of sampled data is the image transformation required for the

purpose of registration. It is the process of taking pixel values in one image (discrete matrix) and transforming them to a continuous image. In other words, it is a method used to estimate the gray values of an image at positions other than the grid points. Interpolation is often realized by convolving the image with an interpolation kernel. Errors in interpolation affect the value of the optimization cost function, which may lead to registration error. It is important to use an interpolation function that is appropriate to that nature of the image data. It is also important to note that there is always a trade-off between the demanded accuracy of the interpolation and the computational complexity.

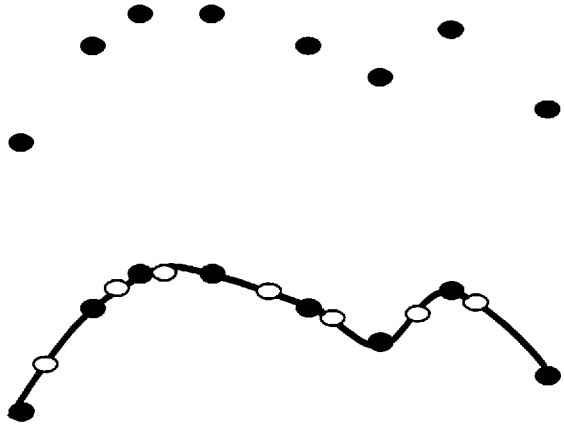

Fig. 3.9 Interpolation.

There are a number of interpolation functions available, each is used in accordance with the application [77]:

a. Nearest Neighbour Interpolation: This is the simplest method of interpolation where the output value equals to the value of the nearest data point. This method is easy to compute but is discontinuous midway between each pair of data points and may lead to inaccurate coregistration.

b. Linear interpolation: continuity can be improved by linear interpolation where each estimated pixel in the output image is a weighted combination with equal distance between 2 points with known values in the input image. It takes a little longer to compute and the slope is not continuous. Bilinear interpolation is a 2D piecewise extension of the linear interpolation.

c. Cubic interpolation: estimates the slope at each data point and then a cubic curve can be fitted in each interval between the data points. The slope is continuous, but at the expense of more computation. Cubic spline interpolation is another way to achieve slope continuity.

d. B-Spline Interpolation: uses a piecewise polynomial to provide a series of patches resulting in a surface that has continuous 1^{st} and 2^{nd} derivatives. It is a local interpolator, which can be exact or used to smooth surfaces. Bezier spline curves (attributed and

named after a French engineer, Pierre Bezier) are polynomial splines represented in terms of a different basis function.

e. Quadratic Interpolation: uses three known data points to estimate the unknown value of the output, based on a quadratic approximating polynomial, used for functions with large variations.

f. Sinc Interpolation [52;60]: This technique uses every voxel in the image to calculate the new value at a single voxel. It is computationally intensive and thus requires limitation leading to the truncated sinc function and the windowed sinc function.

g. Lagrange Interpolation: it is one of the best techniques for interpolating between values using polynomial fits. It is a way to pass a polynomial of degree N-1 through N points. It converges to sinc for large N [78].

h. Mitchell and Netravali's Method: Mitchell and Netravali developed a family of N=4 cubic filters. Their method partitioned the parameter space into regions characterizing artifacts like, blurring, ringing and anisotropy [77].

i. Gaussian Interpolation: This is a method developed by Appledorn which is both locally compact in the signal space and almost band limited in the frequency domain and, in addition, are easy to manipulate [77].

j. Newton Interpolation: interpolating curves with the Newton polynomials [77].

3.5 Misregistration

Even after the registration has been performed, images may still contain artefacts, which may affect the ability to detect regions of activation. It has also been noted that some standard motion correction methods may therefore induce spurious activations [79].

Some of the sources of artefacts are as follow:

1. Interpolation scheme used to resample realigned images leads to motion-correlated residual intensity errors [12;79].
2. The brain is not entirely rigid and images are prone to local deformations due to CSF motion, which lead to misregistration.
3. Aliasing due to gaps between the slices [12].
4. Ghosts in images. EPI is very sensitive to *N/2* Nyquist ghosts, where N represents the field of view [12].

5. Slices not being acquired simultaneously (do not obey rigid body rules of rigid body transformations) [12].
6. Spin excitation history effects [12;52;79].
7. Most registration methods do not account for spatial T2*-weighted signal loss due to changes in the main magnetic filed homogeneity near air/tissue for example (changes depending on spatial orientation) [80].
8. Low-frequency drifts in the voxel time-course in fMRI data sets are quite common [5].

When activation-related signal changes are very small, even slight misregistration will lead to significant artefacts after baseline subtraction. This leads to two types of errors summarized in Table 3.1 [81][38]:

I. Type-I error (False positive): is rejecting the null hypothesis when in fact it is true. An example is identifying a signal, which was not present. The probability of this type of error is known as α.
II. Type-II error (False negative): is accepting the null hypothesis when in fact it is false. An example is not identifying a signal, which was present. The probability of this type of error is known as β.

Statistical Decision	State of the null hypothesis	
	True	False
Reject Null Hypothesis	Type I error (False positive)	Correct
Accept Null Hypothesis	Correct	Type II error (False negative)

Table 3.1 Type-I and Type-II errors.

α and β risks are inter-related, as the decrease of one risk would cause the increase of the other and vice versa. α and β risks are also related to the size of the sample [82].

These errors raise concerns in relation to the reliability and repeatability of the registration process (pre-processing stage). The same person performing under identical experimental conditions may yield different measurements, or, different subjects performing under identical experimental conditions may yield similar measurements [3]. Statistical methods are usually used to process the acquired images. Due to the lack of a universally accepted statistical method to analyse fMRI data, the statistical methods used may be another factor contributing to these concerns. This leads to a need of some form of a quality control methodology, which performs comparisons between different activation detection methods for neuro-fMRI.

3.6 Validation of Motion Correction

It is highly desirable to provide an estimate of how accurate the registration actually is. There are two main reasons for that. The first is to ascertain whether the registration is good enough for a particular clinical application or for algorithm comparison. The second reason is for decision making in regards to patient management. The accuracy of a registration transformation cannot be summarized by a single number as it is spatially varying over the image [63].

There are different approaches to measuring the registration accuracy. One approach utilizes fiducial points, where the root mean square (RMS) distance is calculated between corresponding fiducials after registration and transformation [64]. Another approach is using a gold standard method, where the correct registration transformation is known and it is utilized for comparison purposes. Gold standards can be obtained using simulated data (images are often not very realistic), controlled phantom studies and invasive markers [63;67]. Due to the unrealistic nature of the gold standard calculations, registration accuracy can be obtained by measuring the consistency of the transformations. This is done by calculating the transformations for different images, then applying all the transformations one at a time in turn to complete a circuit. This will give the identity transformation. Due to the correlation between the errors, this approach will tend to underestimate the true error of the algorithm. An

alternative approach is to inspect the images visually but it is prone to the observer producing too many false negatives or false positives.

Medical image registration has attracted considerable research activity in devising and validating algorithms. Although, the accuracy of many schemes have been verified on synthetic data, the ultimate validation is still that the results are clinically useful and trusted. There is ongoing research in measures of accuracy studies [63;66;67].

3.7 Summary

Correction for subject motion is an important step in the analysis of fMRI time-series of the brain. This is because signal changes in correspondence to hemodynamic response to neural activity can be small compared to signal changes resulting from subject motion. This chapter presented the applications of image registration, the classification of registration techniques, registration steps, causes of misregistration and validation of the motion correction. The next chapter presents the post registration step of data analysis using statistical procedures.

Chapter 4

Statistical Procedures for fMRI

4.1 Introduction

In most fMRI setups, images are acquired during alternating task and control conditions. Changes in MRI signals due to brain activity are small compared to noise. Thus, statistical methods and signal averaging are frequently used to distinguish signals from noise in the data. The analysis of the image series is based on the computation of a statistical map and then the extraction of the statistical inferences from it [3;9;12;48;82].

Statistical methods for detecting and localising brain activation are divided into:

1. Non-parametric methods: These test the hypothesis with minimal assumptions and are thus less dependent on a specific statistical model. Often, independence of the samples is assumed [83]. Therefore, nonparametric methods are also

called *distribution free* because they make no assumptions about the frequency distributions of the variables being assessed. Non-parametric methods have an advantage over the parametric methods when the parametric assumptions are not correct [3]. The most widely used of these methods is the chi-square test, which tests whether the population medians are equal [84]. Other widely used nonparametric tests are: Kolmogorov-Smirnov test, Wicoxon rank sum test, median test and Spearman's rank correlation coefficient [47;85;86]. Randomisation/permutation test theory is one type of nonparametric test, and is most appropriate when the sample sizes are small, where it is less likely that the samples will follow the normal distribution. Randomisation/permutation test theory has been introduced by Holmes at al [87;88], and has been proposed for neuro-fMRI by Bullmore et al. [89]. The idea behind this method is simply that the data is exchangeable, if the temporal ordering of the data were to be irrelevant [90]. In other words, consider the data at a particular voxel where there is no difference between the two conditions ("rest" and "activation" conditions). In this case, the data would have arisen whatever the condition and, therefore, it is deemed exchangeable, and the labelling will be arbitrary. In this sense, the data is regarded as fixed and the experimental design as random. The null

hypothesis asserts that the distribution of the data for both conditions have the same mean, and hence are the same. The "mean difference" statistic is calculated for each labelling, which forms the permutation distribution. The distribution is then compared to a threshold and the *p*-value is calculated. For a test at given α level, the null hypothesis is rejected if the *p*-value is less than α, and it will be concluded that there is significant evidence against the null hypothesis of no activation at this voxel at level α [88].

2. Parametric methods: these dominate the current world of neuro-fMRI statistical procedures and are used when the data are normally distributed [60]. They are composed of two stages [11]:

    a. Application of a voxel by voxel time dependent analysis: This starts with the assumption that the data in the image can be accounted for by random noise fluctuations, which is known as the *null hypothesis*. Tests of the significance of the data against the hypothesis are performed. The voxels for which the test statistics exceed the threshold are then classified as active relative to the comparison made [91]. The voxel based

null hypothesis is generally implemented as a correlation measure.

b. A regional analysis of clusters: the significance of any data that fails the hypothesis is tested against observing a particular size of regions.

This approach is reasonably effective for a wide variety of testing methods, but a basic problem is choosing the threshold [91]. Some of the tests that are used are: Student's *t*-test, cross-correlation analysis, Fourier analysis, *z* maps, and receiver operating characteristic analysis (ROC) [81]. The most frequently occurring parametric statistical procedures in current neuro-fMRI use linear methods. The General Linear Model (GLM) is often used because it works well in a wide range of applied areas [53]. It is used to identify regions of grey matter that are significantly related to the particular effects under study. Following the application of the GLM, the significance of any differences is ascertained using the theory of Gaussian random fields [3;92].

3. Simulation methods: used to estimate the significance of data in problems that are otherwise intractable. They are dependent on adequate characterization and modelling of image noise. The number of simulations must be sufficiently high to determine the tails of probability distributions with high precision.

4.2 General Linear Model (GLM)

The General Linear Model (GLM) is a general framework that underlies most of the statistical analyses that are used in applied and social research and it is one of the most important tools in the statistical analysis of data. It is the foundation for the *t*-test, Analysis of Variance (ANOVA), Analysis of Covariance (ANCOVA), regression analysis and many of the multivariate methods including factor analysis, cluster analysis, multidimensional scaling, discriminant function analysis, canonical correlation and others. It is assumed that the fMRI time series is a well described convolution of a certain hemodynamic response function with an experimental design sequence, corrupted by Gaussian noise. Therefore, the problem of fMRI data analysis is reduced to the general linear statistic problem [47]. The GLM is based on two assumptions: a normal distribution of the data residuals and their independence of errors. GLM is used to make statistical inferences by performing univariate tests at each and every voxel to produce a so-called "statistical parametric map" [53]. It uses a statistical

procedure (*t*-test) to test the hypothesis that the data in the image are all due to random noise (with a predefined probability *p*-value). After fitting the model, the hypothesis is valid as long as the residuals are identical and normally distributed.

To explain mathematically [93], if we conduct an experiment, and we measure a response variable Y_j, where j represents the observation, and if each observation contains a set of variables x_{jk}, where k represents the variable index, then the general linear model can explain the variations in Y_j in terms of a linear combination of the variables x_{jk} plus an error term:

$$Y_j = x_{j1}\beta_1 + x_{j2}\beta_2 + .. + x_{jk}\beta_k + \varepsilon_j \qquad (4.1)$$

Where β_k are unknown parameters corresponding to each variable. The model is assumed to fit such that the errors, ε_j, are independent and identically distributed normal random variables with zero mean and variance σ^2.

The general linear model is also known as regression analysis, or more correctly "linear regression". The simplest example of the GLM is a linear regression against one variable, where only one variable x_j is measured for each observation. The model is thus written as follows:

$$Y_j = \mu + x_j\beta + \varepsilon_j \tag{4.2}$$

where μ is the Y intercept when $x = 0$ and β is the regression slope. ε is an error term that describes the vertical distance from the straight line to each point. It is termed an "error" because it is the degree to which the line is in error in describing each point [94].

4.3 The t-test

The *t*-test assesses whether the means of two groups are statistically different from each other. The difference is judged relative to the spread or variance of their scores. In essence, the *t*-test is normalizing the differences between brain scans in a voxel-by-voxel basis. The normalization causes the statistic to be identically behaved, everywhere in the context that there is no activation. The formula for the *t*-test is a ratio of the difference between the two means or averages (represented by x_1 and x_2) to the standard error of the difference as shown below. The standard error of the difference (variability of groups) is the square root of the sum of the variances (square of standard deviation) divided by the number of points in that group.

$$t = \frac{x_1 - x_2}{\sqrt{\frac{\mathrm{var}_1}{n_1} + \frac{\mathrm{var}_2}{n_2}}} \tag{4.3}$$

Where x_1 and x_2 are the means, var_1 and var_2 are the variances and n_1 and n_2 are the number of points in group 1 and group 2 respectively. Therefore, the t statistic is the least squares estimate of the slope, divided by a measure of the error of the slope, and is therefore an index of how far the slope differs from zero, given the error. Once the t value is computed, we need to set a risk level (α), which is the probability of getting a false positive. For statistical comparisons between two groups, a null hypothesis is tested. The null hypothesis is normally that there is no change anywhere in the brain. α is the probability of getting false positives even if the null hypothesis is true. The distribution of the t statistic is known, where each value for t corresponds to the probability of false positives when the null hypothesis is true (α or the uncorrected p-value). Statistical tables are available to test whether the t value is large enough to be significant i.e. that the difference between the groups is not likely to have been a chance finding. The threshold is calculated so that if no activation was present, then the maximum t statistic searched over a given brain volume would exceed that threshold with a probability of α. The t statistic is then compared to the threshold. If the t statistic was larger than the threshold, then activation at that point is declared statistically significant at level α [95;96].

How high should we set the t threshold to make sure that the remaining activations are indeed too high to be expected by chance? This is known as

the multiple comparison problem [96]. There are different methods to deal with this problem. One standard method for dealing with this problem is to use the Bonferroni correction. For the Bonferroni correction, one sets the *p*-value threshold for accepting the test as being significant as $\alpha / $ (number of tests), where α is the false positive rate you are prepared to accept. In most cases the Bonferroni threshold will be too conservative, because the Bonferroni correction assumes the independence of tests and it does not take into account the correlation of voxels with their neighbours. Random Field Theory (RFT) is one of such methods used to solve this problem. Once the *t* statistic is calculated, SPM transforms it to Z scores [83]. The Z scores are the numbers from the unit normal distribution (mean 0 and sd/variance 1) that would give the same *p* value as the *t* statistic. Once the *t* statistic has been converted into Z scores, the smoothness of Z is estimated by calculating the covariance matrix of the partial derivatives of Z. This requires the estimation of the covariance matrix of the partial derivatives of the errors, which is based on the residual fields (FSL uses an alternative smoothness estimator which is accurate for small spatial smoothness). The FWHM is then calculated for the observed smoothness, where FWHM is the width of the smoothing kernel at half the maximum of the height of the Gaussian [95;97]. The primary reason for smoothing is to increase the signal to noise ratio and to allow intersubject averaging by blurring differences between subjects [7;9]. The resels are then used to work out the expected Euler Characteristic (EC) of the image, when

thresholded at various levels of Z scores. The expected EC is the number of clusters in the image after it has been thresholded and it represents the probability of getting one or more clusters at that level of threshold (corrected *p*-value).

Most statistical packages for functional imaging data create statistical parametric maps. They are used to identify functionally specialized regions in the brain. Statistical parametric maps refer to image processes of a statistical parameter. These maps have a value for a certain statistic at each voxel in the brain, which is the result of the statistical test done on the scan data for that voxel. The *t*-test is one of such statistical tests which is used in the SPM package [2;94;98].

4.4 SPM

There are several public domain algorithms available for fMRI data analysis. SPM is a widely used algorithm package written in *Matlab*. It was developed originally by K. Friston [99;100], the methodology and the concept underlying the statistical parametric mapping are described and SPM was made available freely to the functional imaging community in 1991. SPM94 was the first major revision of the SPM software. SPM95, SPM96, SPM99 and SPM2 are based on SPM94, and represent the ongoing theoretical advances and technical improvements. SPM is now

being developed by the methodology group at the Wellcome Department of Cognitive Neurology at UCL.

SPM is based on the General Linear Method (GLM). SPM uses the general linear model to find task-specific, voxel-based differences in the magnitude of the BOLD signal. It applies the GLM to an fMRI time series and tests whether the activation evoked by the task is significantly greater than the activation at a base level [47]. The underlying similarity measure is the squared error term, or more specifically, the sum of the squared differences between images. GLM is used to estimate some parameters that could explain the data. The Gaussian Random Field Theory (RFT) is used to solve the multiple comparison problem that ensues when making inferences over a volume of the brain and takes into account the fact that neighbouring voxels are not independent. It provides a method for correcting *p*-values for the search volume of a SPM [101].

SPM examines every voxel location across all images and computes a parametric map containing a parameterised value at each voxel. The parameterised value is generally some form of a Student's *t*-test, which estimates the likelihood that a comparison of image groups matches a given model that explains their possible differences. The *t*-test is based on the signal change relative to the residual variance. The residual variance is computed from the sum of squared differences between the data and the

model to which it is fitted. Motion artefacts add to this residue and reduce the sensitivity of the test to true activations, therefore, realignment of the data is required prior to the statistical analysis [12]. The resulting statistical parameters are assembled into an image or a map – the statistical parametric map (SPM). In these maps, the statistical parameter represents the amplitude of the differential BOLD measurement relative to noise [6;101].

SPM99 is divided into three main sections:

1. Spatial pre-processing: This contains tools for realigning, slice timing, smoothing, coregistration, normalization, and segmentation.
2. Model specification and parameter estimation: This contains the buttons necessary for specifying the model which best describes the task, and then using that model to fit it to the data.
3. Results: Making inferences about those parameter estimates. Tools in this category display the statistical results of fitting the model to the data.

There is also a separate section that contains miscellaneous functions and utilities that are included with SPM.

4.4.1 Limitations of SPM

Despite its success statistical parametric mapping has a number of fundamental limitations.

1. The *p*-value ascribed to a particular effect is the probability of getting the observed data in the effect's absence. It cannot reject the alternative hypothesis (that the activation has not occurred).
2. The probability of an effect being zero is very small. Having thousands of scans entering some fixed-effect analyses of fMRI data will produce a significant effect at every voxel.
3. Correction or adjustment of *p*-value to resolve the multiple comparison problem. The threshold increases with the search volume which will affect the *p*-value, but the probability that any voxel has activated does not change with the search volume.

4.4.2 SPM99 vs. SPM2

SPM2 was released in May 2003. It has introduced some new features, which attempt to tackle some of the above-mentioned issues.

The focus of the comparison will cover improvements and the new functionalities introduced. Some of the main new features are:

1. Inference: Classical inference was used in SPM99. It uses the Gaussian Random Field theory to correct for the threshold. This approach is less sensitive or powerful with large search volumes because the probability that any voxel has activated does not change with the search volume and yet the *p*-value does. It is used to adjust the *p*-value to protect against false positives over the search volume, which is known as Family Wise Error Rate (FWER). It produces statistical parametric maps (SPM). It is the probability of getting the data, given no activation (the null hypothesis is true). The increase of the search volume induces a multiple comparison problem where correction or adjustment for the *p*-values is required. This causes the classical inference to become less sensitive or powerful [102]. SPM2 introduced Bayesian inference as well as the classical inference. In the Bayesian inference it uses the Empirical Bayesian Theory where the Bayesian estimation requires informative priors on the parameters. The posterior probability used in Bayesian inference is the probability distribution of the activation given the data [103]. The probability of activation at any voxel is the same regardless whether we're analysing that voxel or the whole volume and it does not need a *p*-value adjustment. It produces Posterior Probability Maps (PPM) [102]. In the Classical inference SPM2 introduced a new measure known as the False Discovery Rate (FDR) to correct for the *p*-values.

FWER vs. FDR:

Simultaneous testing of multiple hypotheses requires the setting of a threshold that would deem the activations too high to be expected by chance. This is achieved by using measures of specificity, which represent the probability of not detecting a signal when there is none (true inactive). SPM99 used a Family-Wise Error Rate (FWER) to correct for the threshold which is controlled by random field theories. Family-Wise Error Rate (FWER) is the standard measure of Type I errors in multiple testing [104]. It controls the chance of any false positive [91;105-107].

A new measure for correcting the threshold was introduced in SPM2, known as the False Discovery Rate (FDR). The False Discovery Rate (FDR) is a new approach for the multiple comparison problem. It controls the expected proportion of false positives among the suprathreshold voxels (rejected hypotheses that are false positives) [91;105-107].

$$\text{FDR} = \frac{\#\text{ of falsely rejected voxels}}{\#\text{ of rejected voxels in total}} \qquad (4.4)$$

So when we choose the *p*-value to be 0.05, for FWER this means that we are setting the probability of any false positive (one or more)

in the search volume to 5%, for FDR we will be setting the probability of false positives among the suprathreshold voxels to 5% (on average). The "On average" phrase guarantees that if the experiment is replicated many times, then the FDR over those replications would be no bigger than 5%, but for any particular data analysis, the actual FDR might be larger than 5% [91;108].

FDR is a more lenient measure of false positives. It cannot draw definitive conclusions about the extent of the effect, but we are protected against false negatives claims where there is no activation whatsoever.

From a practical point of view, the FWER is very conservative compared to FDR. Results obtained with FWER will have less activation than those obtained by FDR. If we have results significant at a FWER corrected threshold, we have very strong evidence of our effect. On the other hand, if we find results significant with FDR, but not with FWER, we also have evidence of our effect, but not as strong as with a FWER threshold. FWER tends to have more Type-II errors (false negatives – signal loss), while FDR tends to have more Type-I errors (false positives – more activation) [108].

Note: the *p*-value chosen by the user during data analysis which is used to control either FWER or FDR, is referred to differently in the

publications. In FWER, the p-value supplied by the user is known as α which is used subsequently to calculate the *p*-value ($p = \alpha$ / # of tests). In FDR, the *p*-value supplied by the user is known as *q*, which is used subsequently to calculate the *p*-value [91].

2. Similarity Measure: SPM99 uses an ordinary least square method. It estimates the parameters that would minimize the sum of squares of the residuals. SPM2 uses weighted least square method. It estimates the parameters that would minimize the weighted sum of the squares of the residuals [109].

3. Dynamic causal modelling (DCM): enables inferences about interregional coupling (connection strength) by viewing all measured brain responses as evoked by experiment design. (e.g. how attention increases or decreases the effective connectivity from posterior parietal cortex to V5) [109].

4. Hemodynamic modeling: enables inferences about a single voxel or region to be drawn [109].

5. Hemodynamic Deconvolution: deconvolves the observed fMRI time-series to estimate the underlying neural response [109].

6. Image orientation: SPM99 analyzes data using a left-handed coordinate system where some of the images may appear flipped. SPM2 analyses data using either system (left-handed or right-handed) in accordance with the handedness of the images [109].

7. Temporal autocorrelation: The GLM can be used to explain fMRI data sets as a linear combination of a set of variables plus an error term. Rewriting equation (4.1) as a matrix:

$$\mathbf{Y} = \mathbf{X}\beta + \varepsilon \tag{4.5}$$

Where $\boldsymbol{Y}$ is the fMRI time-series (observed pixel values). $\boldsymbol{X}$ is the design matrix which represents the BOLD response arising from a neural cause. β is a vector of parameters, the magnitude of which would provide information regarding the presence or absence of activation, and ε is the error [97;110-112].

fMRI data is contaminated with artefacts, causing the residuals of an fMRI analysis to be temporally auto-correlated. The artefacts stem primarily from low-frequency drifts due to hardware instabilities, temporally aliased cardiac pulsation and respiratory sources, un-modelled neuronal activity and residual motion artefacts not accounted for by rigid body registration methods [111;112].

There are three typical approaches to finding β. The first method assumes the independence of errors and uses the usual least squares estimate as shown below:

$$\beta = (\mathbf{X}'\mathbf{X})^{-1}\mathbf{X}'\mathbf{Y} \tag{4.6}$$

Where $(\mathbf{X}'\mathbf{X})^{-1}\mathbf{X}'$ is the pseudo-inverse of X. If error autocorrelation is ignored, it will lead to under-estimation of the variance and an overestimation of the significance leading to too many false positives [110]. The other two approaches, pre-whitening and pre-colouring account for dependent errors, where their estimates can be written as:

$$\beta = ((\mathbf{KX})'\mathbf{KX})^{-1}(\mathbf{KX})'\mathbf{KY} \tag{4.7}$$

Where $\boldsymbol{K}$ is the (de)correlating matrix. In pre-whitening, $\boldsymbol{K}$ is chosen such that $\mathbf{KVK}'$ is the identity matrix, where $\boldsymbol{V}$ is the correlation matrix of the errors. In pre-colouring, $\boldsymbol{K}$ is chosen such that $\mathbf{KVK}' \approx \mathbf{KK}'$ [110].

SPM 99 uses a pre-colouring approach: by temporal blurring and smoothing the data, this will cause more dependence but the form of dependence induced will be known. Assume the intrinsic

autocorrelation is negligible compared to smoothing. Then correct the GLM inferences based on the known autocorrelation [1].

SPM2 (and FSL) uses a pre-whitening approach: if we know the autocorrelation exactly then we can undo the dependence by de-correlating the data and the model then proceed as with the independent data. Obtaining accurate estimates of the autocorrelation is a problem and requires some regularisation (spatial smoothing) [1].

The table below provides a summary of the above discussion.

	Advantage	Disadvantage	Software
Independent	Simple	Inflated significance	All
Pre-colouring	Avoids autocorrelation estimates	Statistically inefficient	SPM99
Pre-whitening	Statistically optimal for series characterised by autocorrelation functions	Requires precise autocorrelation estimates	FSL, SPM2

Table 4.1 Table of summary adapted from Nichols [1].

4.5 Reproducibility of fMRI

Image analysis in fMRI activation studies is used mainly to detect and delineate the image areas that have a signal intensity time course, which can be related to the experimental parameters. Statistical parametric maps (SPM) are created where either a non-active or active is assigned to each voxel [83]. The use of fMRI technique for cognitive and clinical purposes requires reliable results [113;114]. Variability often exists in the magnitude, spatial distribution and statistical significance of the resulting fMRI maps due to differences in equipment, and other site-specific differences [115]. Reproducibility and comparability studies of these activation patterns in the brain are required to provide confidence in the results obtained. They need to provide a measure of how well an experimental result can be reproduced in different sessions [47]. Reliable results are required for within single subjects measured at different times, for comparisons between subjects or patients as well as for diagnostic examinations [113].

There have been some Multi-Institutional studies to evaluate the effects of factors such as subject, study site, filed strength, vendor, k-space, visit and repeated run on the fMRI reproducibility. Some have found a significant variability between subjects, less variability in 3T and 4T compared to 1.5T and some variability across runs [115]. While others observed the same general findings across sites regardless of differences in image acquisitions and analytic tools used, suggesting a strong evidence of reproducibility,

reliability and comparability of results [114]. Other studies investigated the reproducibility of activation patterns obtained using 4 Tesla and compared it with 1.5 Tesla systems and found that the reproducibility is dependent on region and subject and better than at 1.5 T [116]. Some studies also found that the reproducibility results are not the same for all activated areas in the brain and that there is a substantial variation in the volume of activation [117]. Other studies investigated the use of contextual information in the detection of fMRI activations and found it to be the most reproducible method in comparison to other methods (i.e. Bonferroni) [83].

More studies are required for an insight into reproducibility of fMRI measurements and especially in confounding factors and improved task design [117].

4.6 Summary

fMRI statistical procedures were discussed, presenting the basic concepts of the linear general model, the *t*-test, a detailed description of SPM99 and its updates in SPM2, and a review of the reproducibility of fMRI. The next chapter will describe the data sets used, the methods utilized in the analysis, the actual investigations of the data sets using the methods described, and the results of these investigations.

Chapter 5

Methods

5.1 Introduction

This chapter begins with a description of the experimental design and data acquisition, followed by a description of the data sets used in the analysis. The data sets cover the somatosensory motor cortex as well as the visual cortex. It then describes the analysis methods utilized in this work (SPM99, SPM2, AIR and the correlation method). It also contains a description of the analysis methods using histograms and empirical methods utilised in the normality study and an explanation of the HRF deconvolution method used in the extraction of HRF signals.

5.2 Experimental Design and Data Acquisition

Due to the low signal-to-noise ratio, subjects usually perform two or more very different tasks. The simplest are simple activation experiments comparing an activation condition with a rest condition, which alternate periodically [90]. Paradigm design is an important issue in the practical application of MRI to mapping brain function. It needs to be investigated as often even minor changes in the stimulus presentation may qualitatively alter the results by implicitly changing the original question. For example, doubts have been raised in regards to whether the use of the neuropsychological test protocol is a good representation of the original scientific question into an MRI-compatible paradigm [29].

5.2.1 Summary of Data

There are 3 data sets used in the analysis:

1. (Data Set 1): The first set is performed on a single healthy experienced right-handed male subject of 42 years old, repeated in 14 sessions. It was a right hand finger tapping experiment. The experiment was self-paced right-hand tapping at a rate of 2.5 taps per second. Auditory instructions of the On-Off pattern of the task was received via the scanner head phones. The tapping was random and non directed. The data were acquired using a Siemens 1.5 T Vision scanner using Numaris v33B and

a Circularly Polarised (CP) coil head. The data used were BOLD EPI fMRI multi-slice images of 128x128 pixels from a single subject, each volumetric data set is composed of 10 slices and each session is composed of 35 volumes (the first 5 volumes were discarded from the analysis to avoid T_1 effects in the initial scans), voxel size (2mm x 2mm x 5mm). TR (interscan interval) = 6 seconds, TE (echo time) = 54ms, FOV of 240 mm, and the slice thickness was 5mm. Slices were aligned with the AC-PC (anterior commissure - posterior commissure) line. The task was a right-hand tapping at a rate of 2.5 taps per second. The tapping followed an off-on pattern (Boxcar function) for 5 volumes each as shown in Fig. 5.1. The boxcar is structured so that it has a unit magnitude throughout the performance of the task and zero amplitude during periods of rest.

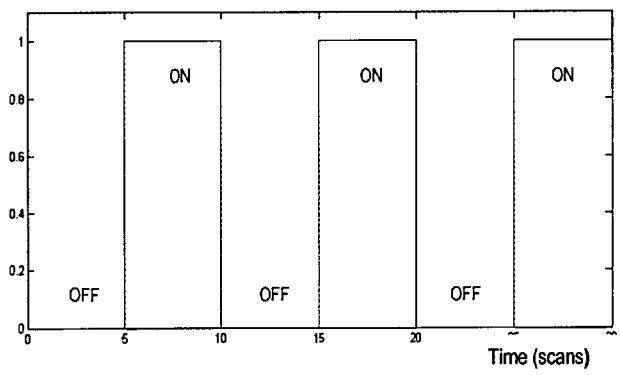

On: indicates the Patient is engaged in finger tapping.
Off: indicates no voluntary motion.

Fig. 5.1 On-Off (boxcar Function).

2. (Data Set 2): Set two is a visual experiment with a full-field flickering chequerboard chosen to evoke the occipital activation and acquired using a 1.5T scanner with a Circularly Polarised (CP) head coil. The visual stimulation was presented to the subjects via a projector set-up at the back of the magnet bore. The stimulus flashed at a frequency of 7 Hz. The data acquired used were BOLD EPI fMRI images of 128x128 pixels from 4 subjects (2 male and 2 female, 2 albino and 2 healthy), each volumetric data set is composed of 12 slices and each session is composed of 84 volumes. The slices were aligned parallel to calcarine fissue and did not cover the whole brain, but only the primary visual cortex. TR (interscan interval) = 3 seconds, TE (echo time) = 54ms, FOV of 240 mm, pixel size 1.88mm x 1.88mm, and the slice thickness was 4mm. The experiment followed an off-on pattern (Boxcar function) for 6 volumes each.

3. (Data Set 3): The third set is also a visual experiment acquired using a Siemens Trio 3T scanner with 8 channel head array coil. The stimulus was a common flashing chequerboard created in *matlab*. It was a circular stimulus measuring 10cm in diameter and flashed at a frequency of 7 Hz. The stimulus comprised of an equal number of segments of two different shades of grey. The contrast between the two shades was user defined with the

maximum contrast being when the two tones were black and white respectively. The contrast was based on a sinusoidal waveform, with black being the peak of the waveform and white the trough. The visual stimulation was presented to the subjects via a projector set-up at the back of the magnet bore. The data used were BOLD EPI fMRI images of 128x128 pixels from 5 subjects, each volumetric data set is composed of 22 slices and each session is composed of 84 volumes. Slices were aligned with the AC-PC (anterior commissure - posterior commissure) line. TR (interscan interval) = 3 seconds, TE (echo time) = 54ms, FOV of 240 mm, pixel size of 1.88mm x 1.88mm, and the slice thickness was 4mm. The experiment followed an off-on pattern (Boxcar function) for 7 volumes each. The blocks of stimulus and rest were repeated 6 times, resulting in 84 measurements being acquired. This data was acquired with two contrasts, 100% and 10% contrast, evoking two different levels of activation.

5.3 Data Analysis Methods

The basic objective in the analysis of functional imaging experiments is to identify voxels that show signal changes that vary with changing brain states of interest across the serially acquired images [7]. We have

compared results obtained using SPM99 and SPM2 with the correlation method based on a simple inner product, where the lengths of a template and the time series extended from one voxel are normalized to unity. The purpose of this is to rapidly be able to alter the predicted activation function, to automatically generate results and to permit automatic HRF extraction. We also studied the effect of the realignment process on activation. We used both SPM and AIR for the realignment process, and used the correlation method to identify areas of activation. A comparison study of the effect of the realignment process on the activation results has then been performed.

5.3.1 SPM99 and SPM2

Chapter 4 contained a detailed description of SPM including a comparison between SPM99 and SPM2.

The data is required to undergo a series of pre-processing steps prior to the analysis. The pre-processing step for SPM99 comprised of three stages as summarized in Table 5.1. The data were first realigned to correct for subject movement and this created output *r*files*, then the realigned data were normalized to a standard space using a modified SPM EPI template and this created *nr** output files. The normalization process is required to account for differences in individual anatomy, but is also applied to single-

subject experiments to allow localization in the standard reference frame [90]. Finally, the *nr** data were smoothed using a smoothing kernel to suppress unwanted high frequency noise and enhancing low frequency signal, this created *snr** output files.

Step	Input	Output
Registration	*.img	1. r*.img,hdr 2. meanoriginalimage.img,hdr (if chosen) 3.realignment_params_*original image.txt 4. spm99.ps
Normalization	1. meanoriginalimage.img 2. r*.img	1. nr*.img,hdr 2. nmeanoriginalimage.img,hdr 3. meanoriginalimage_sn3d.mat 4. spm99.ps
Smoothing	nr*.img	snr*.img,hdr

Table 5.1 Pre-processing steps in SPM99. The left column identifies the step in the processing, the middle column identifies the input files generated on and the right column identifies the output files generated.

The second step was to specify a model, which described the task by convolving the boxcar function with the hemodynamic response function (HRF) to give a function shown in Fig. 5.2. This function mimics the paradigm or stimulation protocol. It represents the ideal brain activation expected and it is the model to be used for fitting the data [29].

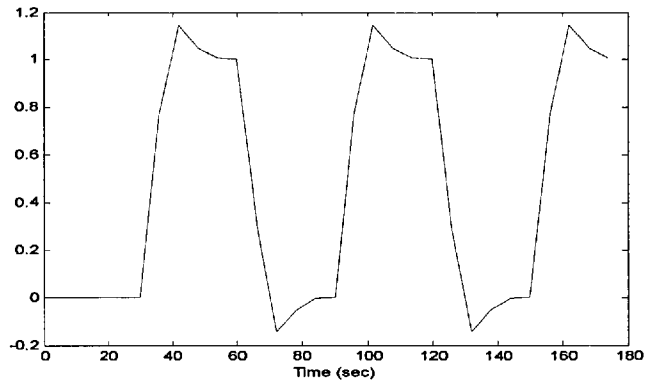

Fig. 5.2 Boxcar function convolved with HRF. We refer to this as the predicted activation signal **μ(n)**.

Then, the specified model was used to fit to the data. SPM99 uses the least square method as a similarity measure. The threshold was chosen to give a *p*-value of 0.001 (the probability of identifying a significant region by chance is 0.001). The activated areas were then displayed, superimposed on a "glass brain" and superimposed in colour on the mean volume.

The pre-processing stage for SPM2 produces the following files shown in Table 5.2:

Step	Input	Output
Registration	*.img	1. r*.img,hdr 2. meanoriginalimage.img,hdr (if chosen) 3. rp_*original image.txt 4. spm2.ps
Normalization	1. meanoriginalimage.img 2. r*.img	1. wr*.img,hdr 2. meanoriginalimage.img,hdr 3. eanoriginalimage_sn3d.mat 4. spm2.ps
Smoothing	wr*.img	swr*.img,hdr

Table 5.2 Pre-processing steps in SPM2. The left column identifies the step in the processing, the middle column identifies the input files generated on and the right column identifies the output files generated.

5.3.2 Automated Image Registration (AIR)

AIR is a registration package developed by the Laboratory of NeuroImaging at the University of California, Los Angeles. It is designed for performing both intra-modality and inter-modality, intra-subject registration. It also performs inter-subject registration such as registering scans of pairs of subjects to each other or registering subjects to atlas template.

The version of the package used is AIR 5.2.5 which was downloaded from the AIR webpage[1]. The software is written in ANSI C [118] and accepts images of the ANALYZE format developed by the Biomedical Imaging Resource at the Mayo Clinic. For each ANALYZE image there are two files associated, a header file (.hdr) and an image file (.img). The header file contains information about the image xyz dimensions, image xyz voxel size, the global maximum and minimum of the image and the size of the header file. The image file is a simple raw data file. It consists of the intensity values of the entire 3D volume saved row by row, plane by plane. The package supports 8 bit and 16 bit images.

5.3.3 Correlation Method

The algorithms of the correlation method are presented in Appendix B. The amount and location of activation detected depends on the reference function chosen. The alternative method uses the inner product as the similarity measure[2]. It is equivalent to the correlation coefficient of two de-meaned signals described by Bandettini et al. [119]. The inner product involves normalizing the lengths of the signals (after removing the means), and the angle between them gives a scaled measure of how close or similar the two signals are in accordance to the following equation:

[1] http://bishopw.loni.ucla.edu/AIR5/
[2] The similarity measure is not a cross correlation, as the cross correlation has a shift. It is a normed inner product.

$$\cos(\theta) = \frac{< x, y >}{\| x \|_2 \| y \|_2} \tag{5.1}$$

Where <x,y> denotes the inner product of x and y, and $||x||_2$ and $||y||_2$ denote the 2-norm of x and y. x represent the trace of voxel values across the volume (time-series) and y represents the model used to fit the data. The value of θ ranges between 0 degrees (good match of signals) and 90 degrees (no match of the signals).

We analysed the data without any pre-processing (realignment) as we have compared results obtained after realignment and found them to be almost identical. We also removed the mean of the data and the template. The same model was used as that in SPM. Changes in the signal were detected by thresholding the signal of the resting state image. The threshold was chosen to give the required p-value in accordance with the following equation [119]:

$$p = 1 - \frac{2}{\pi^{1/2}} \int_0^{TH\sqrt{N/2}} e^{-t^2} dt \tag{5.2}$$

Where N is the number of degrees of freedom and TH is the threshold.

5.4 Methods of Analysis using Histograms

The test of the normality is an important part of the analysis because it is crucial to the inference of SPM. We would also like to investigate the possibility of developing a measure of normality as an indication of the activity/non-activity of the voxels, where active areas show patterns that deviate from normality compared to non-active areas. Subsets of data were chosen from each data set. It included active areas, background out of brain areas, white matter areas and grey matter areas. The subsets were then analysed using a *Matlab* script (Appendix A). The analysis begins with calculating the mean signal of all active voxels within the subset.

$$\text{Mean across all voxels within the subset} = \frac{\sum(i_{xyz})}{N} \qquad (5.3)$$

Where i is the intensity at positions x, y and z for each voxel, and N is the total number of voxels. The mean signal is then subtracted from the signal at each voxel.

$$I_{xyz} = i_{xyz} - \text{mean} \qquad (5.4)$$

The mean of the resultant signals (I_{xyz}) is calculated (as well as the minimum and maximum signals).

$$\text{Mean of } I_{xyz} = \frac{\sum(I_{xyz})}{N} \tag{5.5}$$

A histogram representing the difference between the signal at that region and the mean signal is then produced. The difference was then analysed using the K-S test in *SPSS*® package to check for the normality of the signal distribution and a comparison table was produced.

5.5 HRF Deconvolution

The effect of the variations of the hemodynamic response function on the activation was investigated. This was achieved by comparing the activations obtained using SPM HRF and the ones obtained using the mean extracted HRF. The HRF signal was retrieved from the activation signal by deconvolving it with the boxcar signal. This process was then automated as described below:

After the design matrix has been formulated, the boxcar signal is derived from SPM in the form of a periodic square waveform, $f_B(n)$ of length N. This waveform is then analysed to find the fundamental frequency, a process which obviates the need to re-enter parameters pertaining to the design matrix in the subsequent analysis. It also leaves the route open for later work on deriving the fundamental harmonic from activation data itself.

The process is then as follows:

Compute the DFT of $f_B(n)$ using

$$F_B(k) = \sum_{n=0}^{N-1} f_B(n) e^{2\pi jkn/N} \tag{5.6}$$

Find the bin number at which $F_B(k)$ takes a maximum value

$$k_0 = \arg\max_{k\in[1,N/2-1]} \left\{ \left| F_B(k) \right| \right\} \tag{5.7}$$

From this, an initial signal with the shape of a course-resolutioned skewed discrete triangular function, $\boldsymbol{h_0}$ is defined, with a width equal to k_0. This serves only to initialise the candidate HRF. An example of the initial function is illustrated in Figure 5.3 below.

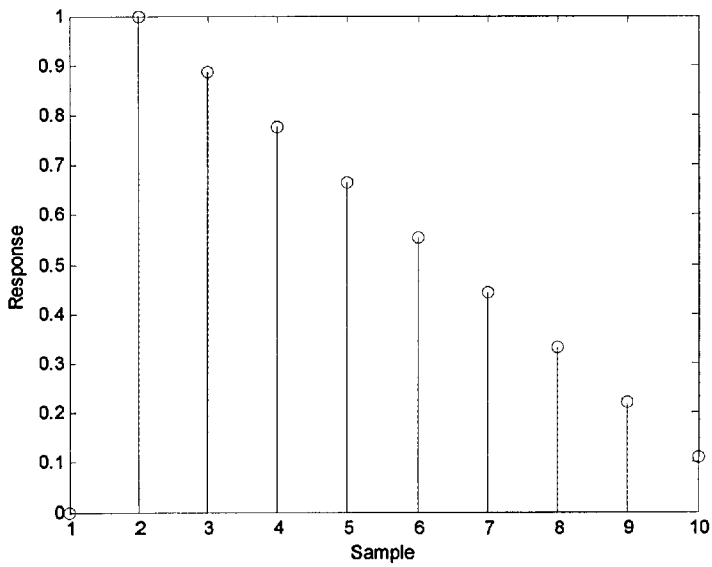

Fig. 5.3 Initial function used to initialise the candidate HRF.

$$\rho_{RS} = \frac{\left\| \mathbf{f}_e(n) - \langle f_e(n) \rangle_n \right\|_2^2}{\left\| \mathbf{f}_s(n) - \langle f_s(n) \rangle_n \right\|_2^2} \tag{5.8}$$

This k_0 dimensional vector is then placed into an optimisation routine to find the estimate of HRF that minimises the residual between the predicted activation and the measured activation, subject to a penalty term that enforces smoothness on the HRF:

$$\mathbf{h}_c = \mathbf{h}_0 \tag{5.9}$$

$$\mathbf{h}_c^{\text{est}} = \arg\min_{\mathbf{h}_c} \left\{ \left\| \mathbf{f}_s(n) - \mathbf{f}_B \otimes \mathbf{h}_c \right\|^2 + \frac{1}{2} \left\| \nabla \mathbf{h}_c \right\|_2^2 \right\} \tag{5.10}$$

And where $\otimes$ denotes convolution between vectors. ∇ denotes the discrete first order derivative along the elements of the vector (discrete time) *not* a derivative in k_0 dimensional space.

$$\rho_{RS} = \frac{\text{Residual Signal Deviation Energy}}{\text{Signal Variation Energy}} = \frac{\left\| \mathbf{f}_e - \langle \mathbf{f}_e \rangle_n \right\|_2^2}{\left\| \mathbf{f}_s - \langle \mathbf{f}_s \rangle_n \right\|_2^2} \tag{5.11}$$

And where

$$\langle \mathbf{x} \rangle_n = \frac{1}{N} \sum_{i=0}^{N-1} \mathrm{x(n)} \qquad (5.12)$$

and $\| \cdot \|_2$ denotes the 2-norm.

Note that we do not use the more common term "variance" although variance is often (**incorrectly**) used in this context. Nevertheless, the closer the ratio ρ_{RS} to 0, the smaller the residual energy is, and therefore the closer the result of the predicted activation to the true activation signal.

The pseudo code for the above mentioned process is as follows:

- Load "activation signal".
- Load "boxcar signal".
- Calculate the length of one period of the "boxcar signal".
- A *candidate_hrf* signal is first set to equal zeros with at most the length of one period of the boxcar signal.
- A subroutine is used to convolve the *candidate_hrf* signal with the "boxcar signal" to give a "predicted signal".
- *fminsearch* is a search tool used within the script to do the following:

    1. The "predicted signal" is compared to the "target signal" (activation signal) by finding the difference between the two signals.
    2. The residual consists of: the difference between the

signals, and a penalty term used to smooth the *hrf* signal.

3. The residual is used to adjust the *candidate_hrf* signal.
4. The process (1 to 3) is repeated until the difference between the two signals is minimized.
5. End;

- The calculated *hrf* (with minimum residual) is convolved with the "boxcar signal" to give the "predicted activation signal".
- Calculate the residual between the "predicted activation signal" and the "target signal".
- Calculate ratio of energy of the residual to the energy of the original activity pattern.
- End;

5.6 Summary

This chapter presented a description of the experimental design and the data acquisition. It also presented a description of the data sets used in the analysis, which comprised somatosensory motor cortex data as well as some visual cortex data. A description of the methods utilized in the investigation (SPM99, SPM2, AIR and the correlation method) were also explained in detail. Histograms utilised in the normality study were described as well as an explanation of the HRF deconvolution method used in the extraction of HRF signals.

Chapter 6

Registration and Reproducibility

6.1 Introduction

Reproducibility and comparability studies of activation patterns in the brain are required to provide confidence in the results obtained. This study investigates the reproducibility of activation patterns obtained using SPM99, SPM2, AIR and the correlation method. The effect of FWER and FDR was also investigated. A normality study was also conducted to investigate the possibility of developing a measure of normality as an indication of the activity/non-activity of the voxels.

6.2 Standard Measures of Reproducibility

The reproducibility of fMRI was discussed in detail in section 4.5. A standard analysis of data using SPM involves finding the total number of active voxels, the strength of the BOLD signal and the position. The following is an analysis of Data Set 1.

6.2.1 SPM Results

Data Set 1 (week 16) was first analysed using SPM99 (SPM parameters are in Appendix C) The first five sets of data were discarded from each session to avoid the T1 effects in the initial scans and to ensure that the magnetization is in a steady state for accurate alignment [8]. After the pre-processing steps of realignment, normalization and smoothing, a model is specified and is fitted to the data with a predefined probability value (*p*-value).

The results show activations in the sensorimotor cortex. The activated areas were then displayed, superimposed on a "glass brain" and superimposed in colour on the mean volume as shown in Fig. 6.1.

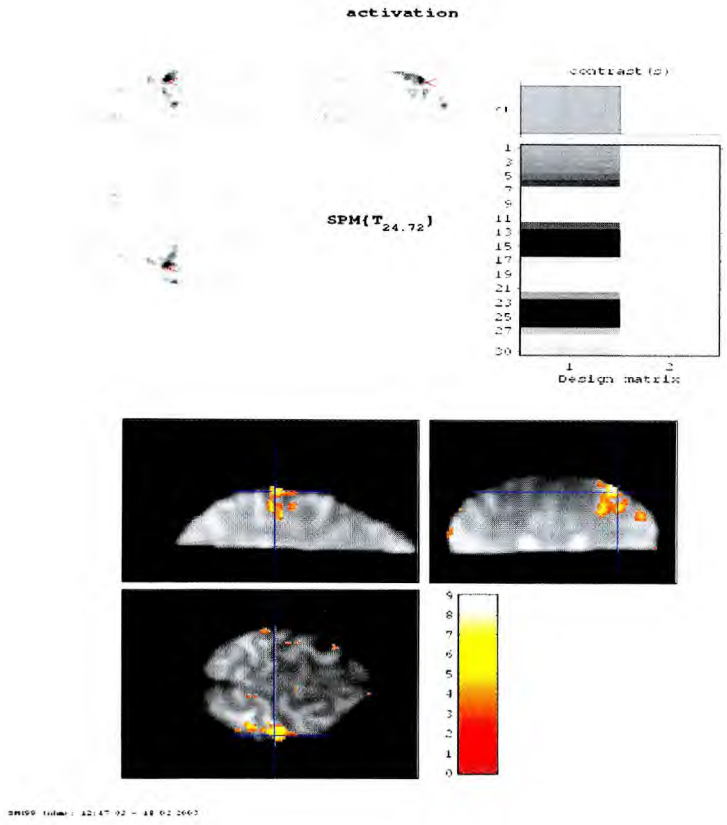

Fig. 6.1 SPM99 Results with a *p*-value of 0.001.

The data on the "glass brain" is the collapsed data in a single plane. The cross-hair indicates the current location relative to the Anterior Commisure (AC). The bar-graph on the right is a graphical representation of the contrast, or pattern of on-off signal. It is known as the design matrix and embodies any non-random and measurable factor that can affect the image intensity [9]. Variations within each dark or light bar are due to the HRF, where the most negative number in the column will be nearest to black and

the most positive will be nearest to white. The grey box at the upper right indicates the particular contrast we're looking at. The image at the bottom of Fig. 6.1 shows single sagittal, coronal, and axial planes with SPM activations overlaid on the mean volume. The colour bar to the right shows the corresponding *t*-value for a particular colour. Activations on brain are voxels that have statistical parameters greater than a given statistical threshold.

The same data (Data Set 1: week 16) were then analysed using SPM2 (SPM parameters are in Appendix C). After fitting the model to the data, the results show the activated areas superimposed on a "glass brain" as displayed below in Fig. 6.2:

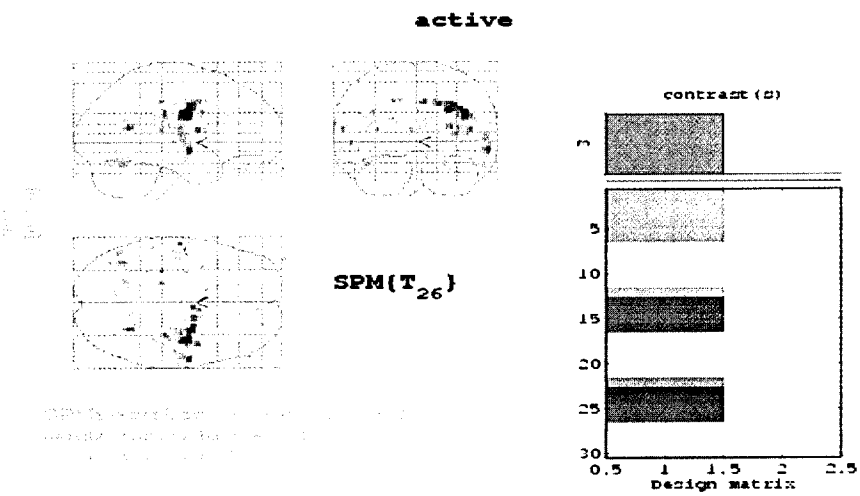

Fig. 6.2 SPM2 activation superimposed on glass brain with *p*-value of 0.001.

6.2.2 Correlation Method Result

The same data (data Set 1: week 16) were then analysed using the correlation method.

The result of the analysis is shown in Fig. 6.3, where we can see the activation areas superimposed on the mean volume (10 slices).

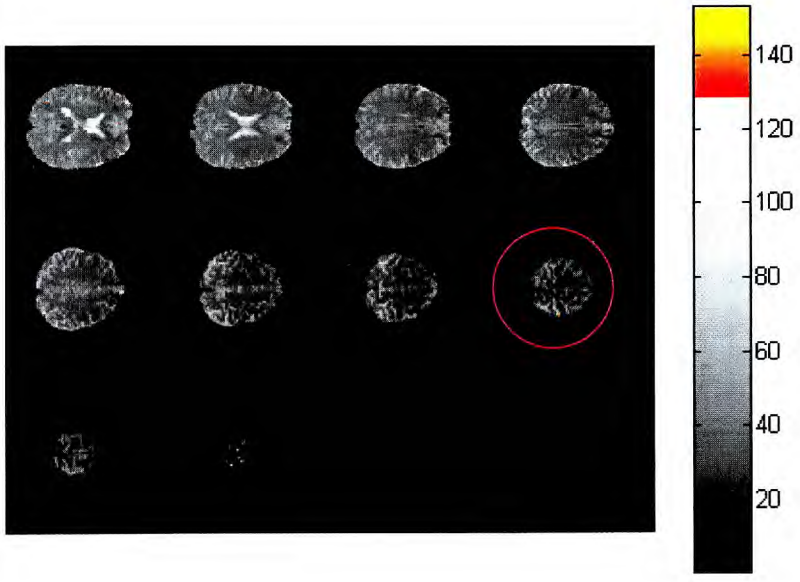

Fig. 6.3 correlation method results with a *p*-value of 0.001. Slices 1-10 are displayed from top left to bottom right. The circled scan (8) is magnified in Fig. 6.4.

We can investigate the activation area in one particular slice. In Fig. 6.4, we have magnified the 8th slice. The activation cluster is composed of 8 voxels.

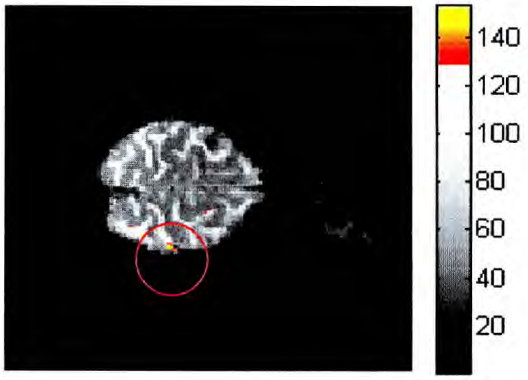

Fig. 6.4 Activation in slice 8 using the correlation method. (The colour overlay represents the activated area).

We trace the signal at each voxel across the data acquisitions and plot it alongside the fitted model. Fig. 6.5 shows the plot at voxel (52,44), we can see that the shape of the model fits the shape of the signal very well. Note that both the actual data ($\mathbf{f}_s$) and the template ($\boldsymbol{\mu}$) are normalized to have unit "length": i.e. (see chapter 5, page 110)

$$|| \mathbf{f}_s ||_2 = 1$$

And $$|| \boldsymbol{\mu} ||_2 = 1$$

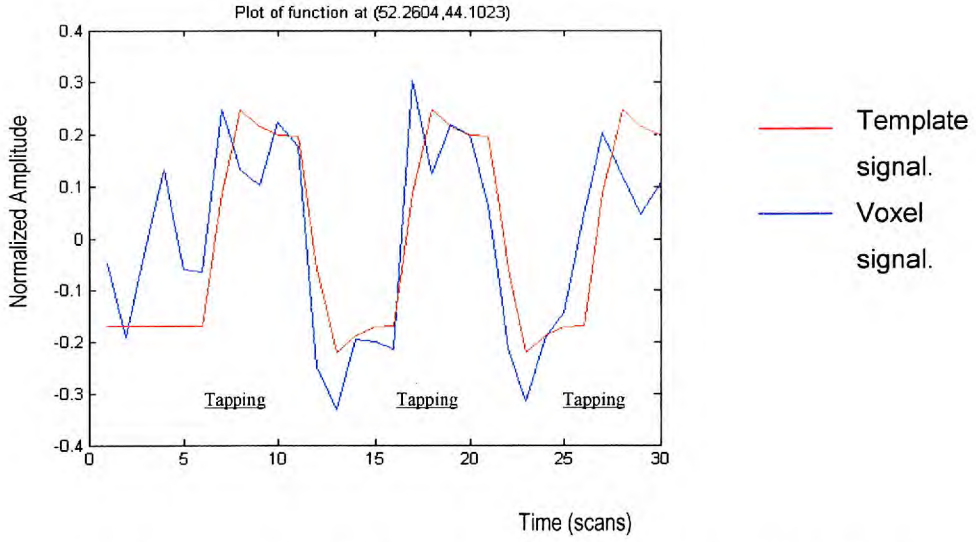

Fig. 6.5 Intensity at each voxel across time at one point in space.

The next step was to investigate the amplitude of the signal at each voxel within the cluster (temporal mean subtracted) as shown in Fig. 6.6.

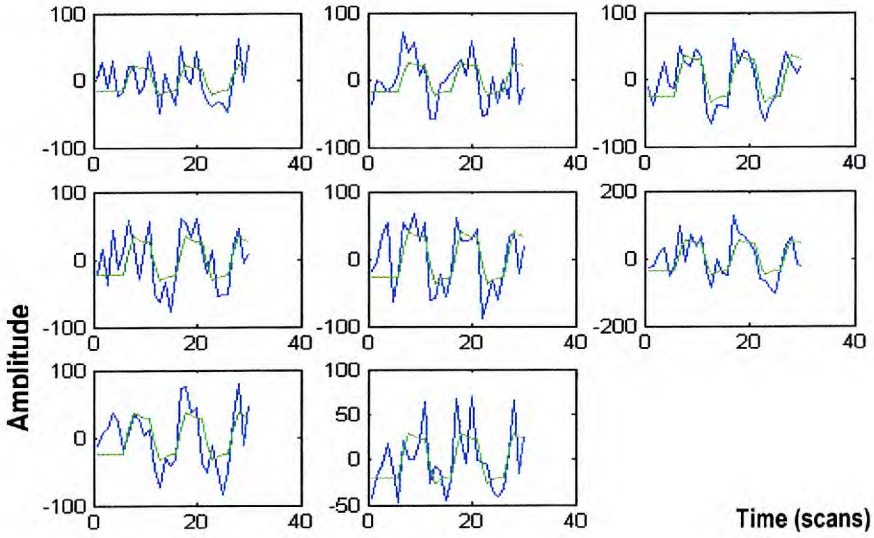

Fig. 6.6 Signal amplitude at each voxel across the volumes.

Table 6.1 below summarises the results of the analysis (percentage of activation) using SPM99, SPM2 and the correlation method.

	SPM99	SPM2	Correlation method
Realigned Data	2.3%	2.6%	0.26%

Table 6.1 Percentage of activation results for the finger tapping data (Data Set 1) with *p*-value of 0.001.

We found that there is more activation in SPM2 and in SPM99 in comparison to the correlation method. The percentage of the active voxels was found to be 2.6% in SPM2 and 2.3% in SPM99 and it was found to be 0.26% in the correlation method.

The analysis was repeated with a 4 subject visual data set (Data Set 2) (128x128x12x84). The results are shown in the Table 6.2 below.

	SPM99	SPM2	Correlation method
Subject 1	0.04%	0.09%	0.11%
Subject 2	0.11%	0.26%	0.11%
Subject 3	0.10%	0.15%	0.06%
Subject 4	0.08%	0.12%	0.12%

Table 6.2 Percentage of activation results for the four subject visual data (Data Set 2) with *p*-value of 0.001.

Both sets of data show similar results where there is more activation using SPM2 in comparison to SPM99, but there seem to be no clear pattern for the results obtained using the correlation method.

In summary, for the finger tapping data, results obtained using SPM2 and the SPM99 showed similar results. In the visual data we were unable to establish a relationship between results obtained using the correlation method and SPM2, as results varied across subjects. The overall observation is that results obtained using SPM2 always show more activation compared to results obtained using SPM99 for both data sets.

6.3 Simulated Data Results

This result has lead to the next step in our analysis, which tries to investigate the accuracy of the results obtained in SPM. This required having a set of data, which enabled us to have total control over the size and strength of the signal in active areas. A fake data set was created to simulate the finger tapping experiment (Data Set 1) and introduced the required active areas. The simulated data was created, by replicating a volume chosen randomly from the real finger tapping data set. Volume 10 of week 16 was replicated 30 times. Two areas (cube of 4x4x4 voxels in size: (56:59,56:59,7:10) and (75:78,75:78,3:6)) of activation were chosen to have an off-on pattern for 5 volumes each, and the strength of the

activation signal was set to be a percentage of the average signal in the image (1%). A normally distributed noise with 0 mean was also added to the image for a realistic simulation of the data. The noise was generated using a randomisation *Matlab* command and negative values were set to 0 (see Appendix A). Data was analysed in SPM99, SPM2 and the correlation method with the same pre-processing steps. Data analysis results in SPM99 are shown below in Fig. 6.7.

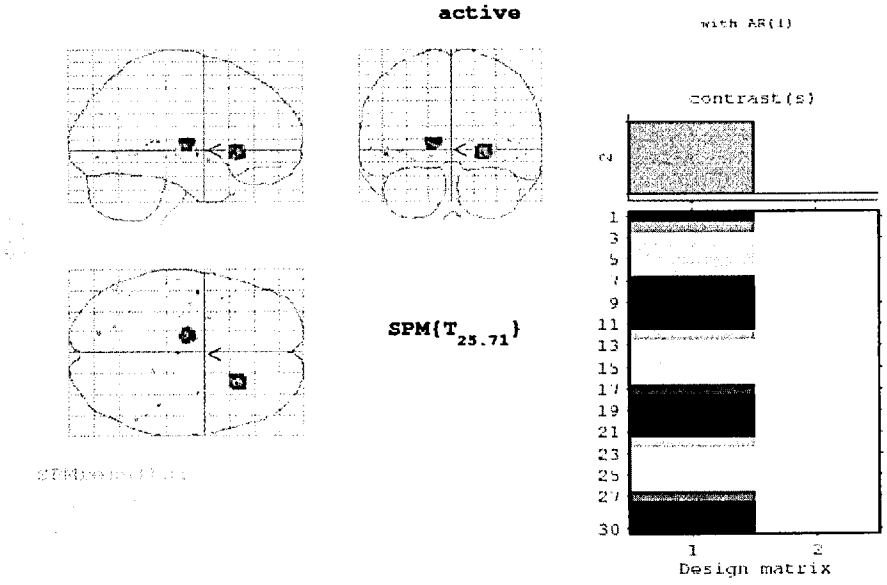

Fig. 6.7 SPM99 results with a *p*-value of 0.001.

Results using SPM99 show a good identification of active areas in the axial plane with 0.12% activation.

Data analysis results in SPM2 are shown below in Fig. 6.8.

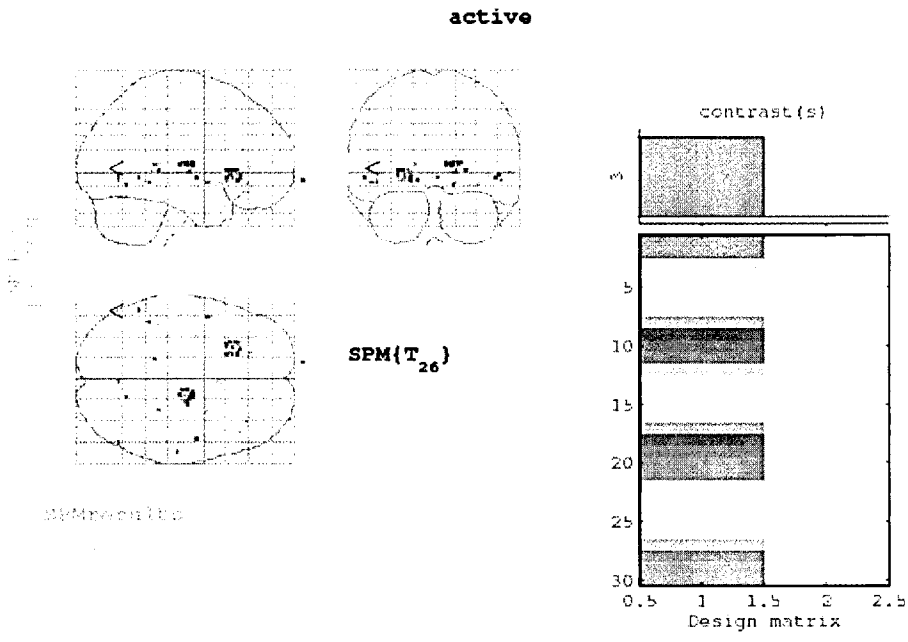

Fig. 6.8 SPM2 results with a *p*-value of 0.001.

Results using SPM2 again show a good identification of active areas in the axial plane with 0.13% activation.

Results using the correlation method correctly identify the two active areas in the precise position and shape as shown in Fig. 6.9. The percentage of the activation was 0.08%.

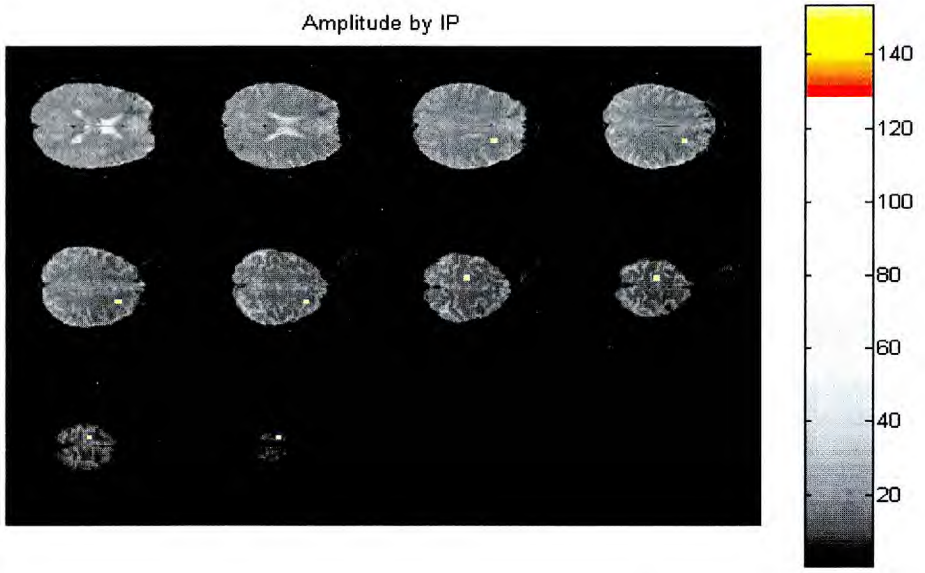

Fig. 6.9 correlation method results with a *p*-value of 0.001.

Therefore, results obtained using SPM99 and SPM2 show similar results and include more activation compared to results obtained using the correlation method.

6.4 Comparison of realigned data Using SPM99, SPM2 and AIR

This study investigates the reproducibility of activation patterns obtained after realigning using SPM99, SPM2 and AIR. The finger tapping data set (Data Set 1) was realigned using SPM99 and SPM2 and AIR, and then

analysed for maximum activation. The following table summaries the results:

	SPM99	SPM2	AIR
Week16	0.82	0.82	0.79
Week17	0.82	0.84	0.76
Week19	0.87	0.83	0.89
Week20	0.86	0.87	0.68
Week22	0.85	0.84	0.80
Week29	0.91	0.89	0.86
Week30	0.80	0.79	0.79
Week33	0.85	0.90	0.80
Week34	0.84	0.91	0.70
Week36	0.87	0.83	0.82
Week37	0.91	0.91	0.91
Week38	0.86	0.86	0.69
Week39	0.87	0.86	0.86
Week42	0.90	0.90	---
Mean (SD)	0.86 (± 0.03)	0.86 (± 0.04)	0.80 (± 0.07)
p-value	SPM99 vs. SPM2 0.861749	SPM99 vs. AIR 0.00778	SPM2 vs. AIR 0.007885

Table 6.3 Similarity measure comparison between SPM99, SPM2 and AIR.

The values above are measures of similarity (calculated using the correlation method). The higher the value, the more similar the signals are. From the above results we can clearly identify that in almost all cases, the

realigned data using SPM show better results in regards to the similarity measure in comparison to the same data realigned using AIR. We can also see that the realigned data using SPM99 show similar results compared to those realigned using SPM2.

The visual data (Data Set 3) was also analysed and the results are shown below in table 6.4:

	Range (Mean) SPM99	Range (mean) SPM2	Range (Mean) AIR
finger tapping (Data set 1: weeks 16,17,33,42)	0.80 - 0.91 (0.87)		
Realigned finger tapping (Data set 1: weeks 16,17,33,42)	0.82 – 0.90 (0.84)	0.79 – 0.91 (0.86)	0.00 – 0.80 (0.59)
Visual (Data Set 3: 100% contrast all subjects)	0.71 – 0.90 (0.81)		
Realigned visual (Data Set 3: 100% contrast	0.77 – 0.91 (0.83)	0.77 – 0.91 (0.83)	0.58 – 0.86 (0.75)
Visual (Data Set 3: 10% contrast all subjects	0.54 – 0.85 (0.71)		
Realigned visual (Data Set 3: 10% contrast	0.00 – 0.85 (0.63)	0.57 – 0.85 (0.75)	0.00 – 0.74 (0.54)

Table 6.4 Mean and range value of similarity measure at active areas.

From the results, we can conclude that for the finger tapping data, the realignment process using SPM99, SPM2 and AIR all cause a decrease in the similarity measure. For the visual data, the realignment process has the effect of: increasing the similarity measure and the cluster size when using SPM2, decreasing the similarity measure when using AIR, but give contradictory results when using SPM99. We can also conclude, that the reduction in contrast (100% to 10%) has the effect of decreasing the similarity measure and the cluster size.

6.5 Comparison of Realigned versus Non Realigned Data in SPM2

An investigation of the effect of realignment was conducted using SPM2. The finger data set (Data Set 1) was realigned using SPM2 and then analysed for maximum activation. The following table summaries the results of the comparison between the realigned and the non realigned data:

	Realigned	Non realigned
Week16	0.82	0.80
Week17	0.84	0.85
Week19	0.83	0.89
Week20	0.87	0.88
Week22	0.84	0.89

Week29	0.89	0.89
Week30	0.79	0.78
Week33	0.90	0.90
Week34	0.91	0.91
Week36	0.83	0.84
Week37	0.91	0.91
Week38	0.86	0.86
Week39	0.86	0.85
Week42	0.90	0.91
Mean (SD)	0.86 (± 0.04)	0.87 (± 0.04)
p-value	0.202464	

Table 6.5 Similarity measure comparison between realigned and non realigned data.

We can see that the non realigned data using SPM2 show better results compared to those realigned. But from the *p*-value, that difference will be deemed insignificant. We would expect a significant difference between the realigned and the non realigned data, but the extent of movement in the data was very small (in the region of 0.1 mm) which might explain these otherwise surprising results.

6.6 Comparison of reproducibility using FWER and FDR in SPM2

The effect of FWER and FDR was also investigated. Data Set 1 was analysed using SPM2 to investigate the reproducibility using FWER and FDR across all the sessions. Figure 6.10 below show the results obtained when realigning the data using SPM2 without using either FWER or FDR. The percentage of the activation was 0.2%.

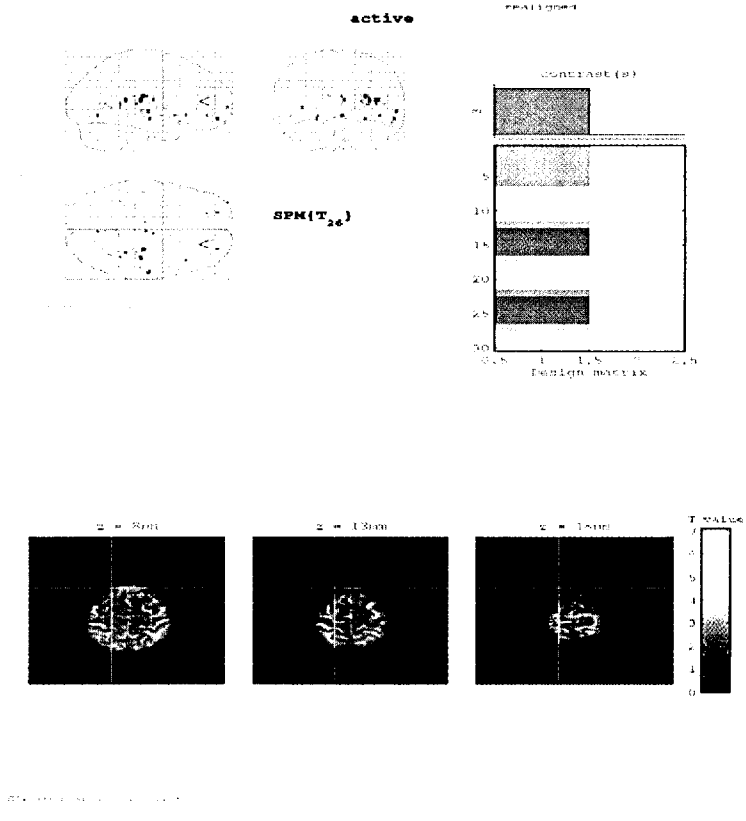

Fig. 6.10 Analysis of data set 1 using SPM2 with a *p*-value of 0.001.

The same data set was displayed using the FWER (*p*-value 0.05) as shown in Figure 6.11 below. The percentage of the activation was 0.01%.

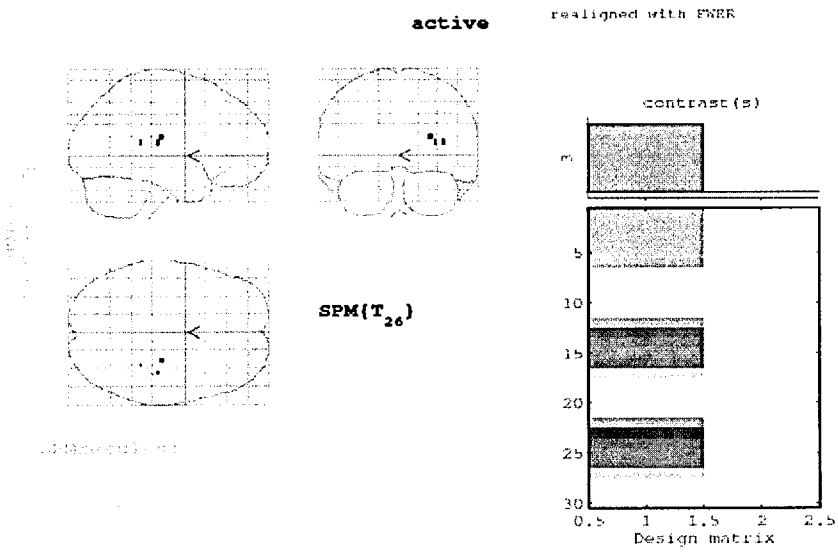

Fig 6.11 Analysis of data set 1 in SPM2 using FWER with a *p*-value of 0.05.

The data was then displayed using the FDR (p-value 0.05) as shown below in Figure 6.12. The percentage of the activation was 0.03%.

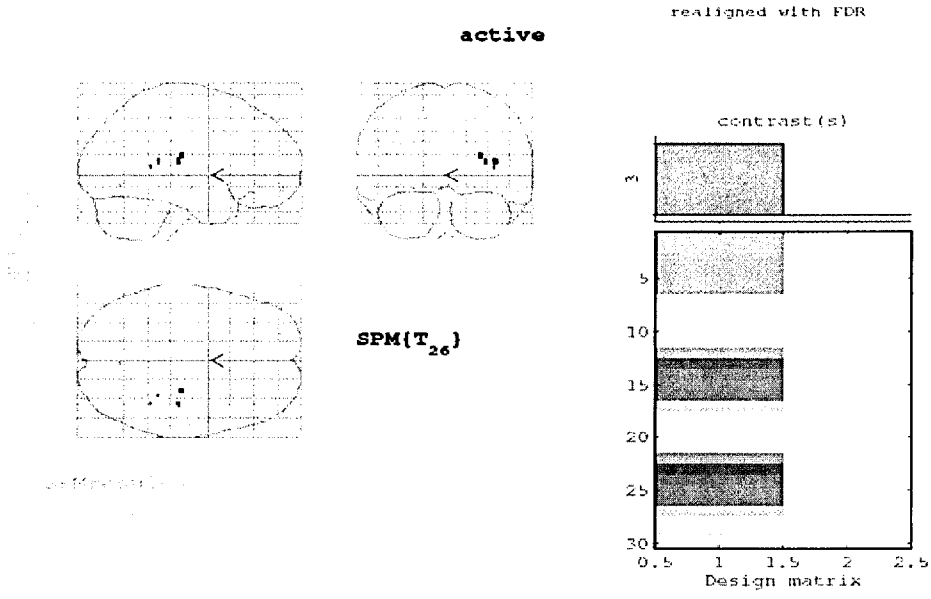

Fig 6.12 Analysis of data set 1 in SPM2 using FDR with a *p*-value of 0.05.

From the figures, we can see that the results presented for the realigned data without using FWER or FDR show a significant increase in the activation compared to results using the FWER and FDR. We can also see that using the FWER give a more conservative result (less activation) compared to using the FDR.

6.7 Normality tests

The test of the normality is an important part of the analysis because it is crucial to the inference of SPM. We would also like to investigate the possibility of developing a measure of normality as an indication of the activity/non-activity of the voxels, where active areas show patterns that deviate from normality compared to non-active (in brain) areas, due to the noise related to the blood flow in the active areas. We would also expect the background (out of brain) areas to be non normal. Subsets of data were chosen from each data set. It included active areas (active), potentially active areas (Pv), background out of brain areas (B), white matter areas (W) and grey matter areas (G). The subsets were then analysed using a *Matlab* script (Appendix A) to produce a histogram representing the difference between the signal at that region and the mean signal as shown in Fig. 6.13 below.

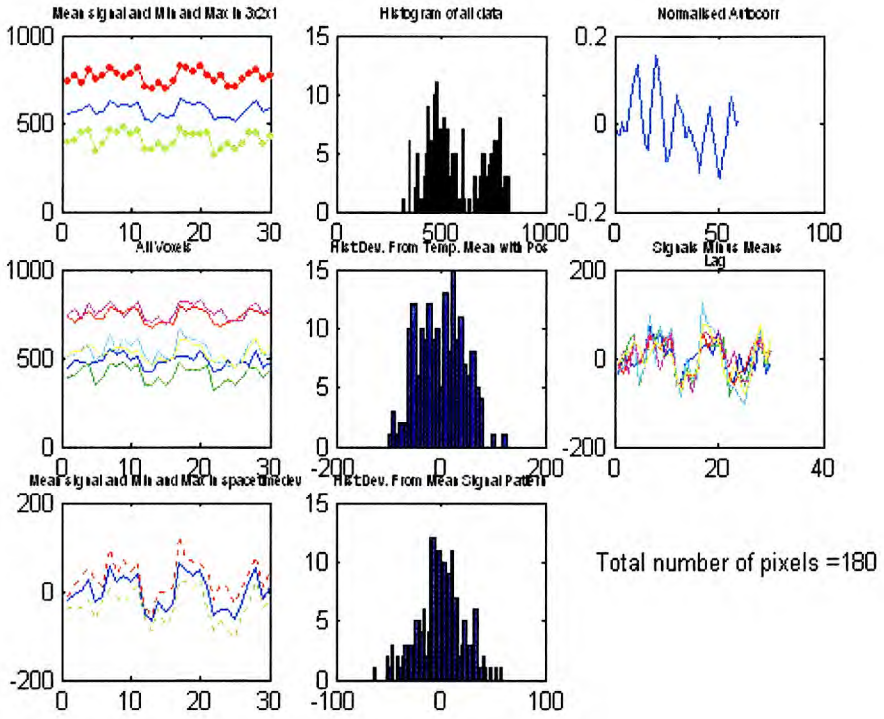

Fig. 6.13 The top left graph is a plot of the mean signal of all the voxels in the subset and the minimum and the maximum signal. The top middle graph is a histogram of the all the data. The top right graph is a plot of the cross correlation. The centre left graph is a plot of the signal at each voxel in the subset. The centre middle graph is a histogram of the deviation from the temporal mean. The centre right graph is a plot of the signals minus the mean. The bottom left graph is a plot of the mean signal of the previous plot (i.e. plot of signals minus the mean) and the minimum and the maximum signal. The bottom middle graph is a histogram of the deviation from the mean.

The difference was then analysed using the K-S test in SPSS package to check for the normality of the signal distribution and a comparison table was produced. The results are displayed in Appendix B. The most significant results are shown in table 6.6:

	Range (Mean) SPM99	Range (Mean) SPM2	Range (Mean) AIR
Finger tapping (data Set 1: weeks 16,17,33,42)	0.76 – 0.99 (0.91)		
Realigned finger tapping (Data Set 1: weeks16,17,33,42	0.33 – 0.97 (0.70)	0.61 – 0.93 (0.81)	0.01 – 0.78 (0.52)
Visual (Data Set 3: 100% contrast all subjects	0.06 – 0.76 (0.44)		
Realigned visual (Data Set 3: 100% contrast	0.19 – 0.99 (0.73)	0.27 – 1.0 (0.78)	0.09 – 0.51 (0.29)
Visual (Data Set 3: 10% contrast all subjects	0.09 – 1.0 (0.73)		
Realigned visual (Data Set 3: 10% contrast	0.12 – 0.98 (0.58)	0.15 – 0.99 (0.60)	0.00 – 0.72 (0.34)

Table 6.6 Mean and range value of signal distribution normality in active areas.

The values above are measures of the normality of the signal distribution. The higher the value, the closer the signal distribution is to normality.

From the results above, we can conclude that realigning the data (finger tapping data and visual data 10% contrast) using SPM99, SPM2 and AIR causes a decrease in the normality of active areas. However, realigning the visual data 100% causes an increase in the normality of the active areas in the data. This study also extended to include the effect of the contrast (100% versus 10%) on the normality of active areas. It was found from the above that there is an increase in the normality with the decrease of the contrast (from 100% to 10%).

The table below summarizes the results related to the normality of the active/non-active areas in the data.

	active	Pv	B	W	G
Finger tapping (16,17,33,42)	0.91	0.84	0.73	0.87	0.77
Realigned finger tapping (16,17,33, 42)	0.81	0.56	0.35	0.85	0.80
Visual 100%	0.44		0.21	0.65	0.59
Realigned Visual 100% (SPM2)	0.78		0.42	0.80	0.63
Visual 10%	0.73		0.26	0.54	0.42
Realigned visual 10% (SPM2)	0.60		0.40	0.77	0.63

Table 6.7 Mean value of signal distribution normality at active and non-active areas.

The results above show that there is a clear difference in normality between active areas and background areas (out of brain areas). However, there seems to be no clear pattern to distinguish the normality between active areas and in brain non-active areas. Therefore, the normality results did not provide conclusive evidence to support our study of using the normality as an indication of the activity/non-activity (in brain areas) of the voxels. Another observation is that the realignment seem to cause an increase in the normality of the in brain non-active areas for the visual data, but causes a decrease in the normality for the in brain non-active areas for the finger tapping data.

6.8 Summary

A standard analysis of data involves finding the total number of active voxels, the strength of the BOLD signal and the position. Analysis of the effect of the realignment process on the activation using different methods (SPM99, SPM2 and the correlation method) was detailed and a comparison of the number of active voxels was carried out. It was found that in general more activation was present using SPM2 compared to SPM99.

A comparison of the similarity measure obtained was performed to identify the differences of aligned data using different analysis methods (SPM99,

SPM2 and AIR). Realigned data using SPM showed better results compared to those obtained using AIR.

Comparing the effect of the realignment process on the similarity measure. From the results, we can conclude that for the finger tapping data, the realignment process using SPM99, SPM2 and AIR all cause a decrease in the similarity measure. For the visual data, the realignment process has the effect of: increasing the similarity measure and the cluster size when using SPM2, decreasing the similarity measure when using AIR, but give contradictory results when using SPM99. We can also conclude, that the reduction in contrast (100% to 10%) has the effect of decreasing the similarity measure and the cluster size.

A comparison of the similarity measure obtained was performed to identify the differences between aligned and non-aligned data in SPM2. Better results were obtained in non realigned data. The extent of movement in the data was checked and found to be very small (in the region of 0.1 mm) which might explain these otherwise surprising results.

The effect of FWER and FDR was also investigated. Results show more activation using FDR compared to FWER.

A normality study was also conducted. The effect of the realignment process on the normality of active areas was investigated. For the finger tapping data and the visual data 10% contrast, realigning using SPM99, SPM2 and AIR caused a decrease in the normality of active areas. However, realigning the visual data 100% caused an increase in the normality of the active areas in the data.

This study also extended to include the effect of the contrast (100% versus 10%) on the normality of active areas. It was found that there is an increase in the normality with the decrease of the contrast (from 100% to 10%).

The normality study showed a clear difference in normality between active areas and background areas (out of brain areas). It also showed that the realignment seem to cause an increase in the normality of the in brain non-active areas for the visual data, but cause a decrease in the normality for the in brain non-active areas for the finger tapping data. The possibility of using the normality as an indication of the activity/non-activity (in brain areas) of the voxels was also investigated. However, the standard K-S test for normality did not indicate a statistically significant difference between active and non active regions within the brain, thus suggesting that a normality test on its own will not be able to distinguish active from non-active regions.

Chapter 7

HRF and Reproducibility

7.1 Introduction

This chapter investigates the HRF signal reproducibility. The effect of the phase shift of the HRF signal on activation is analysed, followed by a detailed description of the empirical extraction of the HRF signal from the data. A comparative study of the effect of different HRF signals has on the similarity measure and the ratio of energy is also carried out. These differences are then presented graphically as ROC curves. Some clinical application of individual's HRF extraction analysis is included.

7.2 Phase shift

In order to optimise the sensitivity of activation detection, the hemodynamic response function should be modelled accurately [120]. The effect of the change in the phase shift of the hemodynamic response function (HRF)

signal convolved with the boxcar signal (predicted activation signal) on the active areas was investigated. The change of the phase shift was tested on the realigned finger tapping data set (Data Set 1). The phase shift was changed between -9dt to + 13dt, where dt is the time increment and is equal to 0.375 sec. The data was then analysed using SPM2 and the correlation method. The results are shown below in table 7.1.

Phase shift	SPM2 (active voxels)	Correlation method (active voxels and similarity measure)
-9 dt (-.3.375 sec)	981	256 (0.73)
-7 dt (-2.625 sec)	1113	286 (0.73)
-6 dt (-2.25 sec)	1216	313 (0.73)
-5 dt (-1.875 sec)	1300	345 (0.73)
-3 dt (-1.125 sec)	1439	383 (0.75)
-2 dt (-0.75 sec)	1486	408 (0.77)
-1 dt (-0.375 sec)	1506	422 (0.78)
0 dt (0 sec)	1510	432 (0.79)
+1 dt (0.375 sec)	1486	435 (0.80)
+2 dt (0.75 sec)	1477	447 (0.81)
+3 dt (1.125 sec)	1462	449 (0.82)
+4 dt (1.5 sec)	1441	446 (0.83)
+6 dt (2.25 sec)	1433	454 (0.84)
+8 dt (3 sec)	1468	468 (0.85)
+10 dt (3.75 sec)	1488	471 (0.86)
+11 dt (4.125 sec)	1477	487 (0.85)
+12 dt (4.5 sec)	1453	488 (0.84)
+13 dt (4.875 sec)	1435	491 (0.83)

Table 7.1 Effect of phase shift on activation in SPM2 and the correlation method.

From the above results we can see that using the correlation inner product method, it was found that the maximum number of activation was at shift +13dt, even though, the maximum similarity measure was found at shift +10dt. In SPM2, the maximum number of activations was found at shift 0dt.

Figure 7.1 below shows a plot of the activation versus the phase shift in SPM2.

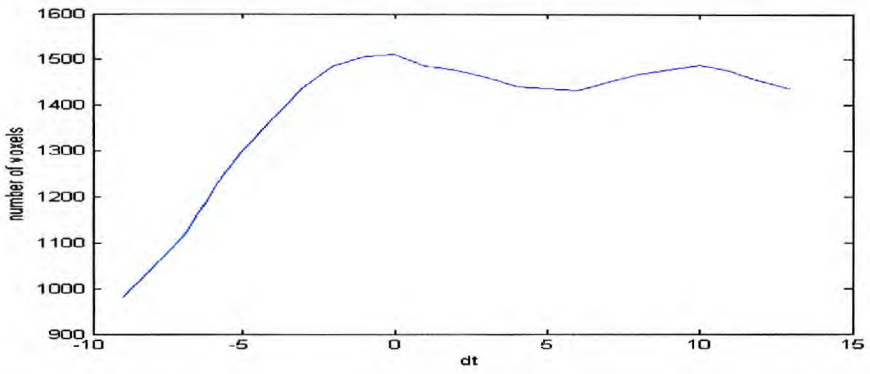

Fig. 7.1 Plot of SPM2 results of number of active voxels versus the phase shift.

We can see that there is a linear relationship between the phase shift and the total number of active voxels for negative phase shifts until 0 phase shift where it reaches a plateau.

Figures 7.2 and 7.3 below display the results obtained using the correlation method.

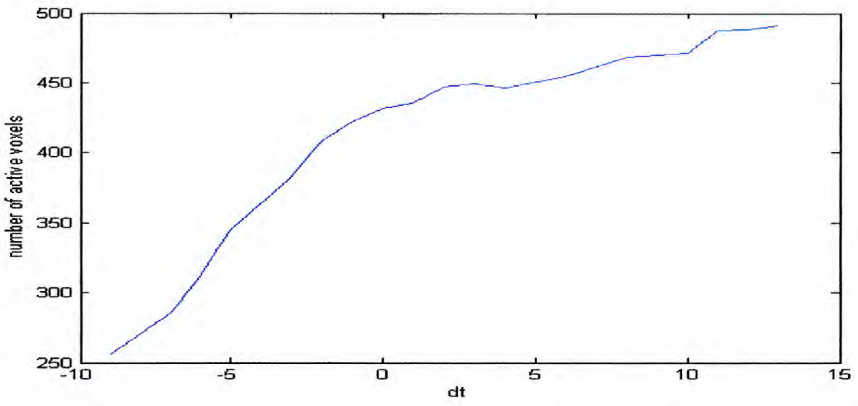

Fig. 7.2 Plot of correlation method results of number of active voxels versus the phase shift.

Again, we can see that there is a linear relationship between the phase shift and the total number of active voxels for negative phase shifts until 0 phase shift.

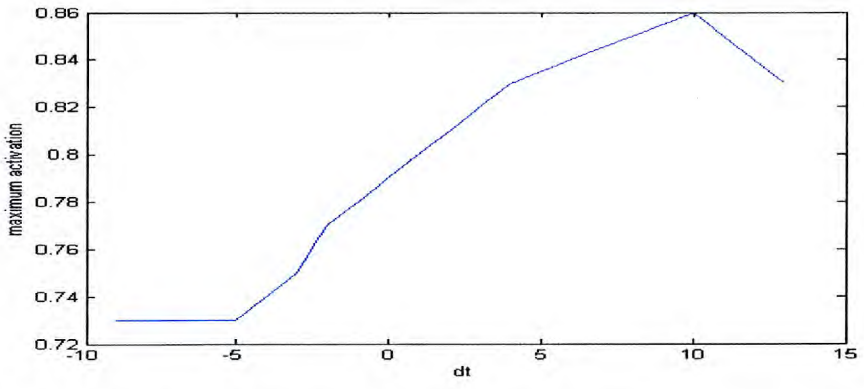

Fig. 7.3 plot of correlation method results of the similarity measure versus the phase shift.

We can see a linear relationship between the similarity measure and the phase shift for the range of -5dt to 10dt. The maximum activation peaks at a shift of 10 dt (3.75 sec) using the correlation inner product method. This corresponds to the position of the second maximum in Figure 7.1 indicating that there is some significance to the shift of 10 dt (3.75 sec). It is not clear why the second peak does not appear in Figure 7.2.

7.3 Empirical HRF extraction

We discussed the method of HRF extraction in chapter 5 section 5.5. Here, w present the results of HRF extraction. It was concluded that the HRF signal varies with subjects, sessions, regions in the brain, etc. So we decided to investigate the effect of variations of the hemodynamic response function on the activation observed in the finger tapping experiment and the visual data. Fig. 7.4 shows the HRF signal extracted from the activation signal used in SPM. In the finger tapping experiment (Data Set 1), the empirical activation signal was extracted from the data (week 16) by collapsing the averaged 2D signal, within the slice, at the maximum activation (50,54,9,:) in the image. The HRF signal extracted from the collapsed average signal at maximum activation is shown in Fig. 7.5. Repeating the analysis with the new activation signal improved the maximum activation of the image and the signal similarity measure changed from 0.79 to 0.87. On the other hand, collapsing the averaged 3D

signal (multi-slice at maximum activation) caused a decrease in the signal similarity measure to 0.70. The HRF signal extracted from the collapsed average 3D signal at maximum activation represents the mean of the activation in 3D cluster (multi-slice) around the maximum activation and is shown in Fig. 7.6. From these results, we can conclude that the choice of hemodynamic response function has an effect on the activation.

From the results shown below, we can see a difference in the shape and the amplitude of the HRF signals.

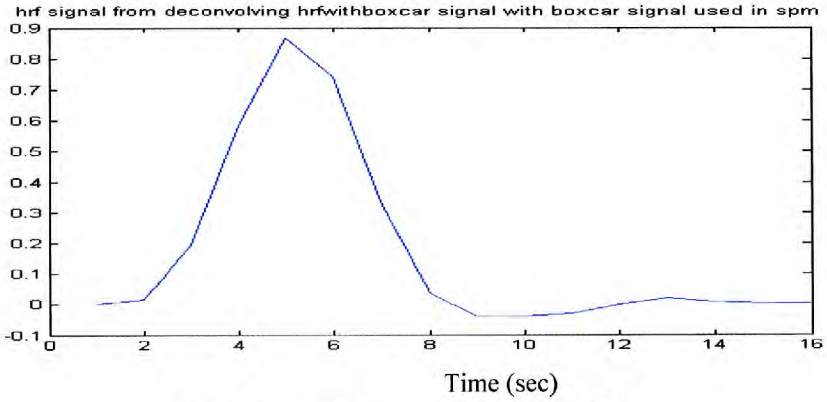

Fig. 7.4 HRF signal used in SPM.

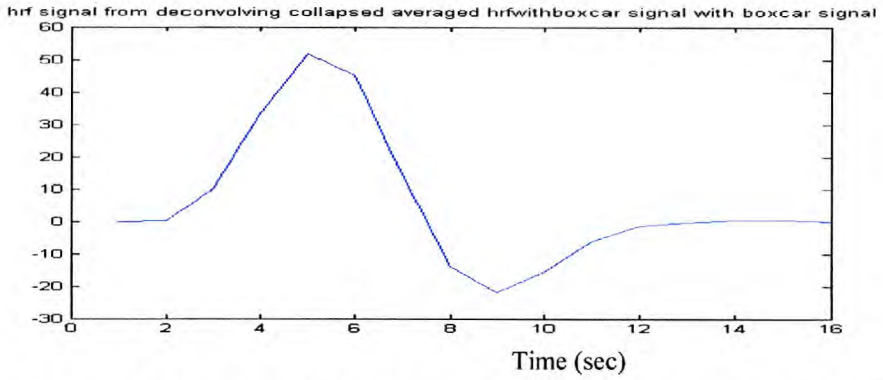

Fig. 7.5 HRF signal of collapsed average signal at maximum activation.

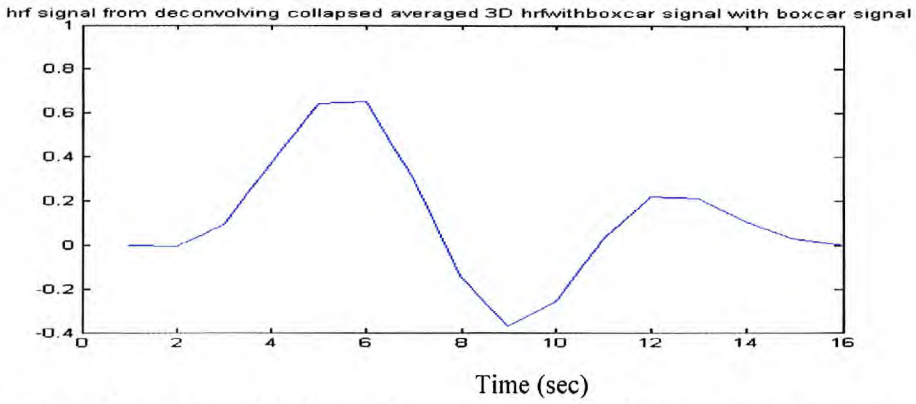

Fig. 7.6 HRF signal of the collapsed average 3D signal at maximum activation.

The next step was to select some data subsets (from Data set 1): 4 to be located in the grey matter (GM), 4 in the white matter (WM), some active areas (A), 2 at potentially active areas (visual cortex: Pv), and 4 background or out-of-brain areas (B). The HRF signal was then extracted at these positions. The results for week 16 are shown below (description of the ratio of energy is detailed in section 5.5):

Week 16:

A1

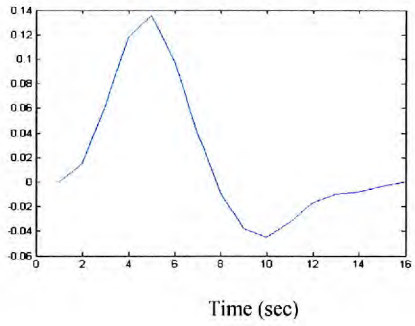

A2

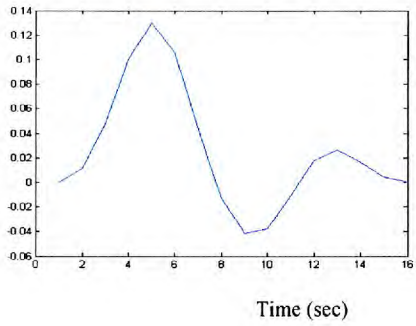

A3

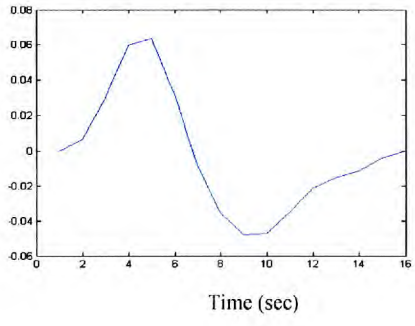

Pv1

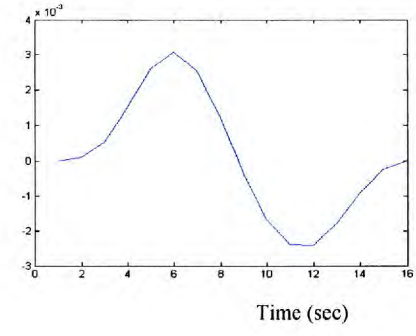

Pv2

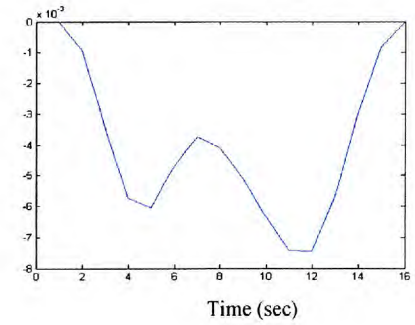

B1

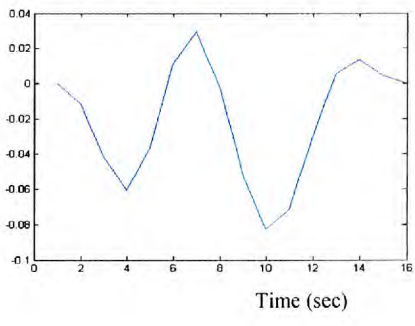

B2

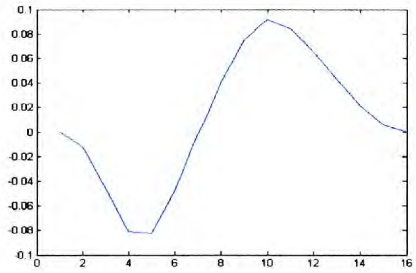

B3

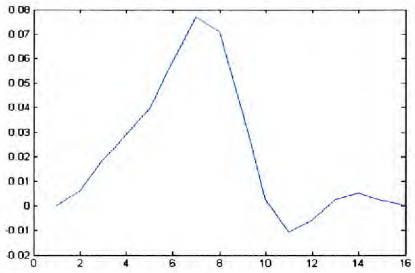

B4

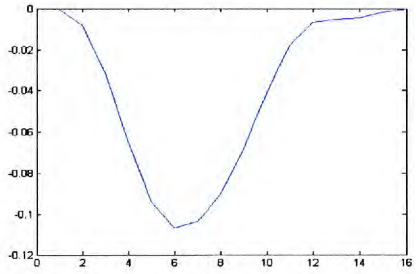

WM1

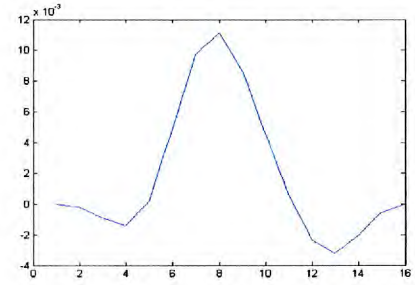

WM2

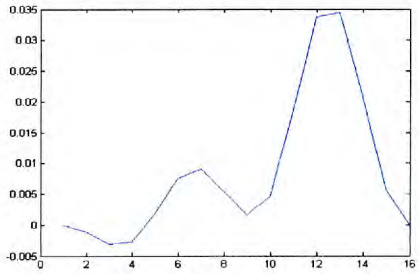

WM3

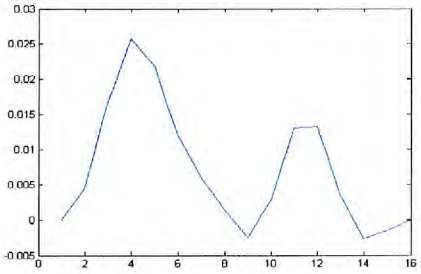

WM4

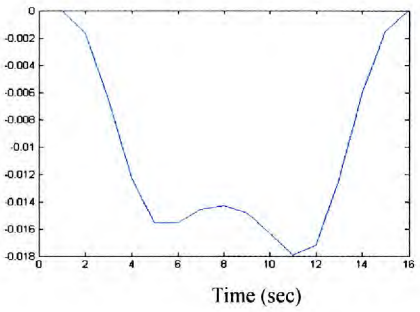

GM1

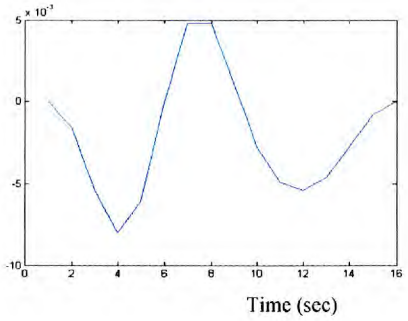

GM2

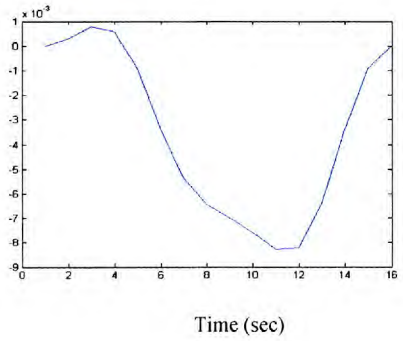

GM3

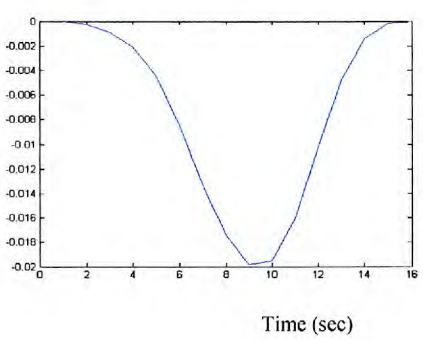

GM4

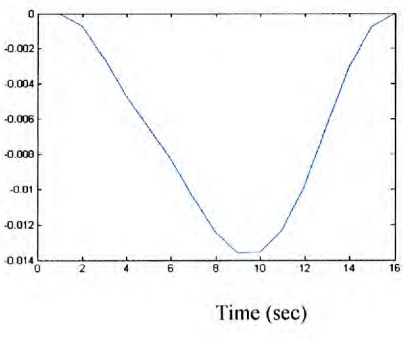

A1:Active area (50,54,9): Ratio of energies = 0.5	A2: Active area (49:50.54,9): Ratio of energies
A3: Active area (43:45,52:53,8): Ratio of energies = 0.47	Pv1: Visual cortex1: Ratio of energies = 0.91
Pv2: Visual cortex2: Ratio of energies = 0.80	B1: Background 1: Ratio of energies = 0.87
B2: Background 2: Ratio of energies = 0.801	B3: Background 3: Ratio of energies = 0.92
B4: Background 4: error: Ratio of energies = 0.89	WM 1: Ratio of energies = 0.95
WM 2: Ratio of energies = 0.90	WM 3: Ratio of energies = 0.77
WM 4: Ratio of energies = 0.92	GM 1: Ratio of energies = 0.88
GM 2: Ratio of energies = 0.98	GM 3: Ratio of energies = 0.80
GM 4: Ratio of energies = 0.82	

Table 7.2 Summary of ratio of energies for each subset for finger tapping data.

It is very evident from the results that we can only retrieve the HRF signal from areas of activation, and that the HRF signal varies at different areas of activation in the brain. It also appears that the ratio of energies of active regions is lower than that of other regions in or out of brain.

The HRF signals of active areas for individual weeks are shown below in figures 7.7 to 7.20:

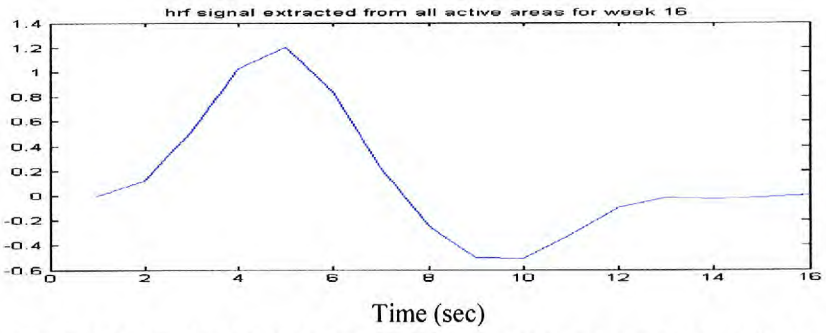

Fig. 7.7 HRF signal extracted from all active areas for week 16.

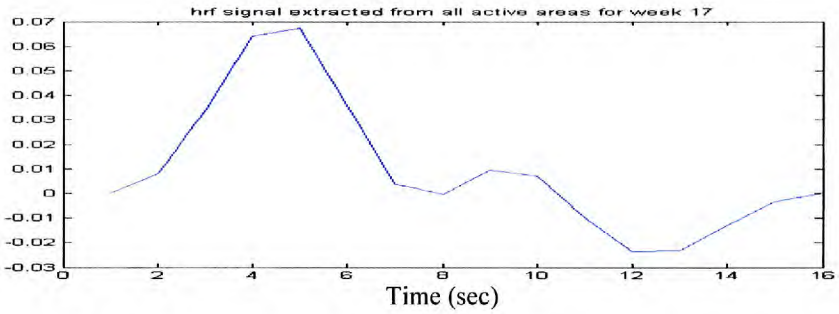

Fig. 7.8 HRF signal extracted from all active areas for week 17.

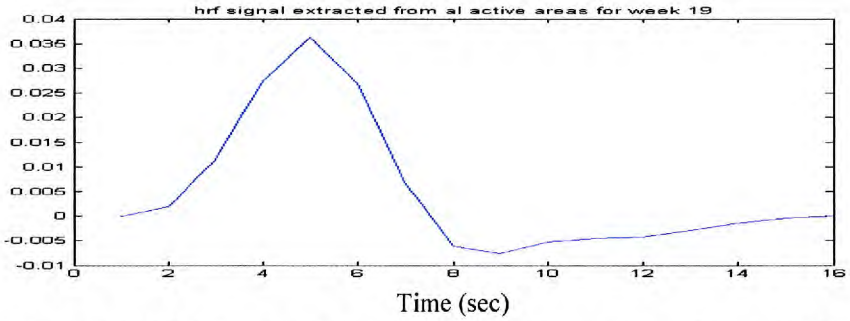

Fig. 7.9 HRF signal extracted from all active areas for week 19.

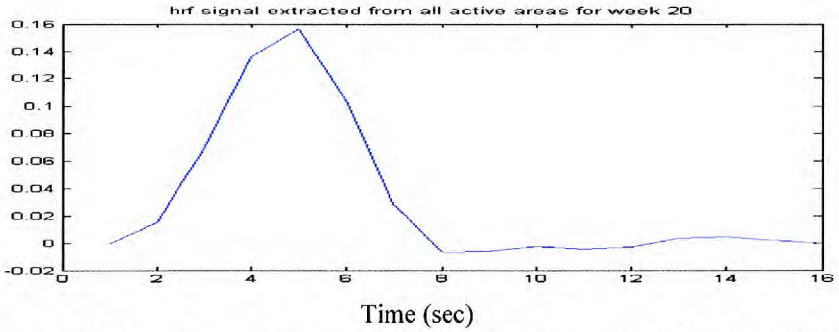

Fig. 7.10 HRF signal extracted from all active areas for week 20.

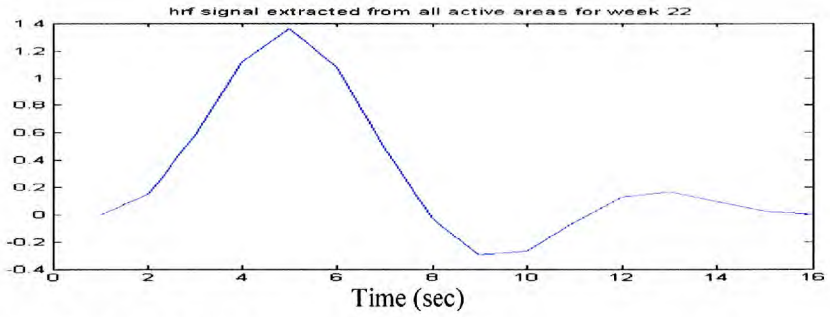

Fig. 7.11 HRF signal extracted from all active areas for week 22.

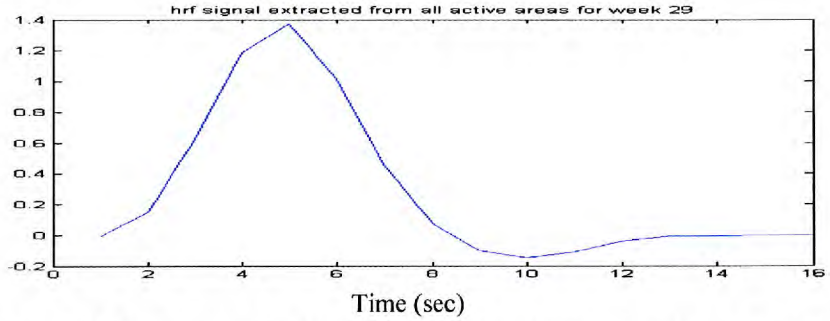

Fig. 7.12 HRF signal extracted from all active areas for week 29.

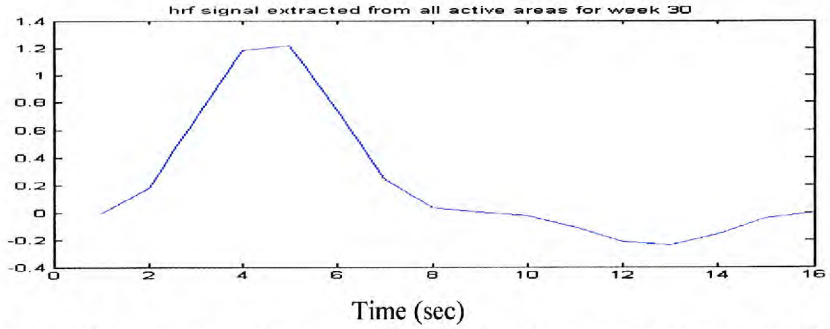

Fig. 7.13 HRF signal extracted from all active areas for week 30.

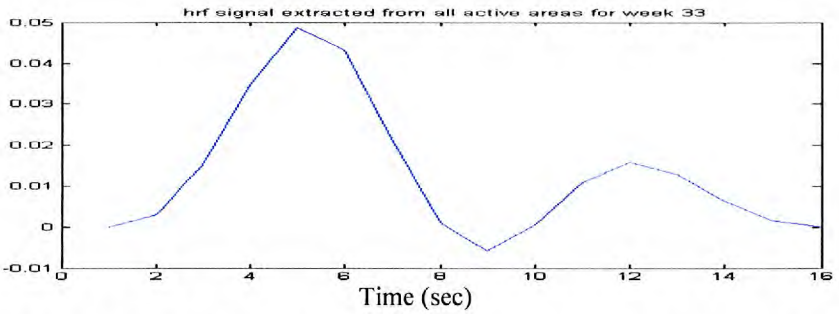

Fig. 7.14 HRF signal extracted from all active areas for week 33.

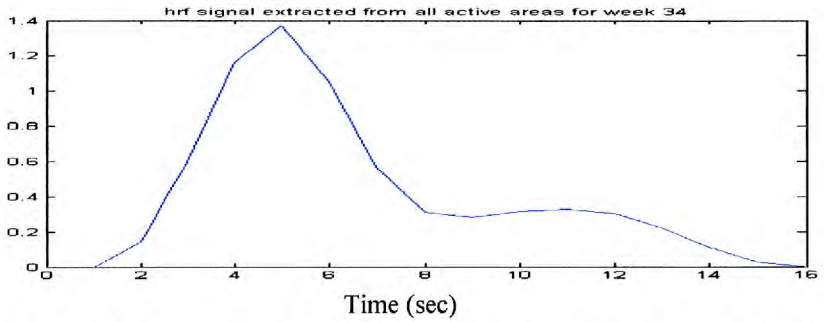

Fig. 7.15 HRF signal extracted from all active areas for week 34.

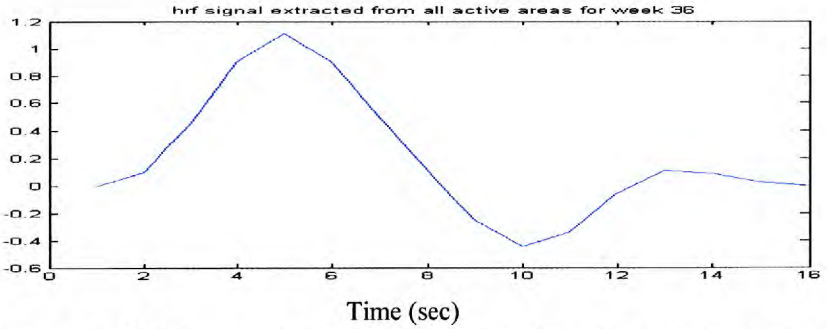

Fig. 7.16 HRF signal extracted from all active areas for week 36.

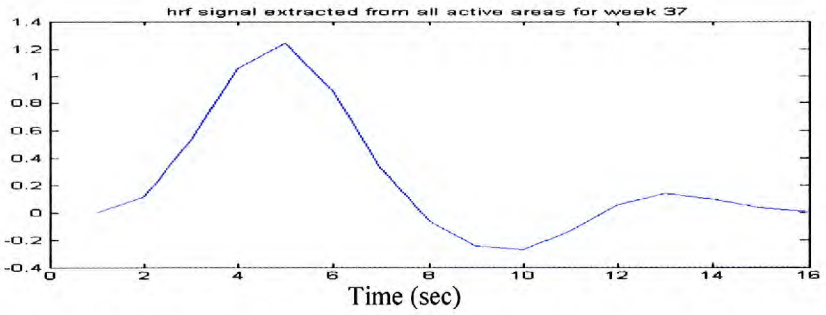

Fig. 7.17 HRF signal extracted from all active areas for week 37.

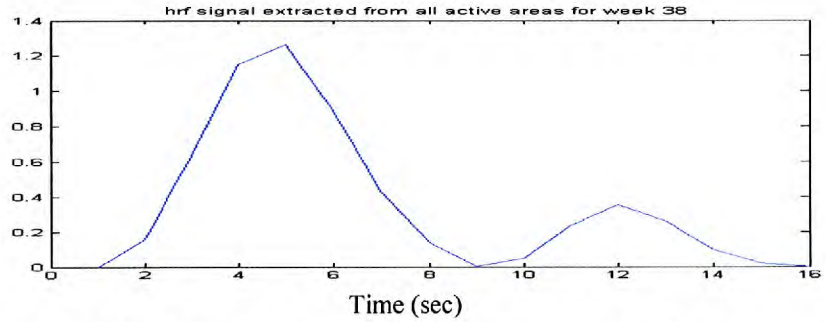

Fig. 7.18 HRF signal extracted from all active areas for week 38.

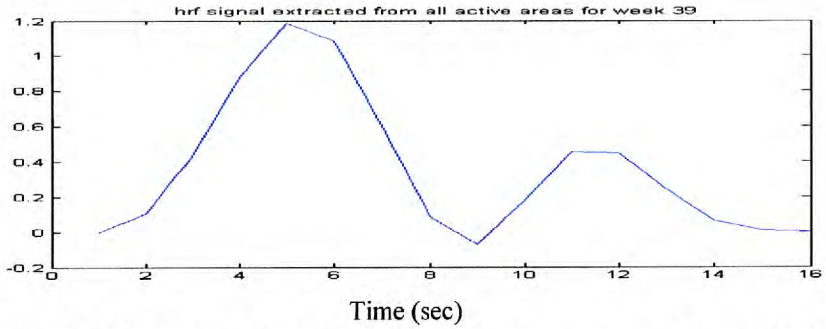

Fig. 7.19 HRF signal extracted from all active areas for week 39.

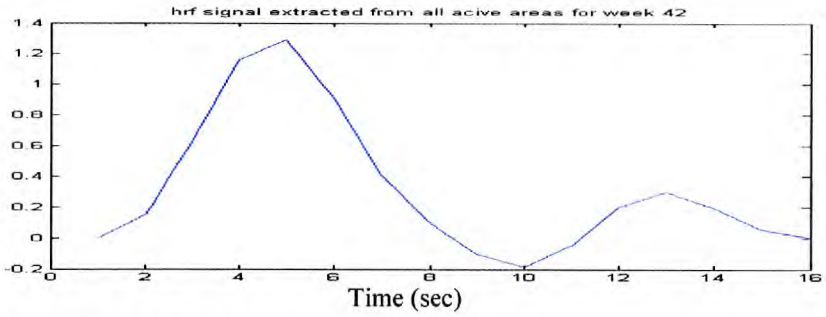

Fig. 7.20 HRF signal extracted from all active areas for week 42.

The standard deviation of the HRF signal and the mean signal of all active areas across the weeks +/- 1 and 2 standard deviation is shown below in Fig. 7.21:

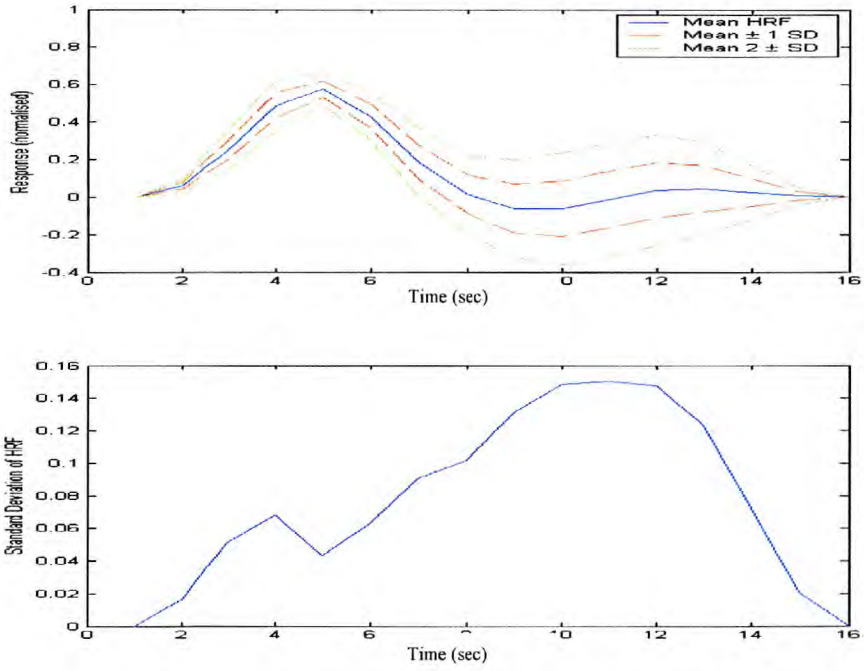

Fig. 7.21 Mean signal and standard deviation of the finger tapping smoothed HRFs.

The same process was repeated for the visual data where the results for subject 1 100% contrast are shown below:

A1

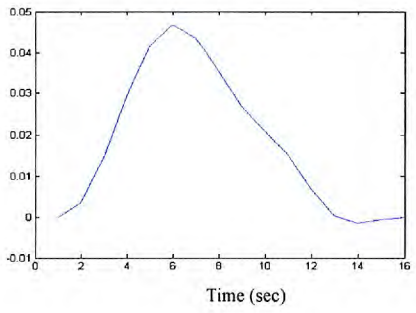

B1

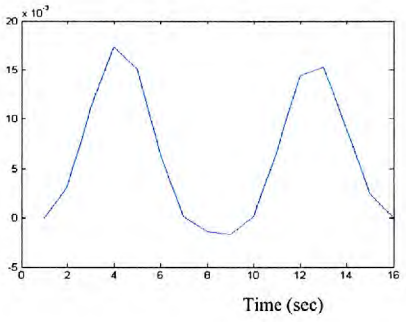

B2

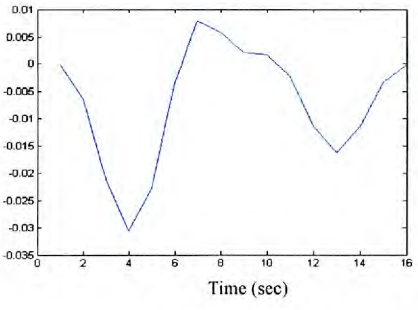

B3

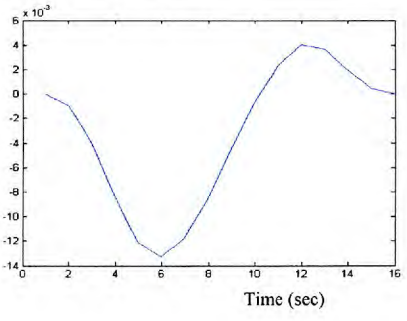

B4

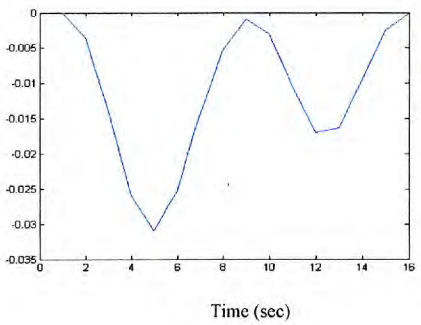

WM1

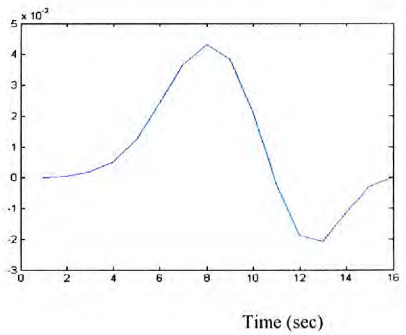

WM2

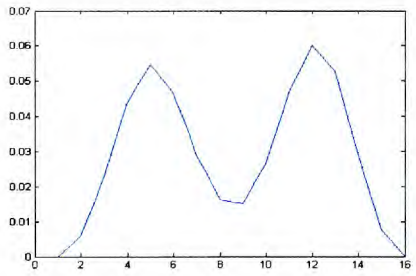

WM3

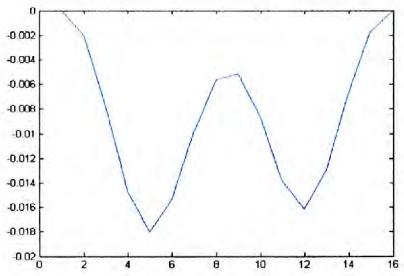

WM4

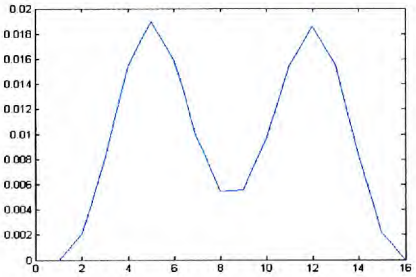

GM1

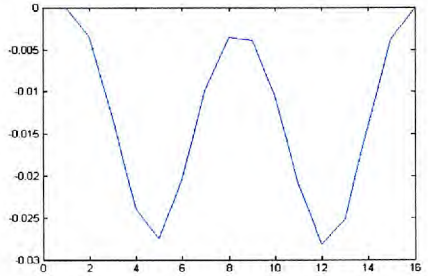

GM2

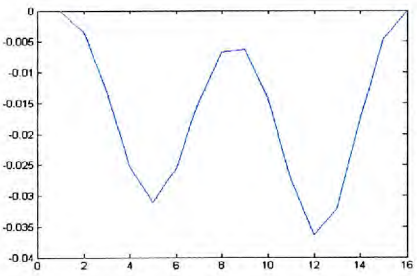

GM3

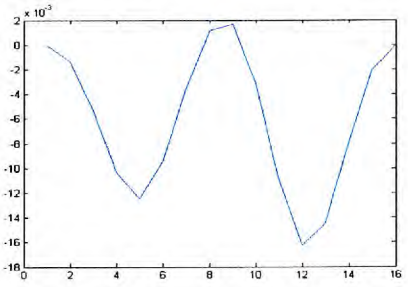

GM4

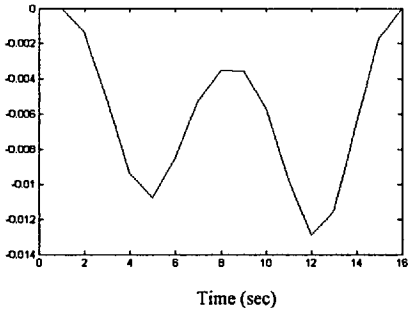

A1: Active (60:62,17,8): Ratio of energies =0.67	B1: Background (18:20,18:20,11): Ratio of energies =0.98
B2: Background 2: Ratio of energies =0.95	B3: Background 3: Ratio of energies = 0.99
B4: Background 4: Ratio of energies =0.98	WM 1: Ratio of energies =0.95
WM 2: Ratio of energies =0.81	WM 3: Ratio of energies =0.86
WM 4: Ratio of energies =0.95	GM 1: Ratio of energies =0.91
GM 2: Ratio of energies =0.82	GM 3: Ratio of energies =0.92
GM 4: Ratio of energies =0.98	

Table 7.3 Summary of ratio of energies for each subset for visual data.

The visual data results confirm the finger tapping results obtained previously.

For the 100% contrast the HRF signals at the active voxels in each subject are shown in Fig. 7.22 to Fig. 7.26 below:

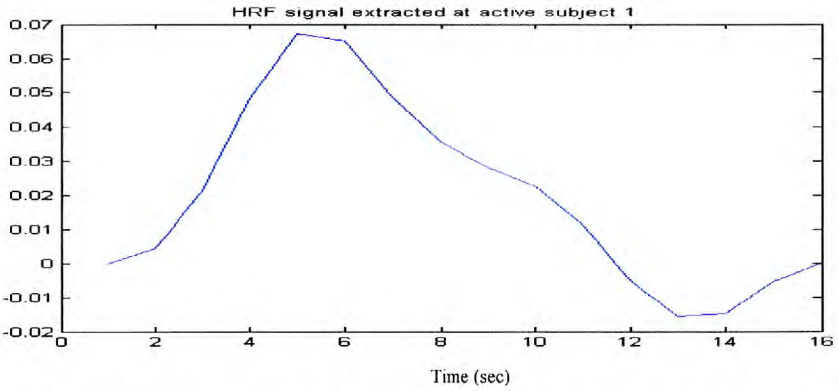

Fig. 7.22 HRF signal at active voxel in subject 1 (100% contrast).

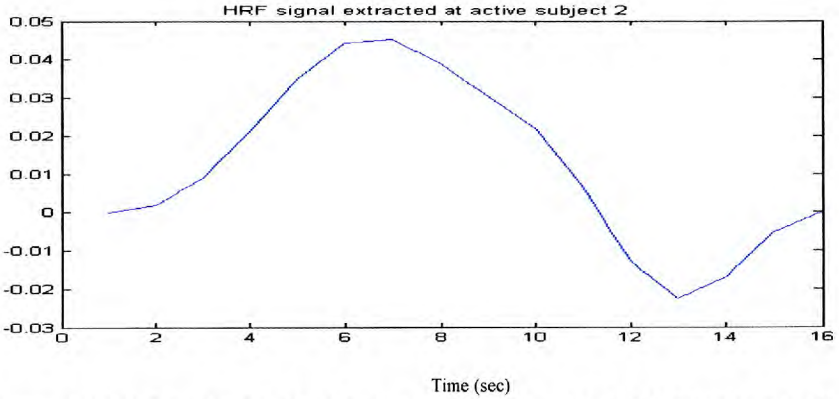

Fig. 7.23 HRF signal at active voxel in subject 2 (100% contrast).

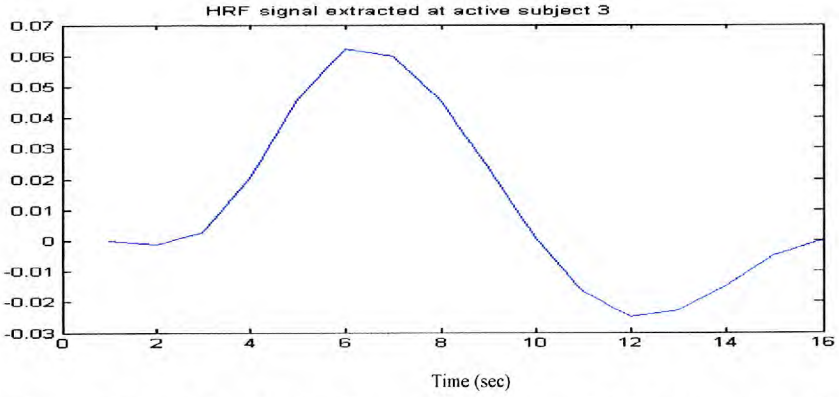

Fig. 7.24 HRF signal at active voxel in subject 3 (100% contrast).

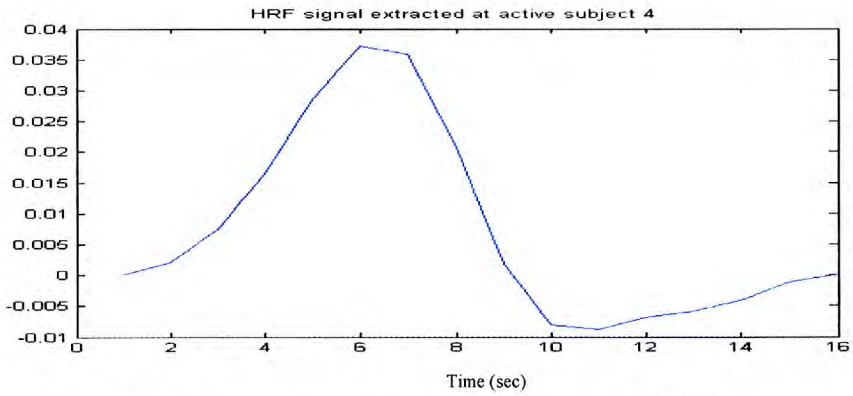

Fig. 7.25 HRF signal at active voxel in subject 4 (100% contrast).

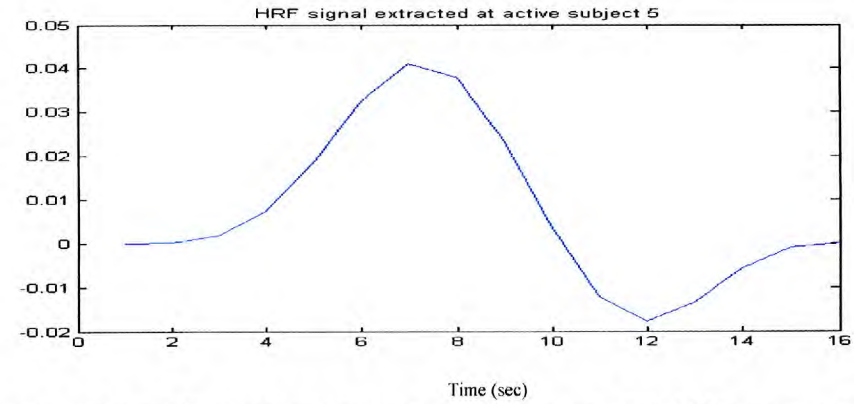

Fig. 7.26 HRF signal at active voxel in subject 5 (100% contrast).

The standard deviation of the HRF signal and the mean signal of all active areas across the subjects (100% contrast) plus and minus one and two standard deviation is shown below in Fig. 7.27:

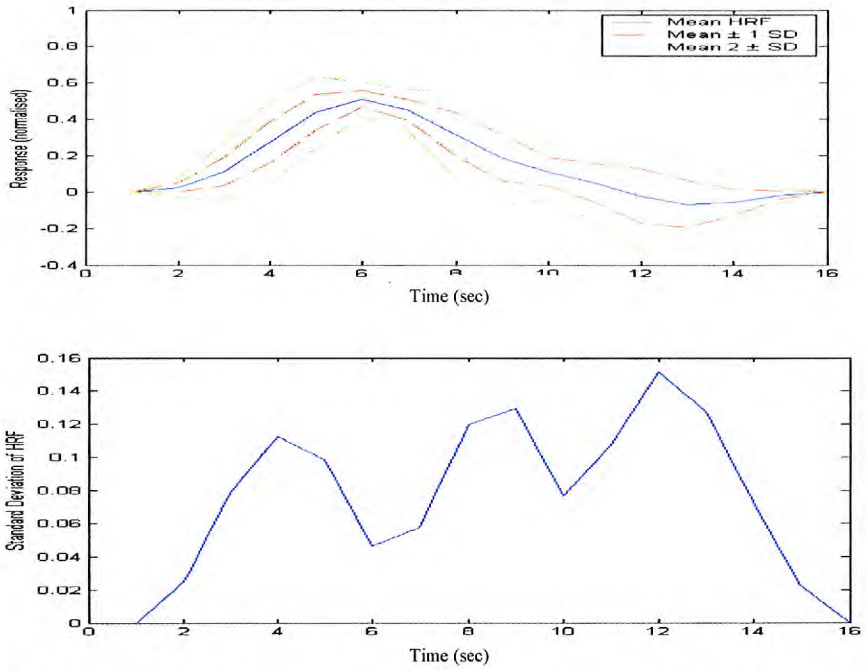

Fig. 7.27 Mean and standard deviation of the visual 100% contrast smoothed HRFs.

For the 10% contrast the standard deviation of the HRF signal and the mean signal of all active areas across the subjects plus and minus one and two standard deviation is shown below in Fig. 7.28:

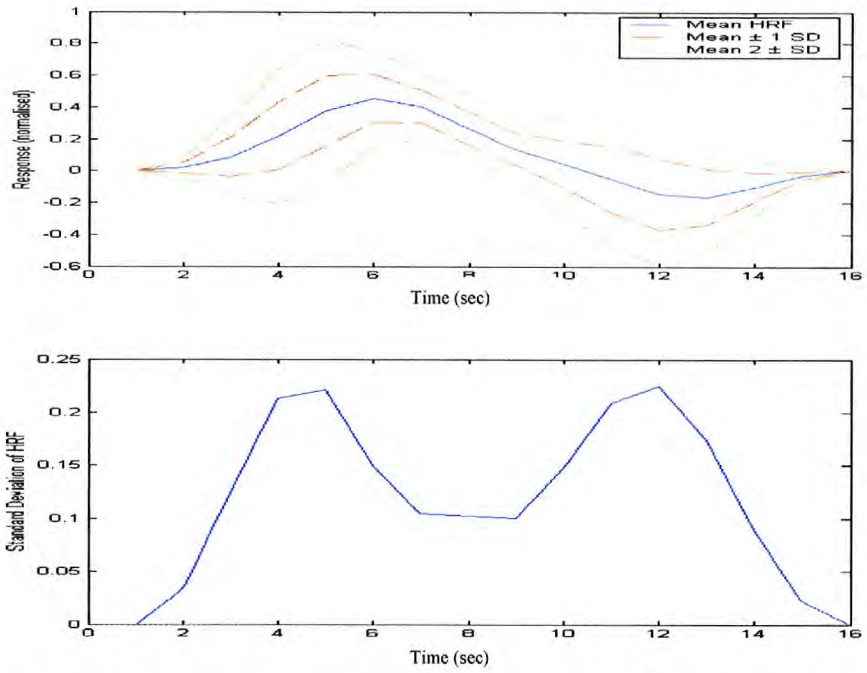

Fig. 7.28 Mean and standard deviation of the visual 10% contrast smoothed HRFs.

7.4 Comparisons of HRFs

Table 7.4 shows a comparison between the mean HRF and the SPM HRF for the finger tapping data (Data Set 1):

	Time to Peak	Ratio of +ve to –ve amplitude
Mean HRF	5 sec.	7.07/1
SPM HRF	5 sec.	8/1

Table 7.4 Comparison of the mean and the SPM HRF signals for the finger tapping data set.

Table 7.5 shows a comparison between the individual's HRF signals in the finger tapping data set (Data Set 1) and the mean HRF signal:

	Time to Peak (sec.)	Ratio of +ve to –ve amplitude
Week 16	5	2.5/1
Week 17	5	3.5/1
Week 19	5	3.5/1
Week 20	5	16/1
Week 22	5	4.5/1
Week 29	5	14/1
Week 30	5	6/1
Week 33	5	10/1
Week 34	5	10/1
Week 36	5	3/1
Week 37	5	4/1
Week 38	5	5/1
Week 39	5	12/1
Week 42	5	6/1
Mean HRF (SD)	5 (0)	7.07/1 ($\pm$ 4.28)

Table 7.5 Comparison between the individual's HRF signals and the mean HRF signals for the finger tapping data set.

Table 7.6 shows a comparison between the mean HRF and the SPM HRF for the visual data (Data Set 3, 100% and 10% contrast):

	Time to Peak	Ratio of +ve to –ve amplitude
Mean HRF 100% contrast	6 sec.	5/1
Mean HRF 10% contrast	6 sec.	5/1
SPM HRF	5 sec.	8/1

Table 7.6 Comparison of the mean 100%, 10% and SPM HRF signals for the visual data set.

Table 7.7 shows a comparison between the individual's HRF signals in the 100% contrast (Data Set 3) and the mean HRF signal:

	Time to Peak	Ratio of +ve to –ve amplitude
Subject 1 (100%)	5 sec.	7/1
Subject 2 (100%)	7 sec.	2/1
Subject 3 (100%)	6 sec.	3/1
Subject 4 (100%)	6 sec.	4/1
Subject 5 (100%)	7 sec.	2/1
Mean HRF (SD)	6.2 sec. ($\pm$ 0.8)	3.6/1($\pm$ 2.1)
p-value for Motor vs. visual	0.033	0.03

Table 7.7 Comparison of the individual 100% and mean HRF signals for the visual data set.

Table 7.8 shows a comparison between the mean finger tapping (Data Set 1) HRF and the mean visual (Data Set 3) HRF signal:

	Time to Peak	Ratio of +ve to –ve amplitude
Mean HRF (Data Set 1)	5 sec.	6/1
Mean HRF (Data Set 3, 100% contrast)	6 sec	5/1
Mean HRF (Data Set 3, 10% contrast)	6 sec.	5/1

Table 7.8 Comparison of the mean 100% visual, 10% visual and finger tapping HRF signals.

We can conclude from the above results that the HRF signal varies between the somatosensory cortex and the visual cortex, and that there are differences between the SPM HRF and the mean HRFs extracted from the finger tapping data (Data Set 1) and the visual data (Data Set 3). There are also very clear differences between the subject's individual HRF signals and the mean signal in terms of the time to peak and the ratio of +ve to –ve amplitude.

The next step was to look for activation using the extracted mean unsmoothed predicted activation signal for the finger tapping, which is shown in Fig. 7.30, and the SPM activation signal for the data shown in Fig. 7.33. Figure 7.29 shows the unsmoothed mean extracted HRF. Figure 7.31 shows an interpolated smoothed mean HRF signal and Figure 7.32 shows the SPM HRF signal.

Finger tapping set with threshold = 0.68, the threshold was chosen to be the highest threshold to give any activation.

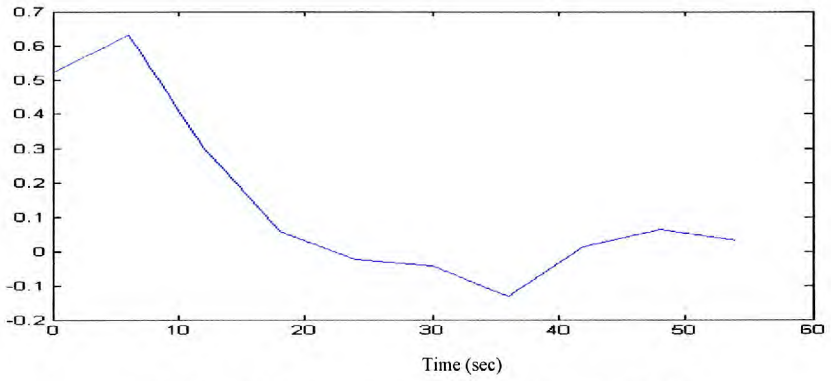

Fig. 7.29 Unsmoothed mean extracted HRF.

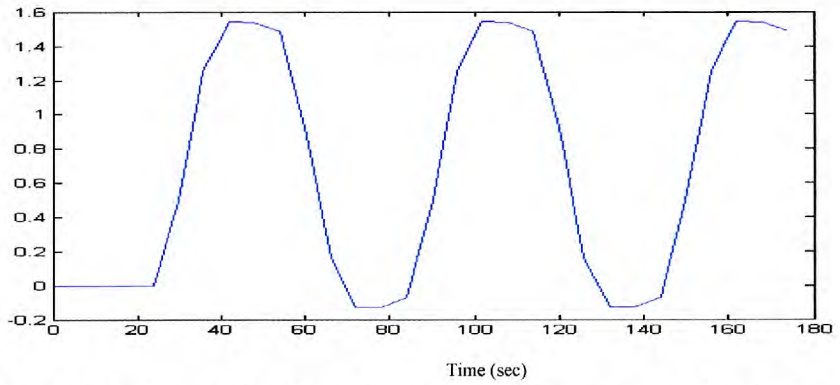

Fig. 7.30 Unsmoothed mean extracted HRF convolved with the boxcar signal.

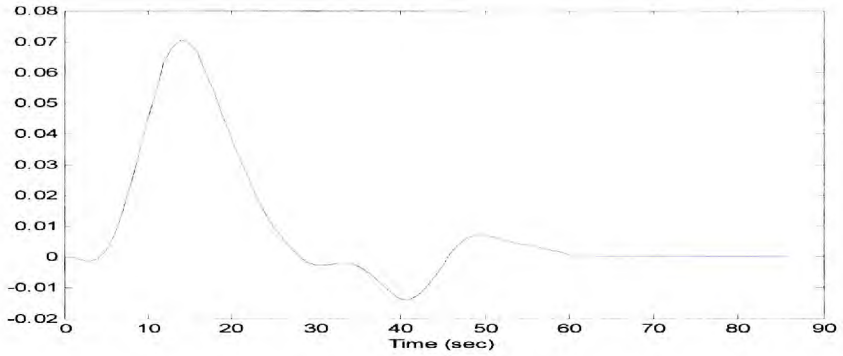

Fig. 7.31 Interpolated smoothed mean HRF (samples at 0.375 per sec.).

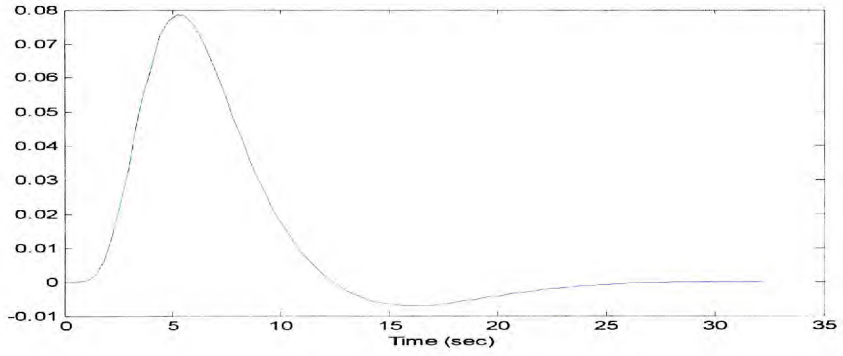

Fig. 7.32 SPM HRF signal.

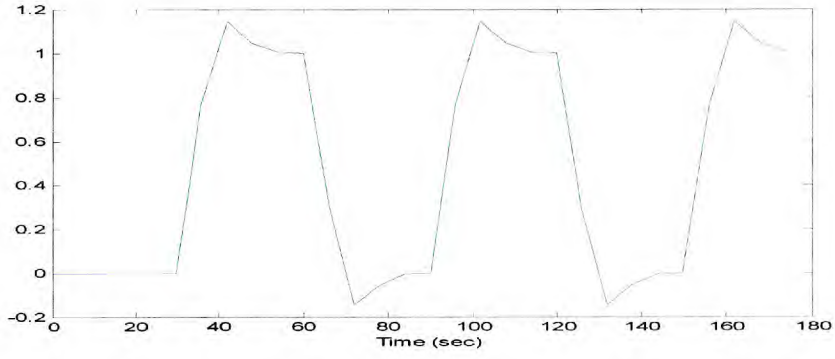

Fig. 7.33 SPM HRF signal convolved with the boxcar signal.

Some of the results are shown below. The activation is superimposed on the slice with the maximum activation, and the graph to the right shows the time series at that particular voxel with the maximum activation.

Week 17: max. activation using the extracted mean unsmoothed predicted activation signal = 0.82 in slice 8 with cluster size of 4 as shown in figure 7.34

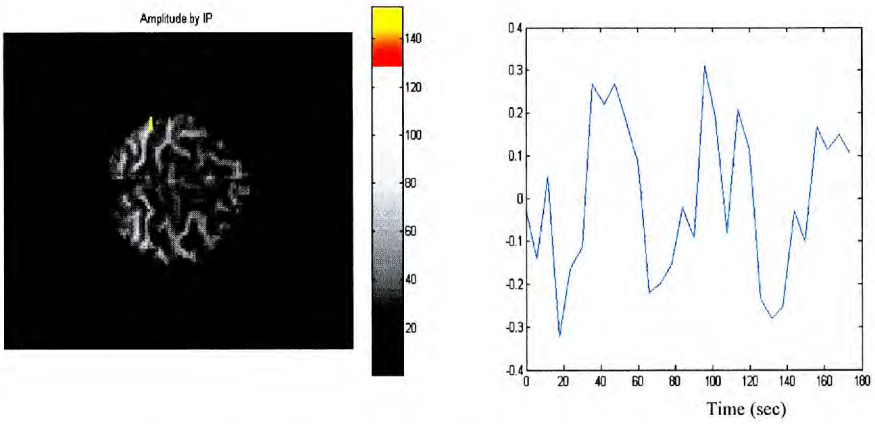

Fig. 7.34 Activation superimposed on brain and plot of active voxel at maximum activation.

Maximum activation using the SPM activation signal = 0.79 in slice 8 with a total number of 3 voxels in the cluster as shown in Figure 7.35.

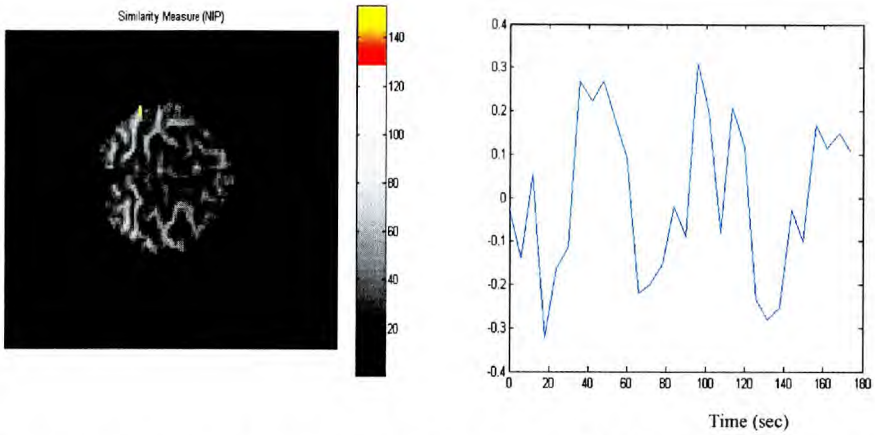

Fig. 7.35 Activation superimposed on brain and plot of active voxel at maximum activation.

From the Figures 7.34 and 7.35 above we can see that the graphs on the right hand side are identical which shows the time series at the voxel with the maximum activation.

The same process was repeated for the visual data using the extracted mean predicted activation signal shown in Figure 7.37 and the SPM activation signal for the data shown in Figure 7.39 with a threshold of 0.6. Again the threshold was chosen to be the highest threshold to give any activation.

Figure 7.36 shows the unsmoothed mean extracted HRF and Figure 7.38 shows the SPM HRF signal.

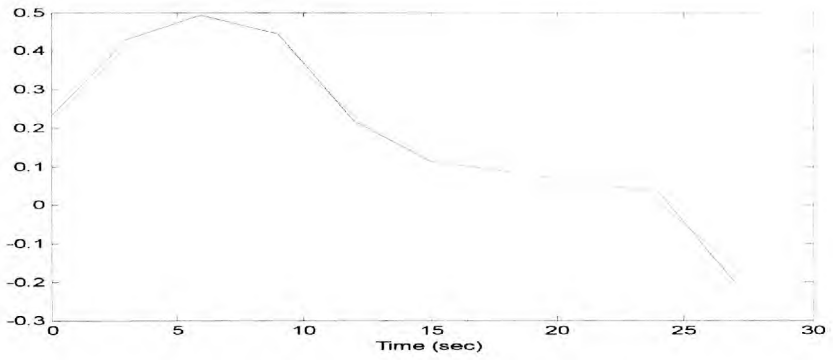

Fig. 7.36 Unsmoothed mean extracted HRF.

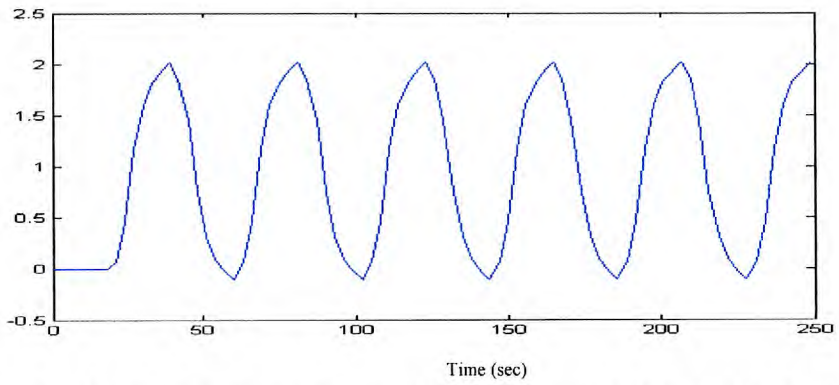

Fig. 7.37 Unsmoothed mean extracted HRF convolved with the boxcar signal.

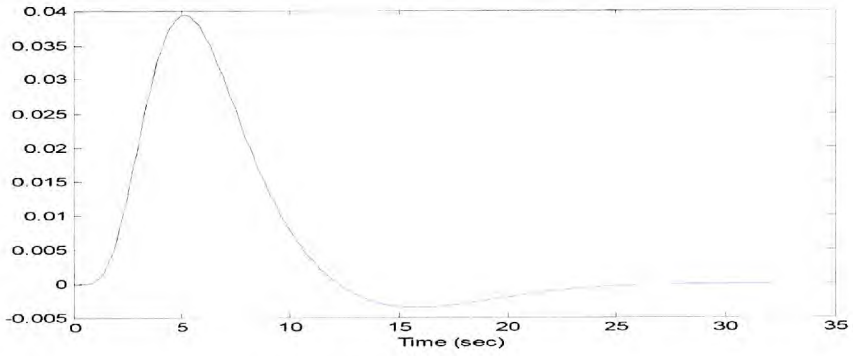

Fig. 7.38 SPM HRF signal.

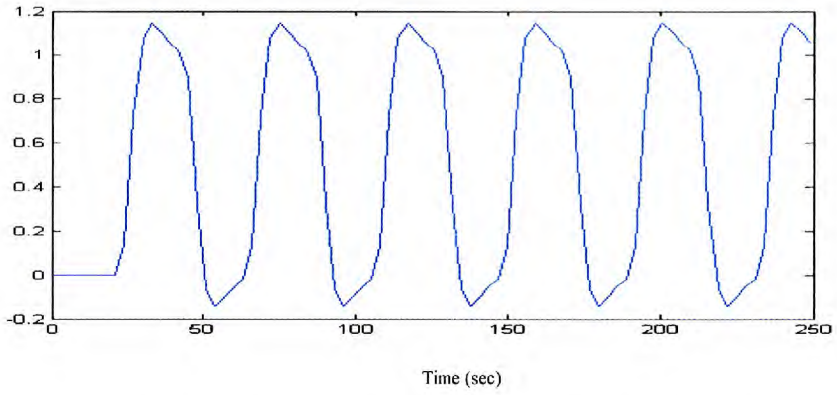

Fig. 7.39 SPM HRF signal convolved with the boxcar signal.

Some of the results are shown below. The activation is superimposed on the slice with the maximum activation and the graph to the right shows the time series at that particular voxel with the maximum activation.

Subject 1:

Maximum activation using the extracted mean unsmoothed predicted activation signal = 0.82 in slice 8 with a total number of 8 voxels in the cluster as shown below in figure 7.40.

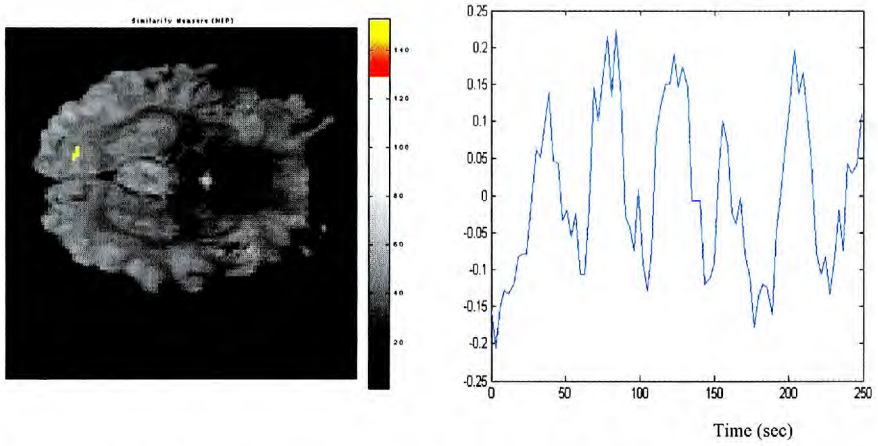

Fig. 7.40 Activation superimposed on brain and plot of active voxel at maximum activation.

Maximum activation using the SPM activation signal = 0.80 in slice 8 with a total number of 8 voxels in the cluster as shown in figure 7.41.

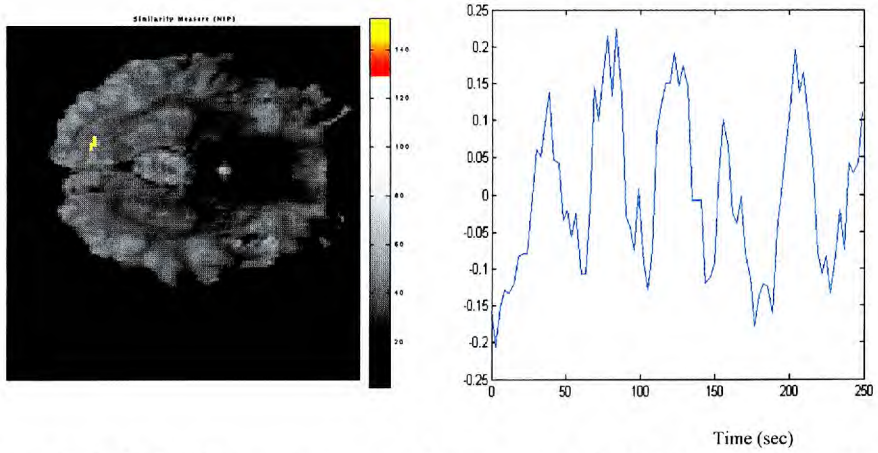

Fig. 7.41 Activation superimposed on brain and plot of active voxel at maximum activation.

Again the Figures 7.40 and 7.41 above show that the graphs on the right hand side are identical which represents the time series at the voxel with the maximum activation.

The same process was repeated for the realigned finger tapping data and the realigned 100% contrast visual data.

Type-I and Type-II errors concept can be applied to the results obtained as shown in Table 7.9 below, which represents a scheme for comparing the results of different method of activation detection.

Statistical Decision	State of the null hypothesis of the correlation method	
	Correlation method results: activation.	Correlation method results: no activation.
SPM results: Reject Null Hypothesis (no activation)	incorrect	correct
SPM results: Accept Null Hypothesis (activation present)	correct	incorrect

Table 7.9 Scheme for comparing results of different methods of activation detection.

The results are summarized below in Tables 7.10 to 7.13:

	Active set using mean HRF	Inactive set using mean HRF
Inactive set using SPM HRF	20	34454
Active set using SPM HRF	24	1

Table 7.10 Finger tapping results.

	Active set using mean HRF	Inactive set using mean HRF
Inactive set using SPM HRF	4	84690
Active set using SPM HRF	33	0

Table 7.11 Visual data 100% contrast results.

	Active set using mean HRF	Inactive set using mean HRF
Inactive set using SPM HRF	19	34157.5
Active set using SPM HRF	23	1.5

Table 7.12 Realigned finger tapping results.

	Active set using mean HRF	Inactive set using mean HRF
Inactive set using SPM HRF	10	84292
Active set using SPM HRF	115	7

Table 7.13 The Realigned visual data 100% contrast results.

In the tables 7.10 -7.13 above, the active/active cell contains the total number of voxels that are active in the data set analysed using SPM HRF and the data set analysed using the mean HRF. The inactive/active cells contain the total number of voxels that are active in the data using SPM HRF but inactive in the data using mean HRF and vice versa. The inactive/inactive cell contains the total number of voxels that are inactive in the data analysed using both SPM HRF and the mean HRF. The above results were represented in the form of Receiver Operating Characteristic (ROC) curves for different thresholds [121]. The curves represent a trade-off between sensitivity and specificity [85]. ROC curves are plotted using α (Type I error) and 1-β (where β is the Type II error). The intersection of the 45° line with the α vs. 1-β plot indicates the threshold for which Type-I and Type-II errors have equal values [81].

For the purpose of creating the ROC curves, the above procedure was repeated for the realigned finger tapping data, the realigned 100% contrast visual data and the realigned 10% contrast visual data, with 10 different thresholds. For the finger tapping data, the threshold range was between 0.068 and 0.68 with increments of 0.068. For the 5 subject visual data, the threshold range was between 0.06 and 0.6 with increments of 0.06. The results are shown below.

ROC curves for finger tapping data (Data Set 1):

All the sessions were realigned with each other using SPM. The realigned data were then analysed for active areas with 10 different thresholds using the SPM activation signal and the mean predicted activation signal. The true active area was chosen by cross analysing all the active areas for the sessions obtained using the SPM signal at maximum activation as shown in the "True Active Recipe" below:

- Realign the 100% contrast and the 10% contrast for each subject together (Data Set 3) and all sessions together (Data Set 1).
- Find the maximum activation using the SPM HRF at a very high threshold (the highest threshold that would produce activation).
- Choose a 3D cluster that is active in both contrasts for each subject (Data Set 3) and in all sessions (Data Set 1).
- This cluster is used as the gold standard.

The true active cluster for the finger tapping data (Data Set 1) was chosen to be a 1x2x3 cluster of coordinates (44 , 52:53 , 6:8).

The ideal ROC curve should have an immediate sharp rise to the saturation point of 1 (True Positive) and continues at that level. We found the ROC curves to give better results for finding activation using the mean predicted

activation signal compared to SPM activation signal in 10 cases out of 14 and only one case shows a better result using the SPM activation signal. Some of the results are shown in Fig. 7.42 and 7.43 below.

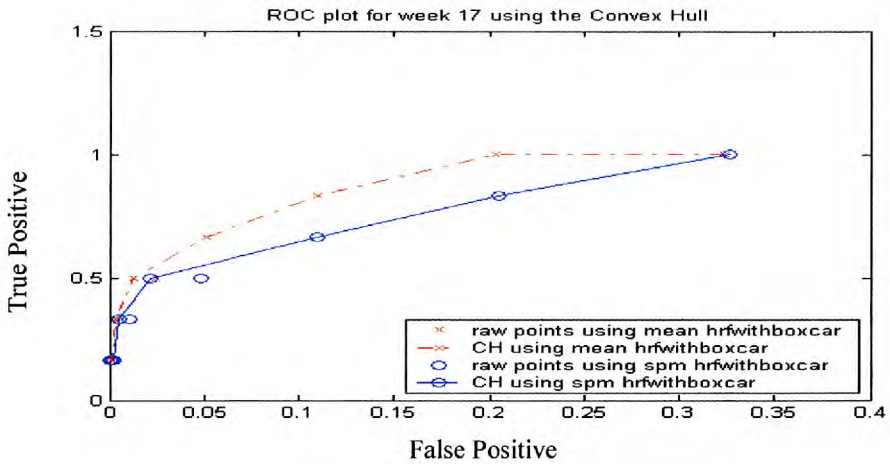

Fig. 7.42 ROC curve for the realigned week 17.

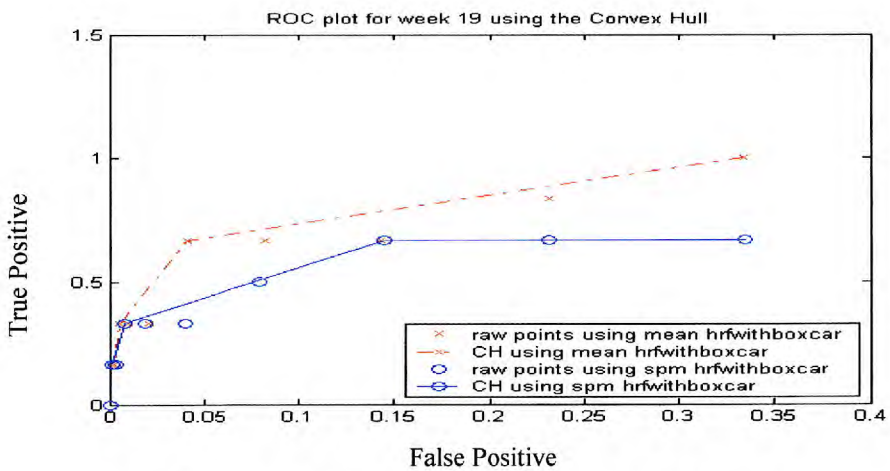

Fig. 7.43 ROC curve for the realigned week 19.

The above figures show better results using the mean predicted activation signal compared to the SPM activation signal.

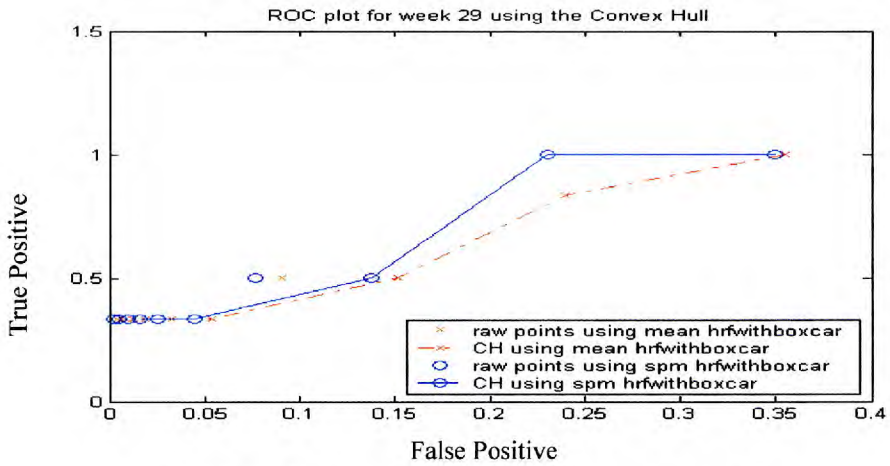

Fig. 7.44 ROC curve for the realigned week 29.

Figure 7.44 above shows better results using the SPM activation signal compared to the mean predicted activation signal.

ROC curves for the Visual data (Data Set 3):

The 100% contrast data was realigned with the 10% contrast data. The realigned data were then analysed for active areas with 10 different thresholds using the SPM activation signal and the mean predicted activation signal. The true active cluster was chosen by cross analysing the active areas obtained using the SPM signal for the 100% contrast and the 10% contrast at maximum activation. The true active cluster was chosen for each subject independently. The true active cluster for subject 1 is 2x4x2 cluster with coordinates of (18:19 , 72:75 , 8:9). The true active cluster for subject 2 is 1x5x3 cluster with coordinates of (19 , 8:10 , 67:71). The true active cluster for subject 3 is 2x3x3 cluster with coordinates of (18:19 ,

67:69 , 8:10). The true active cluster for subject 4 is 2x1x3 cluster with coordinates of (19:20 , 53 , 8:10). The true active cluster for subject 5 is 1x2x2 cluster with coordinates of (20 , 75:76 , 9:10). The ROC curves are shown in the Figures 7.45 to 7.49 below:

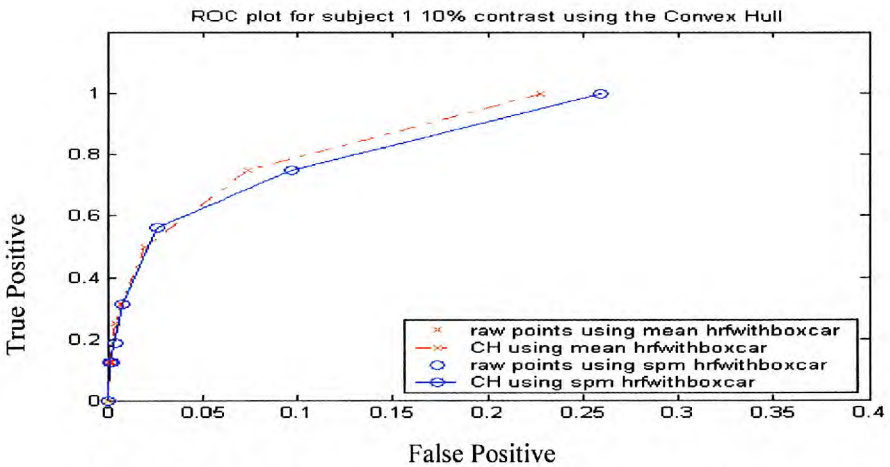

Fig. 7.45 ROC curve for the realigned 10% contrast subject 1.

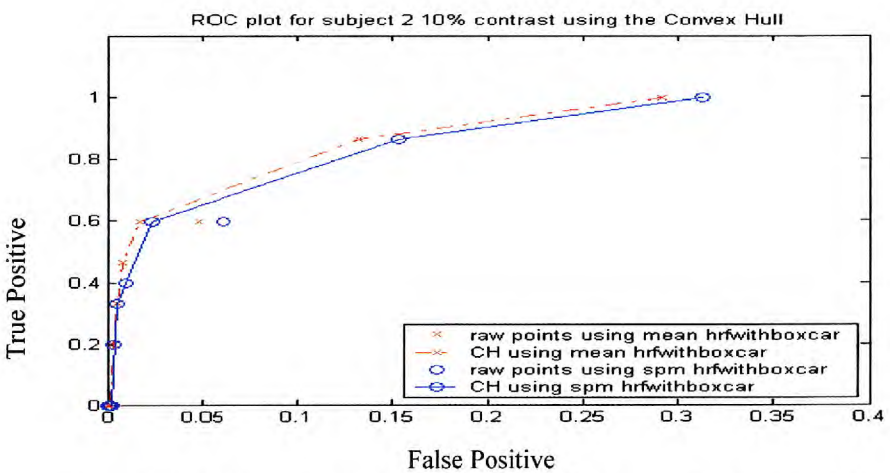

Fig. 7.46 ROC curve for the realigned 10% contrast subject 2.

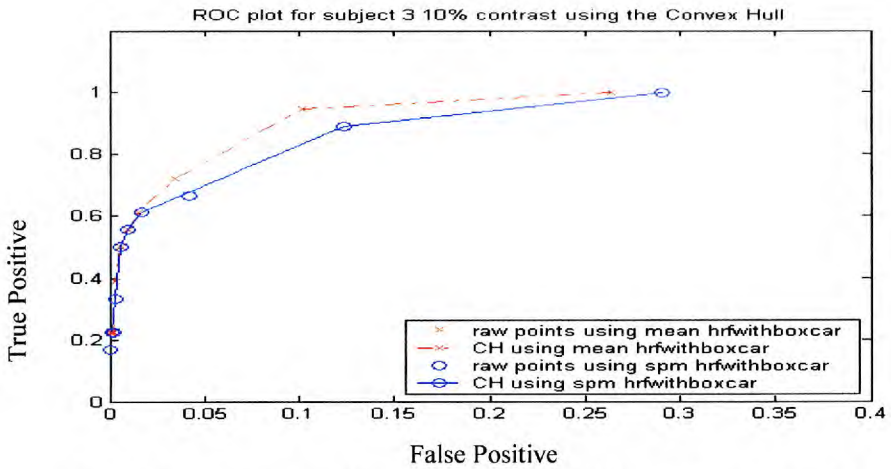

Fig. 7.47 ROC curve for the realigned 10% contrast subject 3.

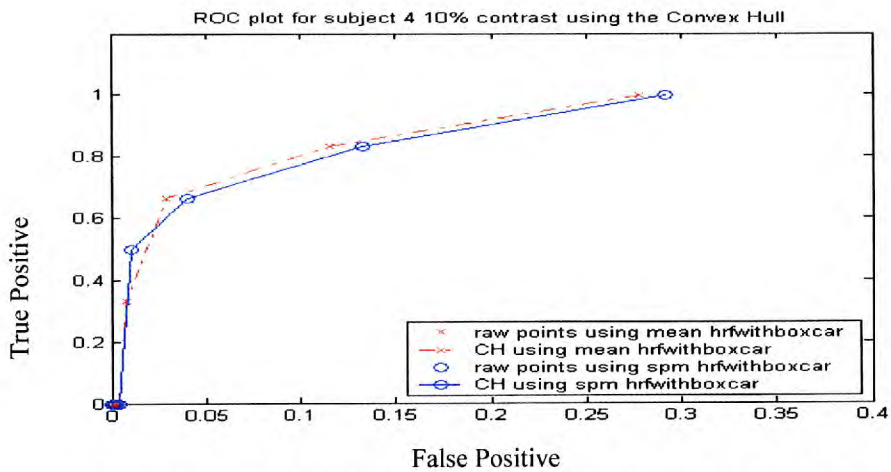

Fig. 7.48 ROC curve for the realigned 10% contrast subject 4.

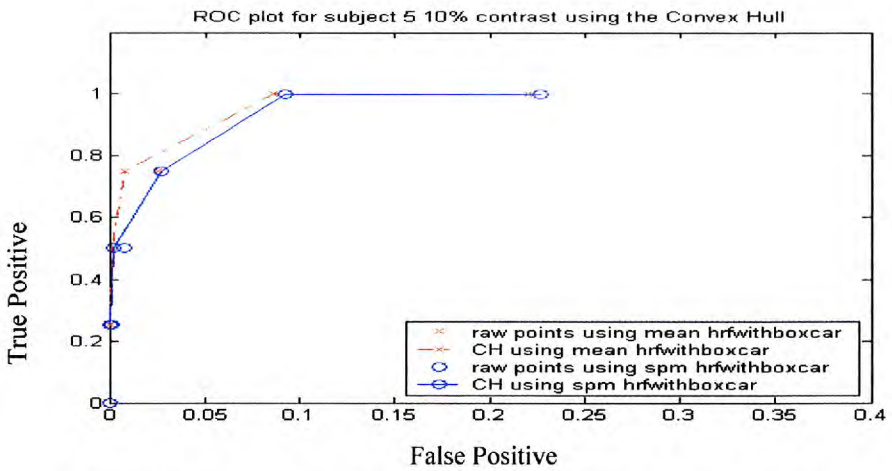

Fig. 7.49 ROC curve for the realigned 10% contrast subject 5.

All the figures above show better results using the mean predicted activation signal compared to the SPM activation signal. Our choice of the True Active cluster in the above analysis is conservative, as there is the possibility that for low thresholds, the false positive count is elevated artifactually which results in the flattening of the ROC curve, therefore the most important part of the ROC curve is the initial slope.

An important issue to consider is the validation of the ROC curve. To do that we looked at ROC curves for a randomized realigned finger tapping session. Week 17 was chosen for the randomization. The 100 run randomization was created using a *Matlab* command. The results for the first 5 runs are shown below:

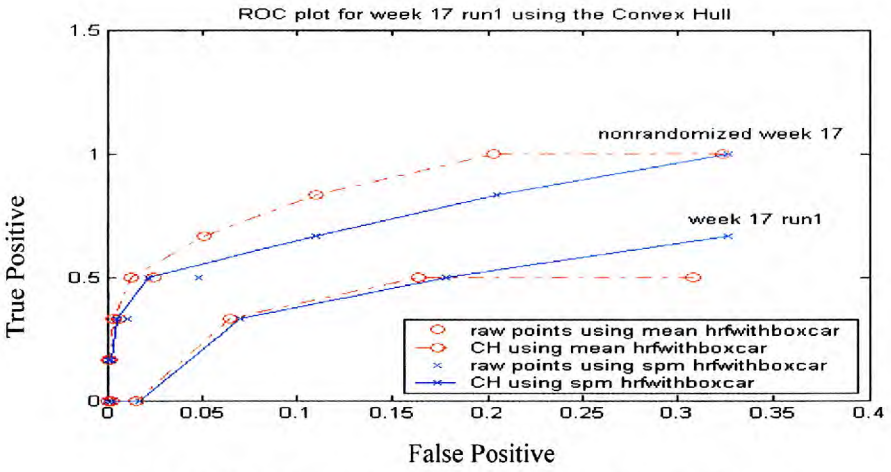

Fig. 7.50 ROC curve for the realigned week 17 run1.

Figure 7.50 above shows the ROC curve for the realigned week 17 run 1. It is obvious from the curve that the randomized data show a flatter curve in comparison to the non-randomized data. The results of the other 4 runs are shown in Figures 7.51 to 7.54 below:

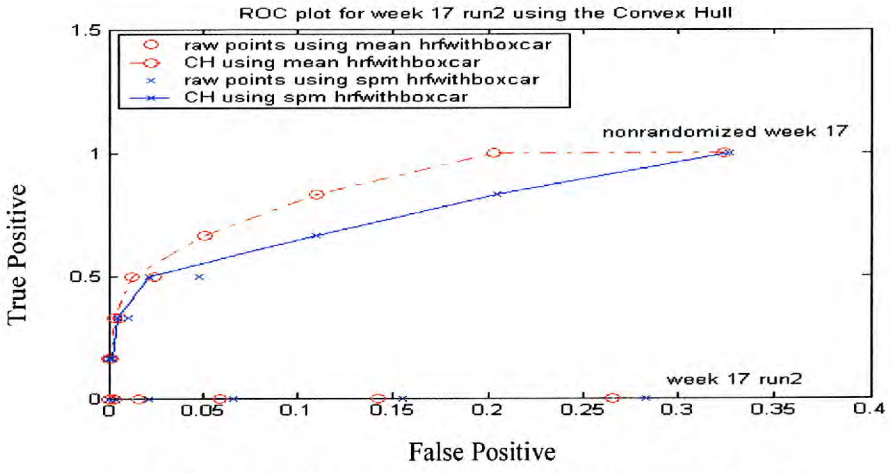

Fig. 7.51 ROC curve for the realigned week 17 run2.

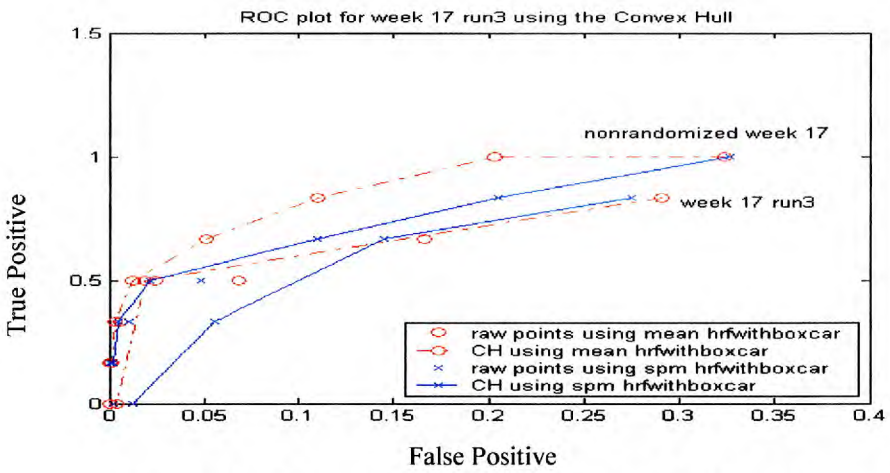

Fig. 7.52 ROC curve for the realigned week 17 run3.

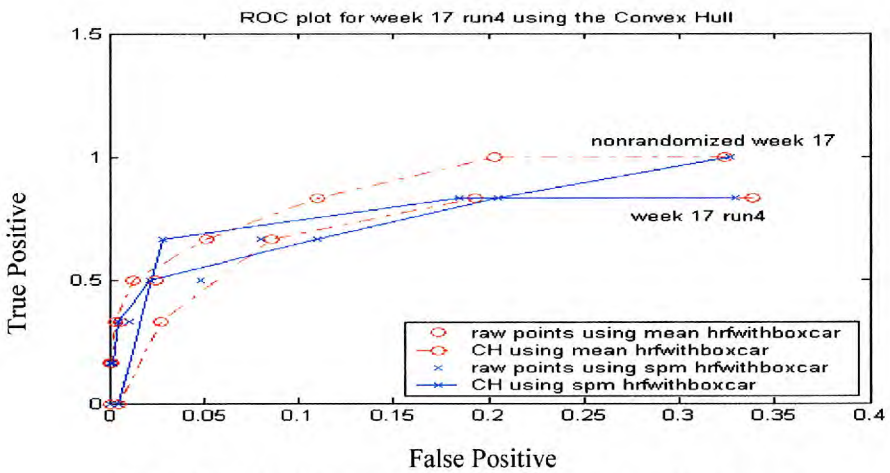

Fig. 7.53 ROC curve for the realigned week 17 run4.

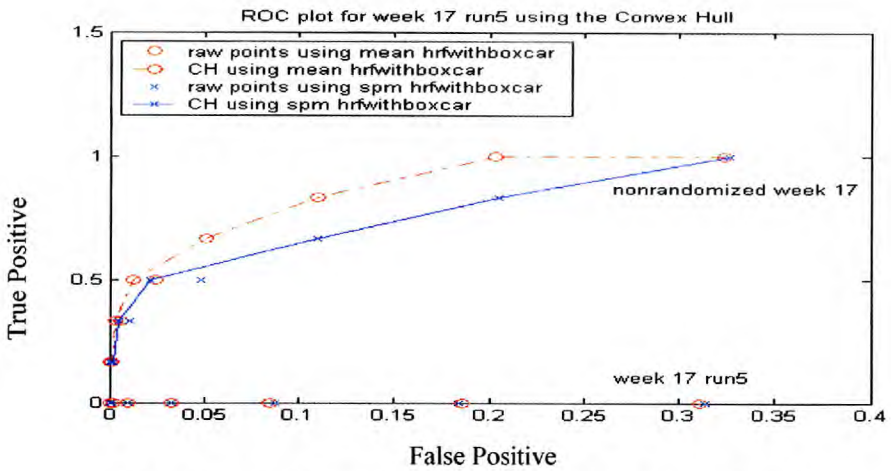

Fig. 7.54 ROC curve for the realigned week 17 run5.

Overall, the results show that the randomized data have a flatter curve in comparison to the non-randomized data. Some of the randomized results illustrate the presence of activation. This is due to the fact that the randomization process does not take into account the on-off pattern, and it was noted that some of the randomized sequences did have a structured format. Repeating the analysis for 100 runs, it was found that there is no significant difference between results obtained using the mean hrfwithboxcar compared to those obtained using the SPM hrfwithboxcar signal. Consulting a statistician[3], we found that although it is possible to plot the mean ROC curves, it was not possible to plot the mean pseudo ROC curve. Therefore the mean false positive signal versus the threshold was presented as shown below in Figure 7.55.

[3] Dr. JefferyNg Sing Kwong, Imperial College London

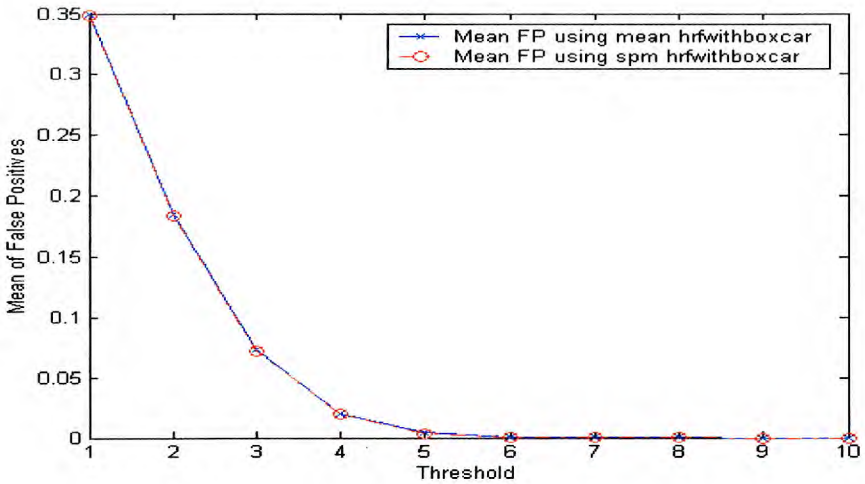

Fig. 7.55 Mean of False Positives vs. the Threshold.

We can also see that as the threshold increases, the number of false positives decreases.

The variance of the false positives from the mean also seem to be very small as shown below in Figure 7.56.

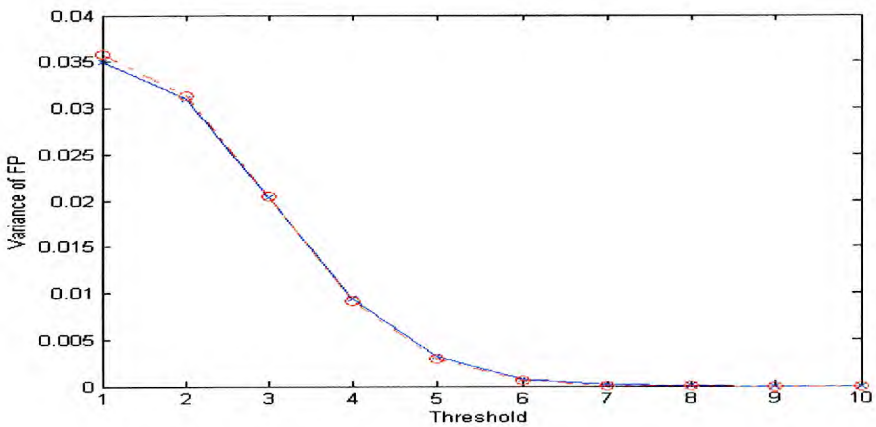

Fig. 7.56 Variance of False Positives from the mean.

7.5 Clinical Application

Two data sets are acquired from 5 subjects with a known tumour on the right side of the brain. The first set was a left hand finger tapping while the other set is a right hand finger tapping. The data were acquired using a Siemens 1.5 T Vision scanner. The data are BOLD EPI fMRI multi slice images of 128x128 pixels, where each volumetric data set is composed of 14 slices and each session is composed of 35 volumes (the first 5 volumes were discarded from the analysis to avoid T_1 effects in the initial scans). TR = 6 seconds. The tapping followed an off-on pattern (boxcar function) for 5 volumes each.

Figures 7.57 and 7.58 show the results for the realigned right hand finger tapping using SPM2 and the correlation method respectively for patient 1.

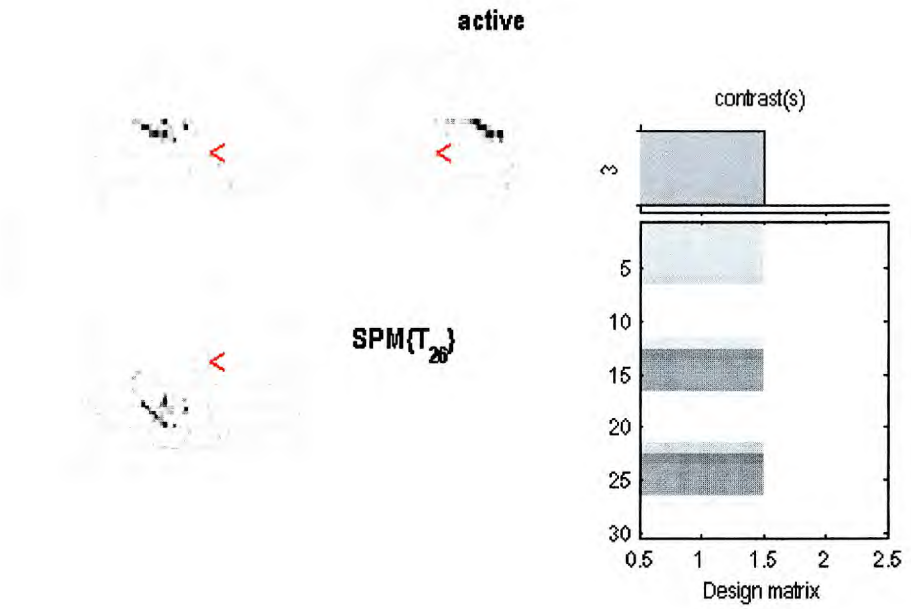

Fig. 7.57 SPM2 results for the right finger tapping activation.

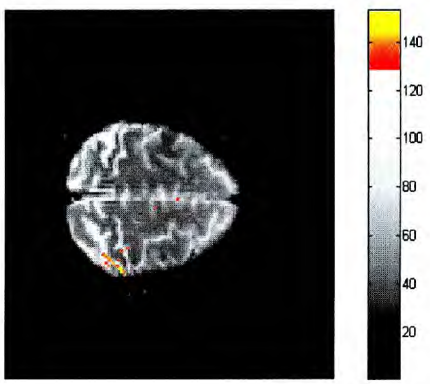

Fig. 7.58 The correlation method results for the right finger tapping activation using the SPM activation signal (patient 1).

Maximum activation is found in slice 11 with a similarity measure of 0.914. The HRF signal at maximum activation (46,38,11) is shown below in Figure 7.59.

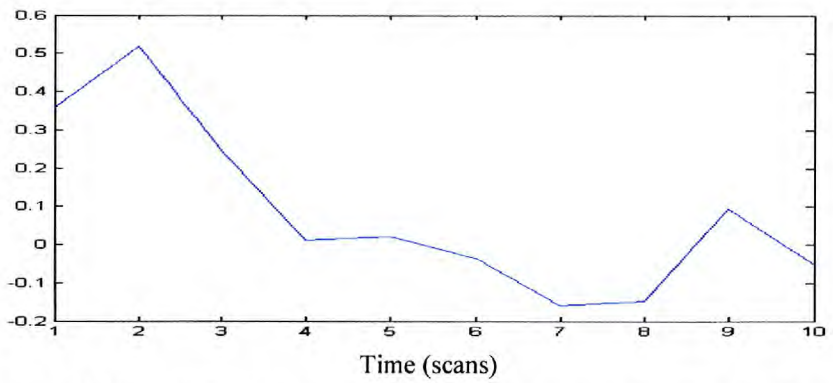

Fig. 7.59 HRF signal extracted from the maximum activation (patient 1 – right hand).

The process was repeated for the other 4 patients and their individual HRF signals are shown below in figures 7.60 to 7.63:

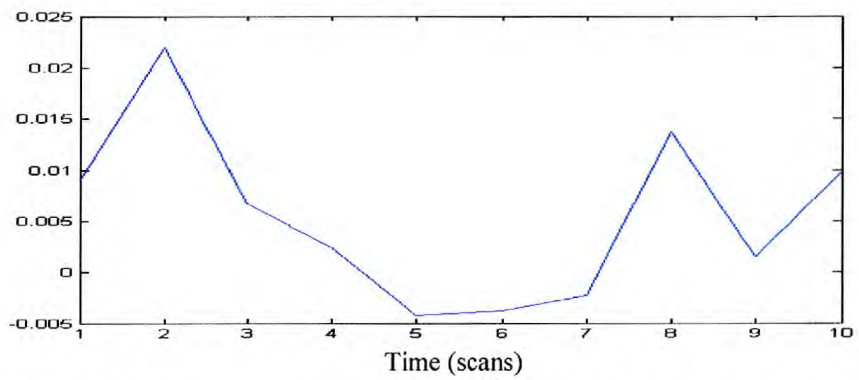

Fig. 7.60 HRF signal extracted from the maximum activation (patient 2 – right hand).

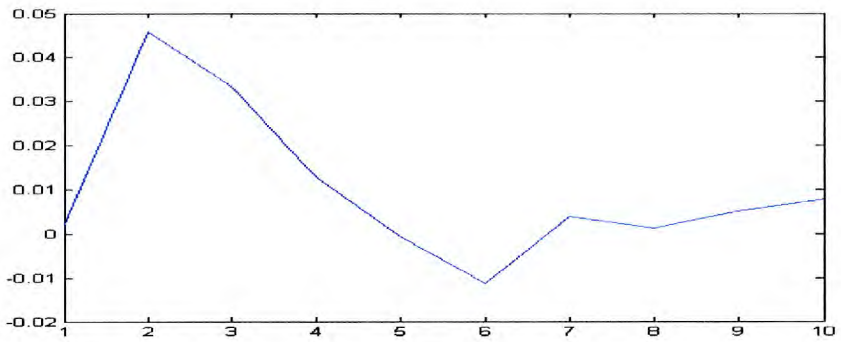

Fig. 7.61 HRF signal extracted from the maximum activation (patient 3 – right hand).

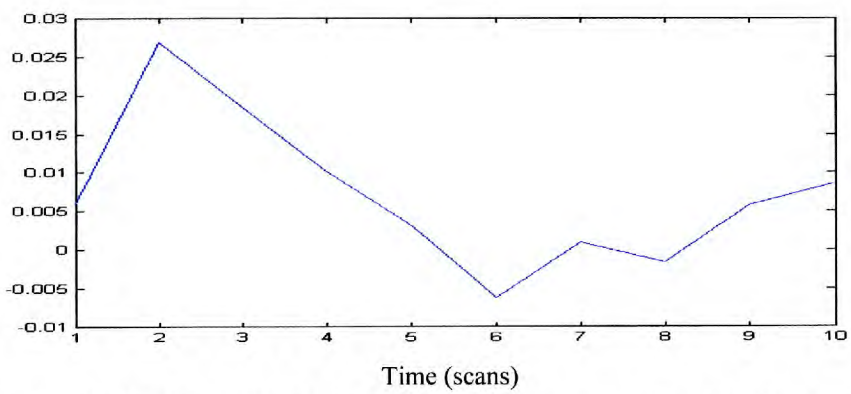

Fig. 7.62 HRF signal extracted from the maximum activation (patient 4 – right hand).

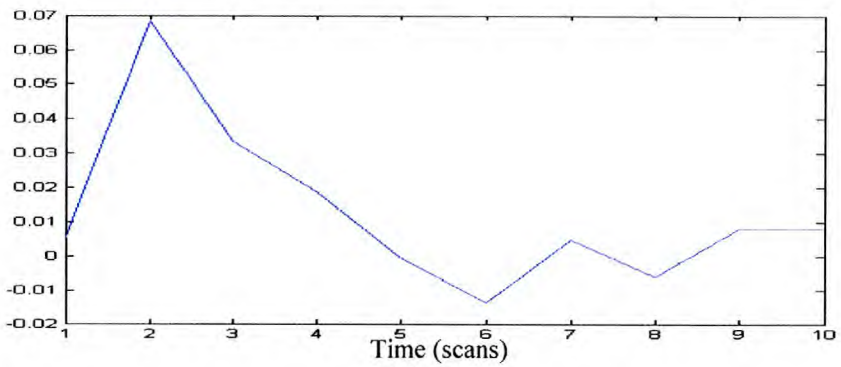

Fig. 7.63 HRF signal extracted from the maximum activation (patient 5 – right hand).

The mean HRF signal for the right hand finger tapping was then calculated and the signal is shown below in figure 7.64:

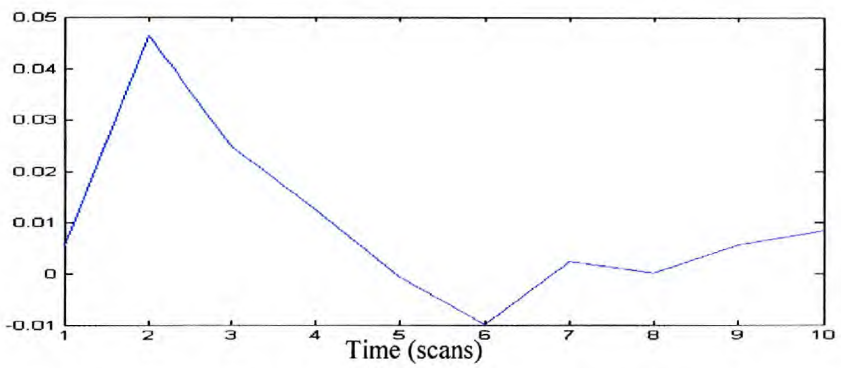

Fig. 7.64 The mean of the HRF signals extracted from the maximum activation across patients (right hand).

And the mean hrfwithboxcar signal is shown below:

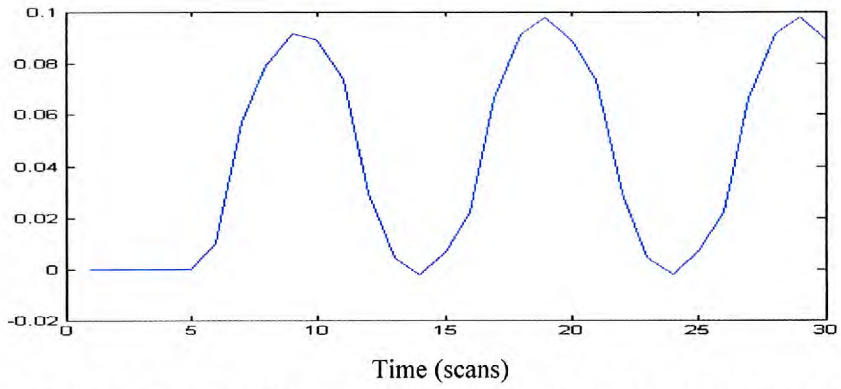

Fig. 7.65 The mean HRF signal convolved with the boxcar signal (right hand).

The process was repeated using the mean extracted HRF signal and the results are shown below in Figures 7.66 to 7.70.

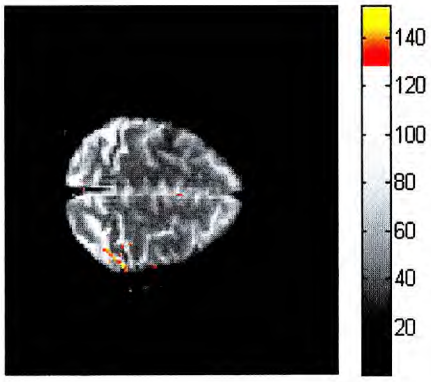

Fig. 7.66 The correlation method results for the right finger tapping activation using the mean extracted activation signal for patient 1.

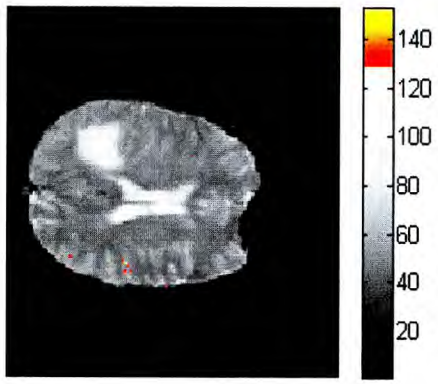

Fig. 7.67 The correlation method results for the right finger tapping activation using the mean extracted activation signal for patient 2.

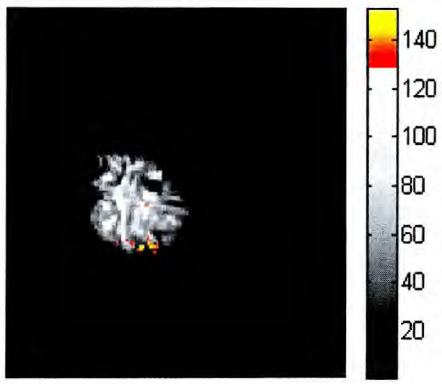

Fig. 7.68 The correlation method results for the right finger tapping activation using the mean extracted activation signal for patient 3.

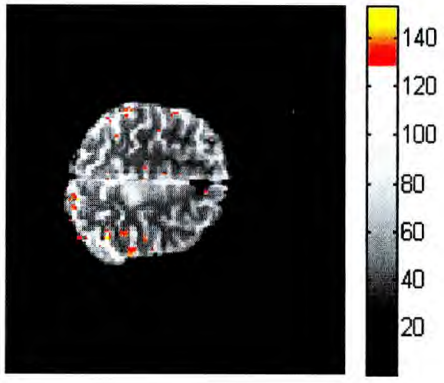

Fig. 7.69 The correlation method results for the right finger tapping activation using the mean extracted activation signal for patient 4.

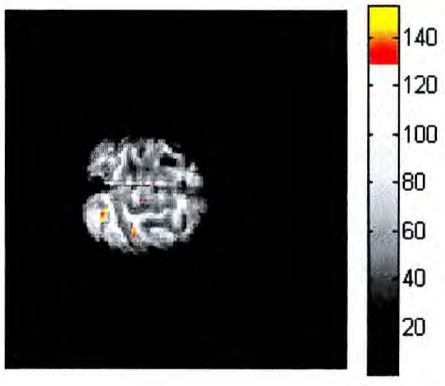

Fig. 7.70 The correlation method results for the right finger tapping activation using the mean extracted activation signal for patient 5.

The maximum activation is found in slice 11 (for patient 1) with a similarity measure of 0.91. The table below summarises the data for all subjects:

Right Hand	Patient1	Patient2	Patient3	Patient4	Patient5
SPM HRF	0.91	0.75	0.86	0.86	0.76
Mean HRF	0.91	0.75	0.84	0.91	0.76

Table 7.14 summary of the similarity measure results for each patient using the SPM HRF and the mean extracted HRF signals (right hand).

From the results above we can conclude that there is no real difference in regards to the similarity measure between the data analysis using the SPM HRF and the mean HRF for the right hand.

The true active cluster for the finger tapping data was chosen to be a 2x1x2 cluster of coordinates (45:46 , 83 , 11:12). The ROC curve for the results obtained using the SPM activation signal and the mean extracted predicted activation signal is shown in Figure 7.71.

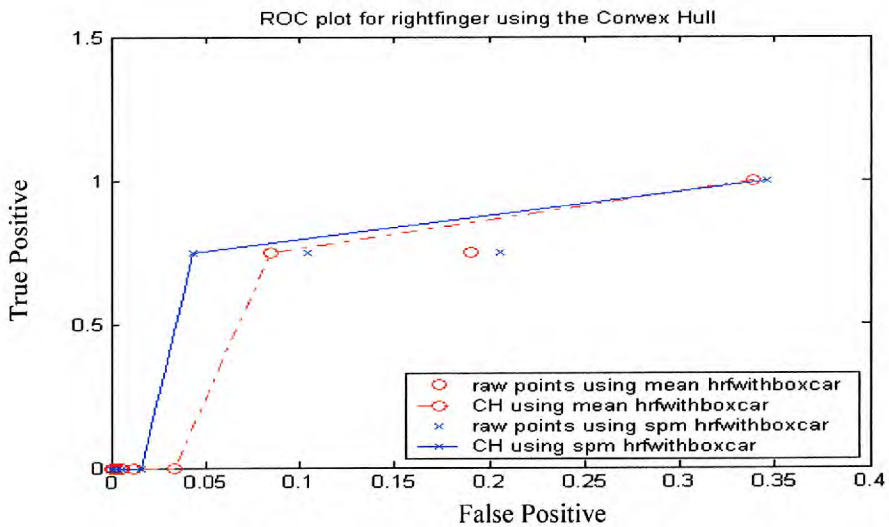

Fig. 7.71 ROC curve for the realigned right finger tapping.

The ROC curve above shows better results using the SPM HRF compared to the results using the mean HRF.

The process was repeated for the realigned left hand finger tapping and Figures 7.72 and 7.73 show the results for the realigned left hand finger tapping using SPM2 and the correlation method respectively for patient 1.

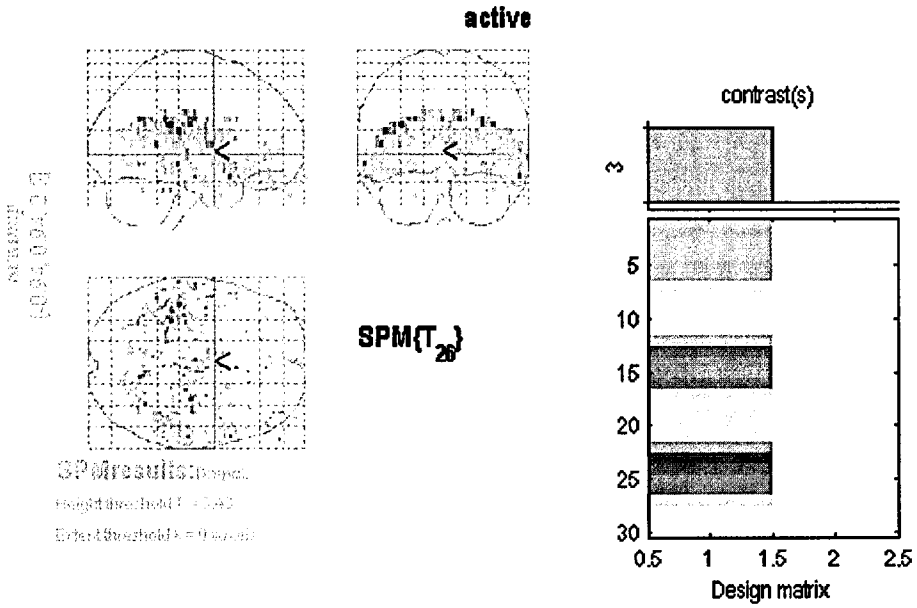

Fig. 7.72 SPM2 results for the left finger tapping activation (patient 1 – left hand).

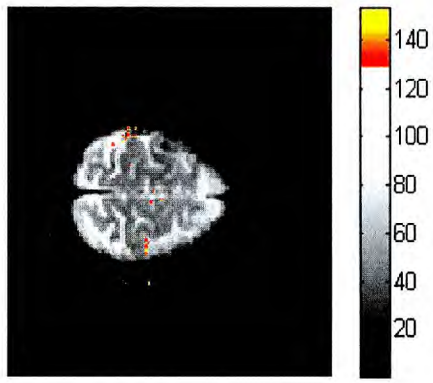

Fig. 7.73 The correlation method results for the left finger tapping activation using the SPM activation signal (patient 1 – left hand).

Maximum activation is found in slice 12 with a similarity measure of 0.913. The HRF signal at maximum activation (82,46,12) is shown below in Figure 7.74.

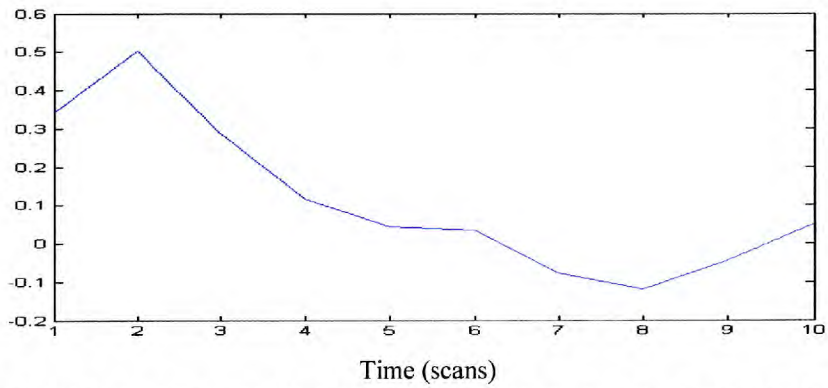

Fig. 7.74 HRF signal extracted from the maximum activation (patient 1 – left hand).

The process was repeated for the other 4 patients and their individual HRF signals are shown below in figures 7.75 to 7.78:

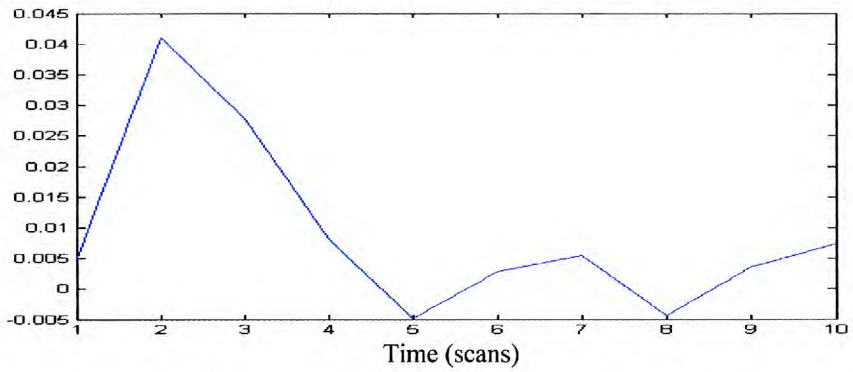

Fig. 7.75 HRF signal extracted from the maximum activation (patient 2 – left hand).

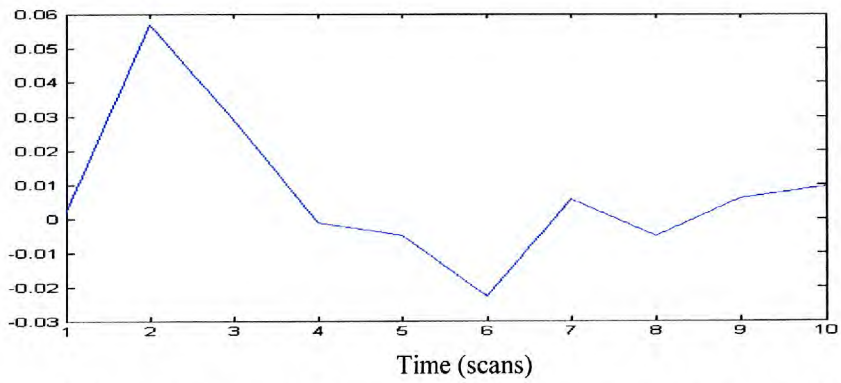

Fig 7.76 HRF signal extracted from the maximum activation (patient 3 – left hand).

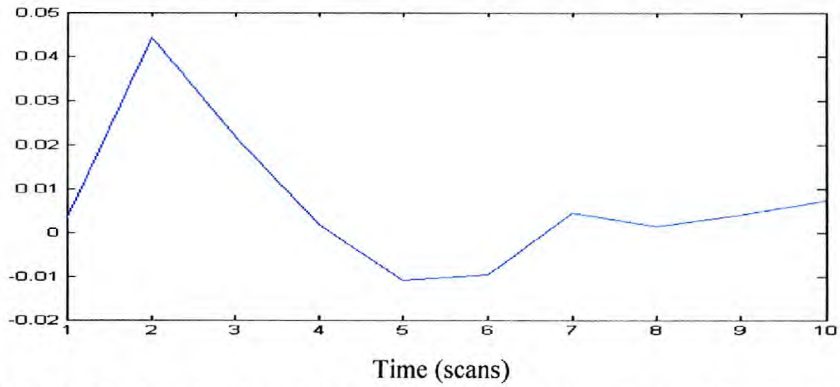

Fig 7.77 HRF signal extracted from the maximum activation (patient 4 – left hand).

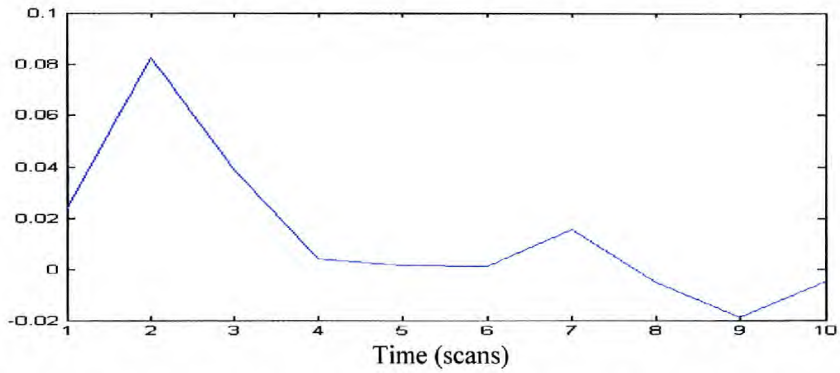

Fig 7.78 HRF signal extracted from the maximum activation (patient 5 – left hand).

The mean HRF signal for the right hand finger tapping was then calculated and the signal is shown below in figure 7.79.

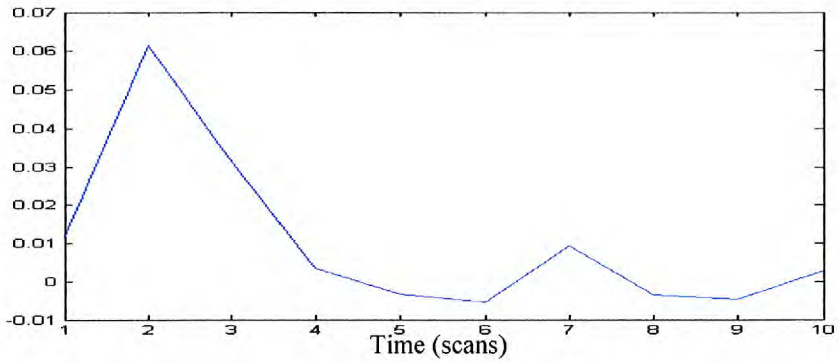

Fig 7.79 The mean of the HRF signals extracted from the maximum activation across patients (left hand).

And the mean hrfwithboxcar signal is shown below:

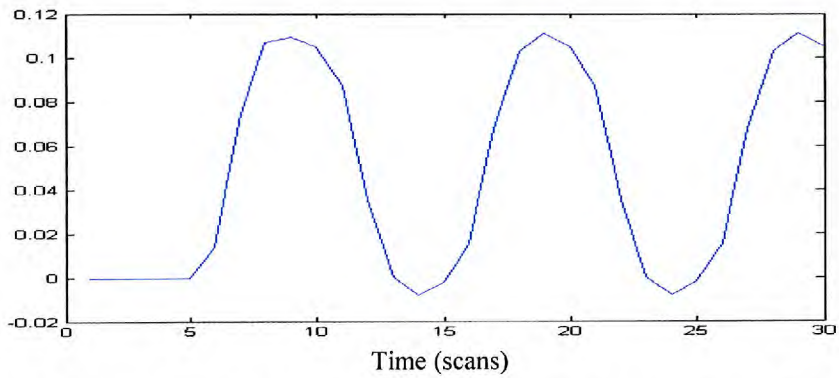

Fig 7.80 The mean HRF signal convolved with the boxcar signal (left hand).

The process was repeated using the mean extracted HRH signal and the results are shown below in Figures 7.81 to 7.85.

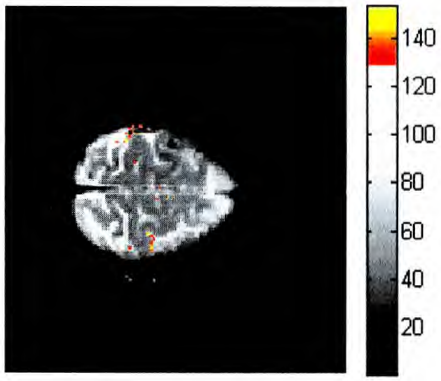

Fig. 7.81 The correlation method results for the left finger tapping activation using the mean extracted activation signal (patient 1).

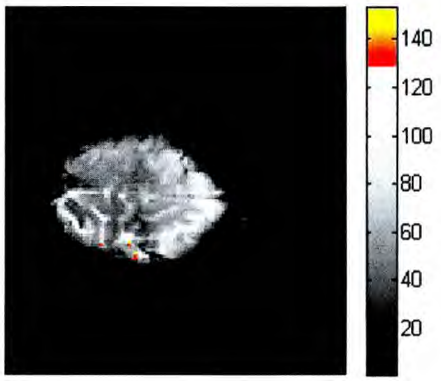

Fig 7.82 The correlation method results for the left finger tapping activation using the mean extracted activation signal (patient 2).

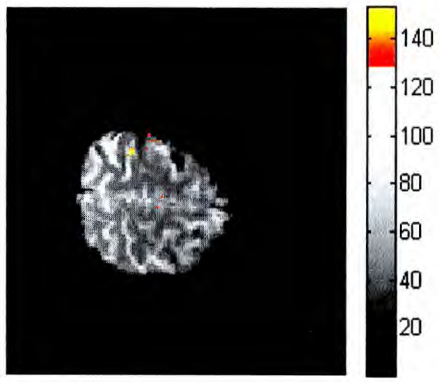

Fig 7.83 The correlation method results for the left finger tapping activation using the mean extracted activation signal (patient 3).

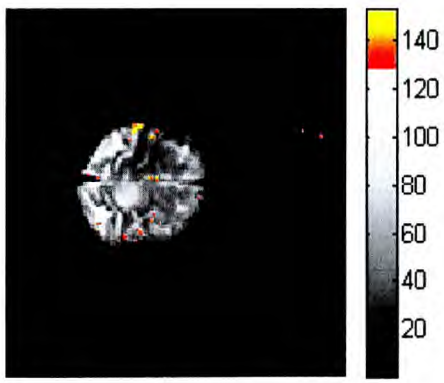

Fig 8.84 The correlation method results for the left finger tapping activation using the mean extracted activation signal (patient 4).

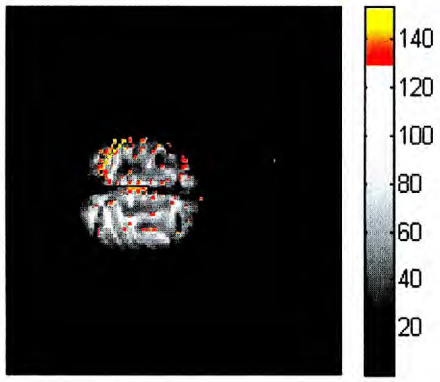

Fig 8.85 The correlation method results for the left finger tapping activation using the mean extracted activation signal (patient 5).

The maximum activation is found in slice 12 (for patient 1) with a similarity measure of 0.905. The table below summarises the data for all subjects:

Left Hand	Patient1	Patient2	Patient3	Patient4	Patient5
SPM HRF	0.91	0.82	0.85	0.87	0.86
Mean HRF	0.92	0.81	0.85	0.87	0.88

Table 7.15 summary of the similarity measure results for each patient using the SPM HRF and the mean extracted HRF signals (left hand).

From the results above we can conclude that there is no real difference in regards to the similarity measure between the data analysis using the SPM HRF and the mean HRF for the left hand.

The ROC curve for the results obtained using the SPM activation signal and the extracted predicted activation signal is shown in Figure 7.86.

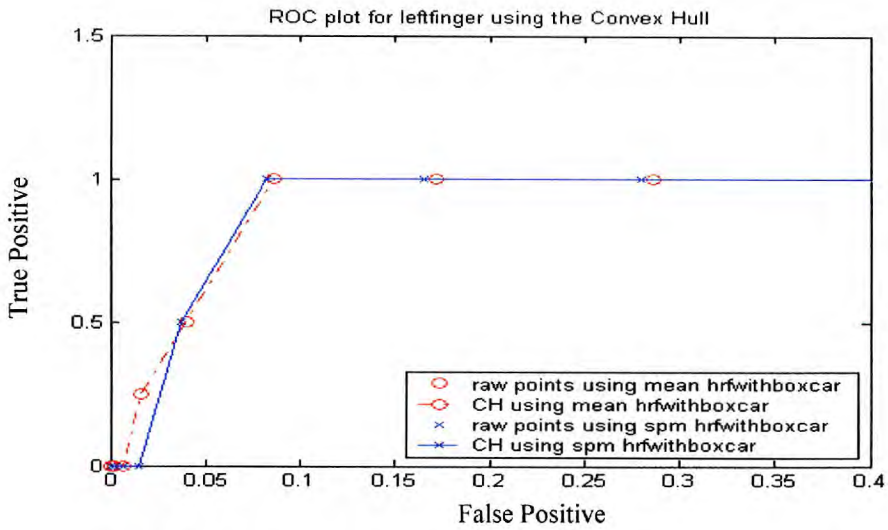

Fig. 7.86 ROC curve for the realigned left finger tapping.

The ROC curve above shows better results using the mean HRF compared to the results using the SPM HRF.

Overall, in the right finger tapping, the results appear to be better using the SPM HRF. In the case of the left finger tapping, the results show that even though the similarity measure did not seem to improve using the mean HRF compared to the SPM HRF, the ROC curve illustrated better results using the mean HRF in the left finger tapping. Considering that the tumour is in the right side of the brain, then we would expect the left finger tapping to most likely be affected, and therefore, our results seem to indicate that an HRF signal extracted from the subject's data tend to produce better ROC curves. This strengthens our argument for the need to customize the HRF

signal as opposed to a standard SPM HRF signal which is based on a group of healthy subjects and does not necessarily apply across all patient groups, some of which may have abnormal vascularization.

7.6 Summary

This chapter presented an investigation which concentrated on the differences in the hemodynamic response function across subjects, sessions, and regions in the brain. We can conclude from the results that the HRF signal varies between the somatosensory cortex and the visual cortex, and that there are differences between the SPM HRF and the mean HRFs extracted from the finger tapping data (Data Set 1) and the visual data (Data Set 3). There are also very clear differences between the subject's individual HRF signals and the mean signal in terms of the time to peak and the ratio of +ve to –ve amplitude.

The effect of the phase shift of the HRF signal on activation is analysed. It was found that using the correlation method, the maximum number of activation was at shift +13dt (4.875 sec), even though, the maximum similarity measure was found at shift +10dt (3.75 sec). In SPM2, the maximum number of activations was found at shift 0dt (0 sec).

A detailed description of the empirical extraction of the HRF signal from the data was described. A comparative study of the effect of different HRF signals has on the similarity measure and the ratio of energy is also carried out. It is very evident from the results that we can only retrieve the HRF signal from areas of activation, and that the HRF signal varies at different areas of activation in the brain. It also appears that the ratio of energies of active regions is lower than that of other regions in or out of brain. This does suggest that there are no other significant event-correlated activations present other than those that are well described by a Hemodynamic Response Function that is close to the initial ($\mathbf{h}_0$) candidate solution (see chapter 5 section 5.5). We can also conclude that the ratio of energy might be used as a test of activity/inactivity even if there is uncertainty in the precise form of the HRF.

The differences in activations obtained using the SPM HRF and the mean extracted HRF signals are compared by presenting them graphically as ROC curves. They showed that in general the results were better using the mean predicted activation signal compared to the SPM activation signal. Some clinical application of our analysis is also included utilising all the methods discussed previously.

The next chapter will provide a detailed discussion of the results obtained, presenting a conclusion of the work and suggestions for future directions of this work.

Chapter 8

Conclusions and Future work

This study has extensively studied and compared the role of commonly used data analysis techniques in functional magnetic resonance imaging. A detailed investigation into the effect of the assumed hemodynamic response function on activation strength and reproducibility has also been performed. Below I summarise the results obtained during this work and compare the results to those in the literature.

Realignment & Maximum activation:

The effect of the realignment process on fMRI activation was previously investigated using generic tools by [49;122;123] using a computer-generated phantom. The effect of the realignment process on activation was here thoroughly investigated using SPM99, SPM2 and AIR as realignment tools. Activation statistics were compared in active and non-active regions in both finger tapping and visual cortex experiments with and without realignment, and using both the in-built detection algorithms in SPM

and using a simple, correlation signal detection process that is analogous to that of SPM (linear model).

We found that the total number of active voxels and cluster size were *greater* using SPM2 compared to SPM99, and that the realignment using SPM in general produced better similarity measures compared to AIR. In selecting 4 weeks of Data Set 1 to compare the effect of alignment on activation strength, we found that for the finger tapping data, the realignment process using SPM99, SPM2 or AIR caused a *reduction* in the maximum similarity measure observed in the brain (Table 6.4). This is addressed more fully below.

For the visual data, the realignment caused an *increase* in the maximum similarity measure using SPM2, a *decrease* using AIR, but gave contradictory results using SPM99 (Table 6.4). Similar work was conducted by Freire et al. [49] which investigated the effect of different realignment methods, based on different similarity measures, on registration. Their study concluded that the German McClure (GM) estimator was found to be more robust than the usual difference of squares measured but that more work is required to compare the various robust metrics that are proposed in the literature. We also noted that the reduction of the stimulus contrast had the effect of *decreasing* the maximum similarity measure. In general, a

bigger similarity measure does imply larger cluster size (suprathreshold regions) and vice versa.

A more extensive (all weeks of Data Set 1) study, presented in Table 6.5, of the effect of realignment against non-realignment using SPM2, confirmed the surprising result of Table 6.5, where the non-realigned data led to similar matches of predicted to actual data compared to the realigned data. This might be due to the fact that the movement present in the data was very small (in the region of 0.1 mm). The effect of attempting to realign data with such small (sub-pixel) movements may actually lead to a reduction in the coherence of the activation pattern due to interpolation errors (see Chapter 3 section 3.4). Non peer reviewed studies[4] have also found that small fast movements can have as much effect on the time course as large slow ones. The effect of realignment in the process of measurement noise may be to introduce precisely such artefacts into the data.

Realignment & Normality:

A normality study was conducted using the K-S test in the *SPSS*® package to investigate the effect of realignment on the active areas. The normality assumption is an important property to establish, as it underlies the most popular signal detection strategies used in fMRI.

[4] http://merlin.psych.arizona.edu/~dpat/Public/Imaging/SPM/spm2docs/spm2_analysis_defaults.html

For the finger tapping data, the realignment was found to cause a *decrease* in the normality of the signal deviation from the temporal mean (mean across time) (see Table 6.6) in the *active* areas of the brain. This is most likely to be due to variation in activation amplitudes within the cluster with respect to the mean activation within the cluster. Further steps to investigate this are proposed in Future Work.

For the visual data, separate comparisons were performed on the normality statistic of active areas for varying stimulus contrast and with and without realignment. For the 10% contrast data, the realignment process (using SPM99, SPM2 or AIR) resulted in a *decrease* in the normality of active areas (Table 6.6), consistent with the finger tapping data (Table 6.6). However, for the visual 100% contrast, the realignment caused an *increase* in the normality of the active areas. This might be due to the 100% contrast leading to near maximum stimulation quite consistently within clusters, implying that all intra cluster voxels shared similar amplitudes.

We found that decreasing the contrast caused an *increase* in the normality of active areas (Table 6.6), but this is in the *absence* of realignment, where the motion is unlikely to be as small as for the finger tapping experiments (longer sequence, and visible motion was present).

The normality study was extended to investigate the effect of realignment on inactive areas as well.

There was a clear difference between the normality of active areas and the background out-of-brain areas, where, the active areas were less normal than the background areas (Table 6.7). This is because background areas are more likely to deviate from the temporal mean due to pure noise effects, and are thus more likely to display normality [124].

The realignment process seems to cause an *increase* in the normality of the in brain non-active areas for the visual data (Table 6.7), but causes a *decrease* in the normality for the in brain non-active areas for the finger tapping data (Table 6.7). There are two possible explanations for this, one of which is that there is significant non-random temporal structure in the non-active brain areas which realignment emphasizes. However, it may also be due to the fact that, as pointed out earlier, that the motion in the finger tapping experiments was sub-pixel, so that the effect of applying a realignment process is to introduce interpolation artefacts. No comparative studies of this nature could be found in the literature.

No conclusive evidence was found to support the hypothesis that the normality may be used as a detector of activity in brain areas, but this cannot be completely ruled out based on the arguments presented above.

Effect of Phase Shift on activation patterns:

By using both SPM2 and a correlation detection algorithm based on the normalised inner product, the effect of introducing phase shifts into the Hemodynamic Response Function on activation detection was also investigated (Chapter 7, section 7.2). The effect of the phase shift was to change the activation levels for both techniques. Using the correlation method produced maximum activation, in terms of the total number of active voxels, at a non-zero phase shift, whilst the maximum activation using SPM2 was found at zero phase shift. For this comparison, standard SPM protocols were used, but the HRF was modified externally.

Comparison of SPM HRF and individualised HRF:

We studied the differences in the Hemodynamic Response Function, and it was concluded that the HRF varies with subjects, sessions, and regions in the brain in strong agreement with findings by other researchers [6;22;24] see also [28;31-33;120]. Subsequently, this has lead to the decision to investigate the effect of variations of the Hemodynamic Response Function and the predicted activation signal on the activation size and signal similarity measure observed in the data. We concluded that the choice of Hemodynamic Response Function affects the predicted activation signal which subsequently has an effect on the activation (cluster) size and signal activation level. This also is in accordance with the literature [120;125]. The average hemodynamic response signal extracted from the slice with

maximum activation generated both a larger activation cluster and higher similarity measures compared to those obtained using the collapsed average signal extracted from multiple slices (3D) at maximum activation. This is probably because the slice timing information was not taken into account in this study (see Future Work).

Activity versus Inactivity: Residual Signal Energy

In this component of the work, the ability to automatically extract individualised HRF's, and HRF's for different brain areas was investigated.

We selected some data subsets: 4 (clusters of voxels) to be located in the grey matter, 4 in the white matter, some active areas, 2 at potentially active areas (visual cortex), and 4 background or out of brain areas. We attempted to extract HRF signals at these positions. It was evident from the results that:

(a) The ratio of the energy of the residual to the energy of the signal in the active regions is much lower than that of other regions in or out of brain, implying that the model of a box-car stimulus convolved with a presumed (non-zero) HRF is invalid in explaining the non-active areas. This implies, as expected, that we can only retrieve the HRF signal from areas of activation, (but see below for a clarification of this).

(b) The HRF signal varies at different areas of activation in the brain, implying also the nature of the stimulus, and varies across sessions for the same individual, and subjects.

This does also suggest that there are no other significant event-correlated activations present other than those that are well described by a Hemodynamic Response Function that is close to the initial ($\mathbf{h}_0$) candidate solution (see Chapter 5 section 5.5). We can also conclude that the ratio of residual to signal energy might be used as a test of activity/inactivity even if there is uncertainty in the precise form of the HRF.

The mean HRF signal of all active areas across all the weeks, in the case of the finger tapping data, and across all subjects for the 10% contrast and the 100% contrast, in the case of the 5 subject visual data, was calculated and then used to look for the activation at these data sets. The process was repeated with ten different thresholds and the results were represented using ROC curves (Figures 7.42 to 7.49). In the case of the finger tapping data, it was evident from the curves that better results were obtained in finding activation using the mean predicted activation signal compared to the SPM activation signal in 10 cases out of 14, and only one case shows a better result using the SPM activation signal. In the case of the 5 subject visual data, all the curves showed better results using the mean predicted activation signal compared to the SPM activation signal (Figures 7.42 to

7.49). This indicates that better results are obtained when using a hemodynamic response extracted from the actual data as opposed to a standard hemodynamic response. The results of other studies [31;120] are consistent with our results.

ROC curves were also illustrated for a randomized realigned finger tapping session with 100 different runs (Figures 7.50 to 7.54). Overall, the results show that the randomized data have a flatter curve, further from the ideal ROC characteristic [121], in comparison to the non-randomized data. This is generally associated with random classification in the detection sense.

Clinical Data Analysis feasibility study

Some clinical applications of our analysis are also included utilising methods discussed previously. The clinical data was 5-subjects all engaged in unilateral finger tapping, all with tumours on the right hand side of the brain.

The HRF was extracted from active areas (during left and right finger tapping, then averaged separately) as detected using the SPM HRF. These individualised, and "side-tailored" HRF's were then applied to detecting activation.

For the right-hand finger tapping, the pseudo ROC curve (Figure 7.71) obtained using the SPM HRF was better compared to that using the extracted HRF from the left side of the brain. In the case of the left finger tapping, the results show that even though the similarity measure did not seem to improve using the extracted HRF compared to the SPM HRF, the pseudo ROC curve (Figure 7.86) illustrated better results. Considering that the tumour is in the right side of the brain, one might expect that, provided adequate data is available to extract an adequate HRF, the left finger tapping ROC's would show greater differences between using an extracted HRF and the SPM HRF, obtained from normal individuals.

The results obtained require careful explanation. First, the problem with averaging a small number of voxels across subjects is that the extracted HRF's might be expected to be quite noisy. Thus, the HRF is less likely to yield an improvement over the SPM HRF, which is extracted over a large number of individuals. In other words, the quality of the individualised HRF estimate is likely to be poor. This would lead to correspondingly poor results in the resulting ROC curve compared to using the SPM HRF. Indeed, the curve in Figure 7.71 illustrates this effect for the normal brain side. Interestingly, for high thresholds of the left-hand finger tapping (right brain, tumour-containing area), the difference using the SPM HRF and the extracted HRF is less pronounced. Indeed, at high thresholds, there seems to be *slightly* better performance due to the extracted HRF than with the

SPM HRF, in terms of lower false-positive rate for the a given (high) threshold, thus capturing more certain activation areas.

However, *great care*, is required in assessing these results because the extracted HRF from a small number of voxels is certain to show great variability. Thus, the difference between ROC curve pairs is quite likely to be due simply to the quality of the estimate of the extracted HRF. In order to be able to make any conclusive statements about these (not unpromising) results, a much greater cohort of patients would be required, and some effort into improving the reliability of the HRF extraction process would be necessary.

Future Work:

There are many more exhaustive tests that could be performed on the available data using the directions suggested by the outcome of this work:

1. Investigation into the effects of different similarity measures on detected activation using correlation methods (i.e. outside of SPM environment). The method employed was selected to be amplitude invariant. Phase invariant similarity measure could also be employed.

2. The experiment suggest that the inter slice averaging to obtain the HRF yields poorer results than within slice averaging. This may be due to the

acquisition time effects on the scanner. Knowledge of the timing of the slices should allow better averaging results, by taking into account the sampling times of the signal acquisition. Furthermore, such timing information could be incorporated into the randomisation process used in chapter 6.

3. More extensive work also needs to be done to compare the effect on detection of realignment when different cost functions and interpolation methods are used. These are discussed in Chapter 3. Among the promising ones are Mutual Information (MI) and moments matching.

4. During this work, several independent tools have been developed for MRI activation detection and HRF extraction. Because of the ease of performing different types of analysis using these tools, they will be maintained and developed. In particular, enhancement to the histogram method (see Chapter 5, section 5.4 and Chapter 6 section 6.7) is being developed which takes into account a distribution to activation amplitudes.

5. More extensive subject studies need to be done to assess the effect of individual HRFs on activation detection and any effects on the spatial extent of active clusters. However, this initial work does indeed suggest that it is both feasible and useful to tailor HRFs to individuals whenever sufficient scan data is available.

Appendix A

Matlab scripts

Matlab script to load data in *.img format

```
function vol = readimg(dimensions,Ntimes,Offset);

% Script to test loading raw data in IMG format.
% Assumes fixed size to volume of 128 x 128 x 10.
% Assumes 2 bytes/voxel.

Numberofvoxels = prod(dimensions);
j = 0;
vol = zeros([dimensions,Ntimes]);

for i = Offset+1:Offset+Ntimes;
        fid = fopen(sprintf('E:\\HumanQAData\\week16\\..
        HQA16vol0 %.2d.img',i),'r','b');
        [X,nread] = fread(fid,numberofvoxels,'uint16');
        fclose(fid);
        X1= reshape(X,dimensions);
        j = j+1;
        vol(:,:,:,j) = X1;
end;
```

Matlab script to calculate the amplitudes of the activation

```
% Script to do some plots of activation profiles, and
% to calculate amplitudes of activation.

% 299 is cluster label at slice 8
a = find(labelled_x(:) == 299);
SizeOfCluster = length(a);

for i = 1:SizeOfCluster
        m,n,o]= ind2sub(dimensions,a(i));
        signal = squeeze(vol(m,n,o,:));
        Amplitude(i) = signal'*hrfwithboxcar/..
        norm(hrfwithboxcar))^2;
        subplot(3,3,i);
        plot(1:30,squeeze(vol(m,n,o,:)),1:30,Amplitude(i)*hrfwith    boxcar)

end;
```

Matlab script for connected component labelling of the clusters

```
function labelled_x = connected_component_labelling3D(x,k)

%k = 3; % number of z dimensions
% clusters 3D matrix and labels the clusters.

labelled_x = bwlabeln(x,6);
map = [0 0 0;jet(200)];

for y = 1:k;
        figure;imshow(labelled_x(:,:,y)+1,map,'notruesize');
        % display the clusters.
end;

% returns values in matrix without repetition.
a = unique(labelled_x);
```

```
numberofvalues = prod(size(a));
firstclusternumber = a(2,1);
lastclusternumber = a(numberofvalues,1);


% calculate the number of clusters in 3D matrix.
numberofclusters = numberofvalues - 1;

% calculate the total number of elements in each matrix
numberofelements = prod(size(labelled_x));

% reshape labelled_x into a string.
reshaped_labelled_x = reshape(labelled_x,1,numberofelements);

% set the size of insignificant clusters matrix.
insignificantclusters = cell(1,numberofclusters);

if numberofclusters >= 1
   d = 1;
   c = reshaped_labelled_x; % reshaped_labelled_x in 2D
        for i = firstclusternumber : lastclusternumber;

        % finds elements in matrix with values equal to cluster
        number.
        b = find(labelled_x==i);

                % check for number of elements in each cluster.
                if prod(size(b)) <= 2

                % save insignificant clusters in insignificantclusters.
                insignificantclusters(1,d) = {b};

                % discard of elements that form an insignificant cluster.

                                for j = 1:numberofclusters
                                r = insignificantclusters{j};
                                c(1,r) = 0;
                        end;
                end;
                d = d + 1;
        end;
else
end;
```

```
labelled_x = reshape(c,size(x));

% display significant clusters only.
for y = 1:k;
        figure;imshow(labelled_x(:,:,y)+1,map,'notruesize');
end;
```

Matlab script to find activation in the data loaded

```
clear;close all;

% Script to look for activation in raw data.

Ntimes = 30; Offset = 4; dimensions = [128 128 10];

%recalls function readimg.
vol = readimg(dimensions,Ntimes,Offset);

k = dimensions(1,3);

%calculate mean of volumes across time.
collapsed_time = mean(vol,4);

% This removes time-averaged values from each voxel.
for i = 1:Ntimes,
        vol(:,:,:,i) = vol(:,:,:,i) - collapsed_time;
end;

load hrfwithboxcar; hrfwithboxcar = dummy(:,1);

% Threshold to get rid of out of brain pixels.
T = uint8(collapsed_time > 150);

hrfwithboxcar = hrfwithboxcar - mean(hrfwithboxcar);
reshaped_vol = reshape(vol,[prod(dimensions),Ntimes]);
normalised_hrf = hrfwithboxcar/norm(hrfwithboxcar);
volnorms = sqrt(sum(reshaped_vol.*reshaped_vol,2));
InnerProduct = (reshaped_vol*normalised_hrf)./volnorms;
InnerProduct = reshape(InnerProduct,dimensions).*double(T);

% Threshold to get rid of in brain insignificant pixels.
```

```
Threshold = 0.5;

mask = (InnerProduct > Threshold);
InnerProduct = mask .* InnerProduct;

for i = 1:Ntimes,
        NormalisedSignals(:,:,:,i) = vol(:,:,:,i)./reshape..
        (volnorms,dimensions);
end

clear volnorms; clear T;

labelled_x = connected_component_labelling3D(InnerProduct,k);
%idispquant(InnerProduct(:,:,8),squeeze(NormalisedSignals(:,:,8,:)));
```

Matlab script to visualize regions of activation

```
% Script to visualise regions of activation.
% Assume we have ccon -labelled regions of activation in 3D vol.

Biggest = max(max(max(collapsed_time)));
Smallest = min(min(min(collapsed_time)));
Scale = (Biggest-Smallest)/128;

collapsed_time = (collapsed_time - Smallest)/Scale;
InnerProduct = InnerProduct.*(labelled_x > 0);

BiggestIP = max(max(max(InnerProduct)));
SmallestIP = min(min(min(InnerProduct)));
ScaleIP = (BiggestIP-SmallestIP)/25;

collapsed_time = collapsed_time + (labelled_x>0).*(InnerProduct/ScaleIP);
[a]=find(reshape(labelled_x>0,[128*128*10,1]));

for i = 1:length(a);
        collapsed_time(a(i)) = 128+InnerProduct(a(i))/ScaleIP;
end;

%D1=smooth3(labelled_x,'gaussian',[3 3 3]);
%p = patch(isosurface(collapsed_time(60:128,1:80,:), 25), 'FaceColor',
'blue', 'EdgeColor', 'none');
%p2 = patch(isocaps(collapsed_time(60:128,1:80,:), 15), 'FaceColor',
'interp', 'EdgeColor', 'none');
```

```
%view([51 -16]); axis tight;  daspect([1 1 .4]);

hotmap = hot(50);
actmap = hotmap(16:40,:);
graymap=grey(128);map = [graymap; actmap];
montage(reshape(collapsed_time,[128,128,1,10]),map);colorbar;

%camlight; lighting gouraud
%isonormals(D1, p);
```

Matlab script to plot histograms of subclusters

```
% Script to generate a "multiplot" of the
% data in block of data.  The function requires
% an input 4D block of data, generating a series
% of plots that illustrate the spatiotemporal
% relationships

% Plots to be done
% (1) Mean signal in block as a function of time
% (2) Cross-Correlation between space-time lines
% (3) PDF total data
% (4) PDF of data along each space-time line
% (5) DFT, one sided of data along space-time means

% Assumes that "vol" is already constructed
% (may need to run analysevols)
Lm = 3;
Ln = 3;
NBins = 50;
time = 84;
timeaxis = 1:time;
for i = 1:time
```

```
    meansignal(i) = mean(mean(mean(newvol(:,:,:,i))));
end;

for i = 1:time
    data = newvol(:,:,:,i);
    maxdata(i) = max(data(:));
    mindata(i) = min(data(:));
end;


subplot(Lm,Ln,1);plot(timeaxis,meansignal,timeaxis,maxdata,'r.-
',timeaxis,mindata,'g.-');
h=title('Mean signal and Min and Max in 1x2x1:(54,49-50,9)voxels');
set(h,'FontSize',6);

data = squeeze(newvol(:,:,:,:));

BinRange = max(maxdata)-min(mindata);
Bins = min(mindata):BinRange/(NBins-1):max(maxdata);
subplot(Lm,Ln,2);[N,H]=hist(data(:),Bins);
bar(H,N);
h=title('Histogram of all data');
set(h,'FontSize',6);

subplot(Lm,Ln,3);
C = xcorr(meansignal-mean(meansignal),meansignal,'coeff');
plot(1:length(C),C);
h=xlabel('Lag');set(h,'FontSize',6);
h=title('Normalised Autocorr');
set(h,'FontSize',6);
```

```
spacetimeline = [];
for i = 1:size(newvol,1);
   for j = 1:size(newvol,2);
      for k = 1:size(newvol,3);
         spacetimeline = [spacetimeline,  squeeze(newvol(i,j,k,:))];
      end;
   end;
end;

subplot(Lm,Ln,4);plot(timeaxis,spacetimeline);
h=title('All Voxels');
set(h,'FontSize',6);

mu = mean(spacetimeline);
mumat=(kron(mu',ones(1,time)))';
spacetimedev = spacetimeline-mumat;

% C = cov(spacetimedev');
% [V,D]=eig(C);
% PI = V(:,30:-1:28);
% subplot(Lm,Ln,5);plot(timeaxis,PI');
% h=title('First 3 Eigenvectors');
% set(h,'FontSize',6);

%Now, let's subtract the mean value from each spacetimeline
subplot(Lm,Ln,5);
hist(spacetimedev(:),40);
h=title('Hist:Dev. From Temp. Mean with Pos');
```

```
set(h,'FontSize',6);

subplot(Lm,Ln,6);

plot(spacetimedev);
h=title('Signals Minus Means');
set(h,'FontSize',6);

subplot(Lm,Ln,7);
mindevsignal = min(spacetimedev');
maxdevsignal = max(spacetimedev');
meandevsignal = mean(spacetimedev');
plot(timeaxis,meandevsignal,timeaxis,maxdevsignal,'r:',timeaxis,mindevsig
nal,'g:');
h=title('Mean signal and Min and Max in spacetimedev');
set(h,'FontSize',6);

NVoxels = 2;
devdev=spacetimedev-kron(ones(1,NVoxels),meandevsignal');
subplot(Lm,Ln,8);
hist(devdev(:),NBins);
h=title('Hist:Dev. From Mean Signal Pattern');
text(2,5,['Total number of pixels =' num2str(prod(size(newvol)))]);
set(h,'FontSize',6);
```

Matlab script to plot ROC curves after the calculation of the false positive and the false negative of activation

```
clear all; %close all;clc

load
C:\research\mymatlab\activation\FTmeanactiveallweeks\activemeanR17 %
loading active areas in visual data using the mean hrf
%load j:\5submeanactive10\activemeanRall510
A1 = Areas; %Areas conatin all the active areas found for 10 different
thresholds

load C:\research\mymatlab\activation\FTspmactiveallweeks\activespmR17
% loading active areas in visual data using the mean hrf
%load j:\5subspmactive10\activespmRall510
A2 = Areas;

ActivationTemplate = zeros(128,128,10); % activation template for the
finger tapping data

% for y = 75:76
%     for x = 20
%       for z = 9:10
%           ActivationTemplate(y,x,z) = 1;
%        end;
%     end;
% end;

% 2x1x3
for y = 44
```

```
  for x = 52:53
     for z = 6:8
        ActivationTemplate(y,x,z) = 1;
     end;

 end;
end;

% collapsed_time = mean(vol,4);
% T = uint8(collapsed_time > 250); % threshold to eliminate out of brain
voxels
% A=find(T(:,:,:)==1); % finds the total number of voxels with value = 1 (in
brain voxels)

% total number of finger tapping in brain voxels = 30366
% total number of 5 subject visual in brain voxels = 84696
% InBrainVoxels = 30366; % for finger tapping

setA1 = cell(1,10);
for threshold = 1: prod(size(A1)) % number of thresholds (i.e. 10)
        % number of active areas for each threshold
        numberofsets1 = prod(size(A1{threshold}.active));
        if numberofsets1 > 1
                for i = 1:numberofsets1
                                setA1 {1,threshold}= [setA1{1,threshold} ;
                        A1{threshold}.active{i}.Positions];
                end;
        elseif numberofsets1 == 1
                setA1 {1,threshold} = A1{threshold}.active{1}.Positions;
        else
```

```
                setA1 {1,threshold} = [];
        end;
end;

for i = 1:10

        temp1 = zeros(128,128,10); % finger tapping
        %temp1 = zeros(128,128,22); % visual data
        if isempty(setA1{i})
                temp1 = temp1;
        else
        tempind1 =
sub2ind(size(temp1),setA1{i}(:,1,:),setA1{i}(:,2,:),setA1{i}(:,3,:));
        temp1(tempind1) = 1; % set all active areas in 1st set to 1
        TruePositive1 = ActivationTemplate .* temp1;
        TPLocation1 = find(TruePositive1==1);
        TP1(i) = size(TPLocation1,1);
        RatioOfTP1(i) = TP1(i) / 6; % 8 is the size of the true positive cluster
chosen in
        ActivationTemplate
        FP1(i) = size(setA1{i},1) - TP1(i);
        RatioOfFP1(i) = FP1(i) / 30360;
        end;
end;

setA2 = cell(1,10);
for threshold = 1: prod(size(A2)) % number of thresholds (i.e. 10)
        numberofsets2 = prod(size(A2{threshold}.active)); % number of
active areas for
        each threshold
```

```
        if numberofsets2 > 1
                for i = 1:numberofsets2
                                setA2 {1,threshold}= [setA2{1,threshold} ;
                        A2{threshold}.active{i}.Positions];
                end;

        elseif numberofsets2 == 1
                setA2{1,threshold} = A2{threshold}.active{1}.Positions;
        else
                setA2{1,threshold} = [];
        end;
end;

for i = 1:10
        %temp2 = zeros(128,128,22); % visual data
        temp2 = zeros(128,128,10); % finger tapping
        if isempty(setA2{i})
                temp2 = temp2;
        else
        tempind2 =
sub2ind(size(temp2),setA2{i}(:,1,:),setA2{i}(:,2,:),setA2{i}(:,3,:));
        temp2(tempind2) = 1; % set all active areas in 2nd set to 1
        TruePositive2 = ActivationTemplate .* temp2;
        TPLocation2 = find(TruePositive2==1);
        TP2(i) = size(TPLocation2,1);

        RatioOfTP2(i) = TP2(i) / 6; % 18 is the size of the true positive
cluster chosen in ActivationTemplate
```

```
        FP2(i) = size(setA2{i},1) - TP2(i);

        RatioOfFP2(i) = FP2(i) / 30360;
        end;
end;
% figure;
% plot(RatioOfFP1,RatioOfTP1,'-.ro',RatioOfFP2,RatioOfTP2,'-xb');

% %axis([0 0.6 0 1.1]);title('ROC plot for subject 5 10% contrast ');

% axis([0 0.4 0 1.5]);title('ROC plot for week 17 run1 ');

% h = legend('using mean hrfwithboxcar','using spm hrfwithboxcar',4);
%h = legend('100% contrast','10% contrast',2);

%New Improved ROC; does not need Gaussian-ness and is easy.
%Called the "Convex Hull of the ROC"

FMM1 = RatioOfFP1;
TMM1 = RatioOfTP1;
idx1 = unique(convhull(FMM1, TMM1));
FMMCH1 = FMM1(idx1(1:end-1));
TMMCH1 = TMM1(idx1(1:end-1));
%figure;plot(FMM1,TMM1,'mx',FMMCH1,TMMCH1,'m');
FMM2 = RatioOfFP2;
TMM2 = RatioOfTP2;
idx2 = unique(convhull(FMM2, TMM2));
FMMCH2 = FMM2(idx2(1:end-1));
TMMCH2 = TMM2(idx2(1:end-1));
```

```
%figure;
plot(FMM1,TMM1,'ro',FMMCH1,TMMCH1,'-
.ro',FMM2,TMM2,'bx',FMMCH2,TMMCH2,'-bx');
%axis([0 0.4 0 1.2]);title('ROC plot for subject 5 10% contrast using the
Convex Hull');
axis([0 0.4 0 1.5]);title('ROC plot for week 17 run5 using the Convex Hull');
h = legend('raw points using mean hrfwithboxcar','CH using mean
hrfwithboxcar','raw points using spm hrfwithboxcar','CH using spm
hrfwithboxcar',4);
```

Matlab script to calculate the mean signal and the standard deviation for a group of signals

```
% Script to load and check reproducibility
DirList = dir ('res_*');
TR = 1;  % Hack
Q =[];
for i = 1:length(DirList)
        DirName = DirList(i).name;
        FileList = dir([DirName,'/',DirName,'A*']);
        eval(['cd ',DirName]);
        for j = 1:length(FileList);
                LoadString = ['load ',FileList(j).name];
                eval(LoadString);
                Q = [Q,hrf'];
        end;
        cd ..;
end;

 Q = Q';
```

```
% Because these have different energies (arising from possibly different
 % amplitude signals), we normalise all the signals by the 2-norm

[M,N] = size(Q);

for i = 1:M
        NQ(i,:) = Q(i,:)/norm(Q(i,:));
end;

MNQ = mean(NQ);

S = std(NQ);
SL = MNQ - S;  SU = MNQ + S;
S2L = MNQ - 2*S; S2U = MNQ + 2*S;
H1=plot((1:N)*TR,MNQ);hold on;

H2=plot((1:N)*TR,SL,'r--');
H3=plot((1:N)*TR,SU,'r--');
H4=plot((1:N)*TR,S2L,'g--');
H5=plot((1:N)*TR,S2U,'g--');
legend([H1,H2,H4],'Mean HRF','Mean \pm 1 SD','Mean 2 \pm SD');
xlabel('Time (scans)');
ylabel('Response (normalised)');

figure(2);
plot((1:N)*TR,S);
xlabel('Time (s)');
ylabel('Standard Deviation of HRF');
```

Matlab script to create simulated data

```
%clear;
%close all;

% Script to create activation in raw data
Ntimes = 30;Offset = 0;dimensions = [128 128 10];percentage1 =
1.5;percentage2 = 1.5;
vol=readimgfake(dimensions,Ntimes,Offset); % recalls function
readimgfake


% hrfwithboxcar shifted to give an on-off pattern
load hrfwithboxcarhighres; % original hrfwithboxcar
hrfwithboxcar = X([0:29]*fMRI_T + fMRI_T0 + 32,:);
hrfwithboxcar=hrfwithboxcar(7:30);
hrfwithboxcar=[hrfwithboxcar;hrfwithboxcar(5:10)];

%    m1 = 1;
%    for slice1 = 7:10;  % positions of activation in area 1 - cube: 4x4x4)
%       for positionofactivationx1 = 56:59;
%          for positionofactivationy1 = 56:59;
%             activationvalue1(positionofactivationx1,positionofactivationy1)
= [(vol(positionofactivationx1,positionofactivationy1,slice1,1))];
%             activationarray1(m1)
=[activationvalue1(positionofactivationx1,positionofactivationy1)];
%             m1 = m1 + 1;
%          end;
%       end;
%    end;

m1 = 1;
   for slice1 = 7:9;  % positions of activation in area 1 - star: 3x3x3)
      for positionofactivationx1 = 56;
        for positionofactivationy1 = 57;
           activationvalue1(positionofactivationx1,positionofactivationy1) =
[(vol(positionofactivationx1,positionofactivationy1,slice1,1))];
           activationarray1(m1)
=[activationvalue1(positionofactivationx1,positionofactivationy1)];
           m1 = m1 + 1;
         end;
      end;
      for positionofactivationx1 = 57;
        for positionofactivationy1 = 56:58;
```

```
            activationvalue1(positionofactivationx1,positionofactivationy1) =
[(vol(positionofactivationx1,positionofactivationy1,slice1,1))];
            activationarray1(m1)
=[activationvalue1(positionofactivationx1,positionofactivationy1)];
            m1 = m1 + 1;
          end;
        end;
        for positionofactivationx1 = 58;
          for positionofactivationy1 = 57;
            activationvalue1(positionofactivationx1,positionofactivationy1) =
[(vol(positionofactivationx1,positionofactivationy1,slice1,1))];
            activationarray1(m1)
=[activationvalue1(positionofactivationx1,positionofactivationy1)];
            m1 = m1 + 1;
          end;
        end;
    end;


   % activation created by finding the average and then adding a
percentage of activation
   valueofactivationmean1 = mean(activationarray1);
   percentageofactivation1 = valueofactivationmean1 * percentage1/100;
   valueofactivationmax1 = valueofactivationmean1 +
percentageofactivation1;
   valueofactivationmin1 = valueofactivationmean1 -
percentageofactivation1;
   boxcaractivation1 = hrfwithboxcar * (valueofactivationmax1 -
valueofactivationmin1) + valueofactivationmin1;

%    % activation created by finding the maximum and minimum
%    valueofactivationmax1 = max(activationarray1);
%    valueofactivationmin1 = min(activationarray1);
%    high1 = repmat(valueofactivationmax1,1,5);
%    low1 = repmat(valueofactivationmin1,1,5);
%    cycle1 = [high1 low1];
%    boxcaractivation1 = repmat(cycle1,1,3);
%    boxcaractivation1 = hrfwithboxcar * (valueofactivationmax1 -
valueofactivationmin1) + valueofactivationmin1;
%    %boxcaractivation1 = boxcaractivation1 .* hrfwithboxcar'; % activation
convolved with hrfwithboxcar signal

% for slice1 = 7:10;  % slices that contain activation in area 1 - cube: 4x4x4
%       for positionofactivationx1 = 56:59;
%          for positionofactivationy1 = 56:59;
%             for count = 1:Ntimes;
```

```
%                vol(positionofactivationx1,positionofactivationy1,slice1,count)
= boxcaractivation1(count);
%              end;
%           end;
%        end;
% end;

   for slice1 = 7:9;  % slices that contain activation in area 1 - star: 3x3x3
      for positionofactivationx1 = 56;
         for positionofactivationy1 = 57;
            for count = 1:Ntimes;
              vol(positionofactivationx1,positionofactivationy1,slice1,count) =
boxcaractivation1(count);
            end;
         end;
      end;
      for positionofactivationx1 = 57;
         for positionofactivationy1 = 56:58;
            for count = 1:Ntimes;
              vol(positionofactivationx1,positionofactivationy1,slice1,count) =
boxcaractivation1(count);
            end;
         end;
      end;
      for positionofactivationx1 = 58;
         for positionofactivationy1 = 57;
            for count = 1:Ntimes;
              vol(positionofactivationx1,positionofactivationy1,slice1,count) =
boxcaractivation1(count);
            end;
         end;
      end;
   end;


%    m2 =1;
%    for slice2 = 3:6;  % positions of activation in area 2 - cube: 4x4x4)
%       for positionofactivationx2 = 75:78;
%          for positionofactivationy2 = 75:78;
%             activationvalue2(positionofactivationx2,positionofactivationy2)
= [(vol(positionofactivationx2,positionofactivationy2,slice2,1))];
%             activationarray2(m2)
=[activationvalue2(positionofactivationx2,positionofactivationy2)];
%             m2 = m2 + 1;
%          end;
%       end;
```

```
%    end;

m2 =1;
   for slice2 = 3:5;   % positions of activation in area 2 - star: 3x3x3)
      for positionofactivationx2 = 75;
         for positionofactivationy2 = 76;
            activationvalue2(positionofactivationx2,positionofactivationy2) =
[(vol(positionofactivationx2,positionofactivationy2,slice2,1))];
            activationarray2(m2)
=[activationvalue2(positionofactivationx2,positionofactivationy2)];
            m2 = m2 + 1;
         end;
      end;
      for positionofactivationx2 = 76;
         for positionofactivationy2 = 75:77;
            activationvalue2(positionofactivationx2,positionofactivationy2) =
[(vol(positionofactivationx2,positionofactivationy2,slice2,1))];
            activationarray2(m2)
=[activationvalue2(positionofactivationx2,positionofactivationy2)];
            m2 = m2 + 1;
         end;
      end;
      for positionofactivationx2 = 77;
         for positionofactivationy2 = 76;
            activationvalue2(positionofactivationx2,positionofactivationy2) =
[(vol(positionofactivationx2,positionofactivationy2,slice2,1))];
            activationarray2(m2)
=[activationvalue2(positionofactivationx2,positionofactivationy2)];
            m2 = m2 + 1;
         end;
      end;
   end;

   % activation created by finding the average and then adding a
percentage of activation
   valueofactivationmean2 = mean(activationarray2);
   percentageofactivation2 = valueofactivationmean2 * percentage2/100;
   valueofactivationmax2 = valueofactivationmean2 +
percentageofactivation2;
   valueofactivationmin2 = valueofactivationmean2 -
percentageofactivation2;
   boxcaractivation2 = hrfwithboxcar * (valueofactivationmax2 -
valueofactivationmin2) + valueofactivationmin2;

%    % activation created by finding the maximum and minimum
%    valueofactivationmax2 = max(activationarray2);
```

```
%     valueofactivationmin2 = min(activationarray2);
%     high2 = repmat(valueofactivationmax2,1,5);
%     low2 = repmat(valueofactivationmin2,1,5);
%     cycle2 = [high2 low2];
%     boxcaractivation2 = repmat(cycle2,1,3);
%     %boxcaractivation2 = boxcaractivation2 .* hrfwithboxcar'; % activation
convolved with hrfwithboxcar signal
%     boxcaractivation2 = hrfwithboxcar * (valueofactivationmax2 -
valueofactivationmin2) + valueofactivationmin2;

%     for slice2 = 3:6;   % slices that contain activation in area 2 - cube:
4x4x4
%       for positionofactivationx2 = 75:78;  % positions of activation in area
2)
%         for positionofactivationy2 = 75:78;
%           for count = 1:Ntimes;
%
vol(positionofactivationx2,positionofactivationy2,slice2,count) =
boxcaractivation2(count);
%           end;
%         end;
%       end;
%     end;

   for slice2 = 3:5;   % slices that contain activation in area 2 - star: 3x3x3
     for positionofactivationx2 = 75;  % positions of activation in area 2)
       for positionofactivationy2 = 76;
         for count = 1:Ntimes;
           vol(positionofactivationx2,positionofactivationy2,slice2,count) =
boxcaractivation2(count);
         end;
       end;
     end;
     for positionofactivationx2 = 76;  % positions of activation in area 2)
       for positionofactivationy2 = 75:77;
         for count = 1:Ntimes;
           vol(positionofactivationx2,positionofactivationy2,slice2,count) =
boxcaractivation2(count);
         end;
       end;
     end;
     for positionofactivationx2 = 77;  % positions of activation in area 2)
       for positionofactivationy2 = 76;
         for count = 1:Ntimes;
           vol(positionofactivationx2,positionofactivationy2,slice2,count) =
boxcaractivation2(count);
```

```
            end;
          end;
        end;
    end;


% Addition of noise to the data
for i = 1:Ntimes,
    noise = randn(dimensions);
    % remove negative values (set to zero);
    noise=reshape(noise,[(prod(dimensions)),1]);j = find(noise<0);  for
k=1:length(j) noise(j(k))=0; end; noise=reshape(noise,dimensions);
    vol(:,:,:,i) = vol(:,:,:,i) + noise;
end
```

Matlab script to find the mutual active areas between two sets of data

```
clear all; close all;
i = 1; % i selects the threshold 1:10
% algorithm to check if two data sets have any active voxels in common
%load
C:\research\mymatlab\activation\FTspmactiveallweeks\activespmR16 %
loading active areas in visual data using the mean hrf
load J:\5subspmactive100\activespmRall5100 % loading active areas in
finger tapping using the mean hrf
A1 = Areas{i};


%load
C:\research\mymatlab\activation\FTspmactiveallweeks\activespmR17 %
loading active areas in visual data using the mean hrf
load J:\5subspmactive10\activespmRall510% loading active areas in visual
data using the spm hrf
A2 = Areas{i};
```

```
temp1 = zeros(128,128,22); % finger tapping data
temp2 = zeros(128,128,22);

% finding the number of active voxels in data set 1

numberofsets1 = prod(size(A1.active));
setA1 = [];
if numberofsets1 > 1

        for i = 1:numberofsets1

        setA1 = [setA1 ; A1.active{i}.Positions];
        end;
        else setA1 = A1.active{1}.Positions;
end;

% finding the number of active voxels in data set 2
numberofsets2 = prod(size(A2.active));

setA2 = [];
if numberofsets2 > 1
        for j = 1:numberofsets2
                setA2 = [setA2 ; A2.active{j}.Positions];
        end;
        else setA2 = A2.active{1}.Positions;
end;

tempind1 = sub2ind(size(temp1),setA1(:,1,:),setA1(:,2,:),setA1(:,3,:));
Totalactive1 = prod(size(tempind1));
```

```
%disp(['Total number of active voxels in set using the mean hrf = '
num2str(Totalactive1)])
temp1(tempind1) = 1; % set all active areas in 1st set to 1
tempind2 = sub2ind(size(temp2),setA2(:,1,:),setA2(:,2,:),setA2(:,3,:));
Totalactive2 = prod(size(tempind2));
%disp(['Total number of active voxels in set using the spm hrf = '
num2str(Totalactive2)])



%temp(tempind2) = temp(tempind2) + 1;
%temp(setA2(:,1,:),setA2(:,2,:),setA2(:,3,:)) =
temp(setA2(:,1,:),setA2(:,2,:),setA2(:,3,:)) + 1; % increment all active areas
in temp by one.
temp2(tempind2) = 1;
a = temp1.*temp2;
b = find(a==1);
[x,y,z]=ind2sub(size(temp1),b);
F=[x y z]; % contains all voxel that are active in both sets
```

Appendix B

Results

The table below contains the measures of normality and the total number of active voxels for subsets selected for all the data analysed. "Active" indicates area of activation, "pv" indicates area of potential visual activation, "B" indicates background out of brain area, "W" indicates a white matter area, and "G" indicates a grey matter area.

	Active/ number of voxels	active2	active3	pv1/ nov	pv2/ nov	B1/nov	B2/nov	B3/nov	B4/nov	W1/ nov	W2/ nof	W3/ nov	W4/ nov	G1/nov	G2/nov	G3/nov	G4/nov
FT16	0.76/60	0.89/ 120		0.92/ 1920	0.98/ 1920	0.69/ 270	0.78/ 270	0.70/ 270	0.74/ 270	0.90/ 120	0.79/ 120	0.98/ 120	0.50/ 120	0.65/ 120	0.56/ 120	0.94/ 120	0.72/ 120
FT17	0.94/120	0.99/ 90		1.00/ 1920	0.96/ 1920	0.87/ 270	0.80/ 270	0.76/ 270	0.84/ 270	0.89/ 120	0.96/ 120	0.96/ 120	0.89/ 120	0.95/ 120	0.92/ 120	0.31/ 120	0.97/ 120

FT33	0.995/240	0.79/180		0.50/2250	0.72/1080	0.68//270	0.74/270	0.64/270	0.34/270	0.84/180	0.97/120	0.97/120	1.00/120	0.67/120	0.73/120	1.00/120	0.56/120
FT42	0.99/180	0.96/120		0.81/1920	0.80/1920	0.36/270	0.89/270	0.90/270	0.89/270	0.93/120	0.97/120	0.82/120	0.52/120	0.68/120	0.98/120	1.00/120	0.71/120
FT16_SPM2	0.70/60			0.32/1920	0.64/1920	0.23/270	0.42/270	0.59/270	0.25/270	1.00/120	0.87/120	0.98/120	1.00/120	0.63/120	0.90/120	0.82/120	0.73/120
FT17_SPM2	0.91/90			0.79/1920	0.62/1920	0.43/270	0.17/270	0.27/270	0.21/270	0.86/120	1.00/120	0.95/120	0.29/120	0.89/120	0.94/120	0.67/120	0.48/120
FT33_SPM2	0.92/240	0.74/240	0.93/300	0.88/1350	0.65/1080	0.50/270	0.61/270	0.16/270	0.19/270	0.99/180	0.82/120	1.00/120	0.60/120	0.97/120	0.81/120	0.74/120	0.69/120
FT42_SPM2	0.61/240	0.84/180		0.18/1920	0.36/1920	0.23/270	0.32/270	0.60/270	0.38/270	0.82/120	1.00/120	0.86/120	0.50/120	0.73/120	0.79/120	0.99/120	0.99/120
FT16_SPM99	0.54/60	0.97/180															
FT17_SPM99	0.33/120																
FT33_SPM99	0.97/90	0.67/240															
FT42_SPM99	0.72/360																
FT16_AIR	0.76/60	0.78/120															
FT33_AIR	0.01/180																

KSmoco	0.50/480			0.15/1920	0.11/1920	0.06/480	0.00/480	0.00/480	0.03/480								
Ksnomoco	0.38/180			0.17/1920	0.09/1920	0.23/480	0.01/480	0.02/480	0.64/480								
KSnomoco1	0.90/600			0.08/1920	0.01/1920	0.00/480	0.00/480	0.00/480	0.00/480								
100_51	0.53/252					0.04/756	0.36/756	0.04/756	0.02/756	1.00/336	0.56/336	0.71/336	0.92/336	0.01/336	0.20/336	0.16/336	0.95/336
100_52	0.06/672					0.11/756	0.10/756	0.29/756	0.18/756	0.77/336	0.72/336	0.44/336	0.72/336	0.38/336	0.48/336	0.81/336	0.71/336
100_53	0.38/840					0.05/756	0.34/756	0.15/756	0.17/756	0.55/336	0.58/336	0.19/336	0.88/336	0.00/336	0.24/336	0.86/336	0.62/336
100_54	0.46/336					0.01/756	0.09/756	0.22/756	0.21/756	0.87/336	0.36/336	0.64/336	0.94/336	0.76/336	0.87/336	0.34/336	0.68/336
100_55	0.76/336					0.55/756	0.23/756	0.68/756	0.27/756	0.53/336	0.22/336	0.70/336	0.63/336	0.99/336	0.97/336	0.91/336	0.84/336
100_51r_SPM2	0.97/504					0.30/756	0.60/756	0.12/756	0.55/756	0.83/336	0.27/336	0.94/336	0.54/336	0.30/336	0.85/336	0.28/366	0.17/366
100_52r_SPM2	1.00/672					0.55/756	0.85/756	0.27/756	0.21/756	0.90/336	0.63/336	0.58/336	0.95/336	0.36/336	0.93/336	0.97/336	0.65/336
100_53r_SPM2	1.00/1512	0.99/672	0.37/840			0.28/756	0.19/756	0.24/756	0.80/756	1.00/336	0.94/336	0.92/336	0.90/336	0.88/336	0.94/336	0.15/336	0.60/336
100_54r_SPM2	0.55/504					0.32/756	0.15/756	0.39/756	0.81/756	0.71/336	0.599/336	0.92/336	0.69/336	0.98/336	0.654/336	0.23/336	0.88/336

100_55r_SPM2	0.99/336	0.88/504	0.27/336			0.68/756	0.45/756	0.34/756	0.38/756	0.90/336	0.96/336	0.81/336	0.99/336	0.71/336	0.53/336	0.61/336	0.93/336
100_51r_SPM99	0.19/336	0.73/336															
100_52r_SPM99	0.78/420	0.35/504															
100_53r_SPM99	0.99/756	0.66/840	0.99/672														
100_54r_SPM99	0.96/168	0.61/336															
100_55r_SPM99	0.84/168	0.88/252															
100_51r_AIR	0.19/252	0.32/252															
100_52r_AIR	0.38/504	0.09/252															
100_53r_AIR	0.51/840	0.17/672															
100_54r_AIR	0.46/168	0.28/168															
100_55r_AIR	0.19/84																
10_51	1.00/168					0.08/756	0.36/756	0.01/756	0.15/756	0.65/336	0.85/366	0.00/336	0.53/336	0.02/336	0.95/336	0.86/336	0.93/336

10_52	0.73/336	0.86/336				0.37/756	0.06/756	0.08/756	0.61/756	0.55/336	0.30/336	0.29/336	0.90/336	0.57/336	0.15/336	0.37/336	0.15/336
10_53	0.94/336					0.14/756	0.38/756	0.07/756	0.46/756	0.43/336	0.27/336	0.73/336	0.46/336	0.01/336	0.40/336	0.63/336	0.27/336
10_54	0.77/84	0.98/168				0.03/756	0.11/756	0.42/756	0.65/756	0.87/336	0.98/336			0.25/336	0.46/336		
10_55	0.45/84	0.09/84				0.19/756	0.23/756	0.78/756	0.01/756	0.54/336	0.98/336	0.49/336	0.94/336	0.46/336	0.90/336	0.62/336	0.36/336
10_51r_SPM2	0.15/252					0.50/756	0.98/756	0.46/756	0.86/756	0.68/336	0.90/336	0.92/336	0.86/336	0.90/336	0.08/336	0.85/336	0.17/336
10_52r_SPM2	0.23/840	0.99/504				0.96/756	0.30/756	0.07/756	0.17/756	0.83/336	0.76/336	0.98/336	0.48/336	0.82/336	0.46/336	0.88/336	0.66/336
10_53r_SPM2	0.51/504	0.60/504				0.08/756	0.55/756	0.07/756	0.09/756	0.88/336	0.90/336	0.39/336	0.87/336	0.78/336	0.85/336	0.30/336	0.92/336
10_54r_SPM2	0.96/336	0.96/336				0.17/756	0.71/756	0.57/756	0.42/756	0.82/336	0.90/336	0.93/336	0.87/336	0.87/336	0.42/336	0.87/336	0.09/336
10_55r_SPM2	0.57/84	0.50/84	0.56/84			0.23/756	0.07/756	0.59/756	0.10/756	0.88/336	0.43/336	0.56/336	0.56/336	0.90/336	0.23/336	0.59/336	0.93/336
10_51r_SPM99	0.73/168																
10_52r_SPM99	0.85/672	0.47/252															
10_53r_SPM99	0.61/504	0.12/336															
10_54r_SPM99	0.33/168	0.98/168															

10_55r_SPM99	-																
10_51r_AIR	0.49/168	0.62/168															
10_52r_AIR	0.72/504	0.17/252															
10_53r_AIR	0.003/252	0.09/168															
10_54r_AIR	0.27/84																
10_55r_AIR	-																

The table below contains the similarity and normality measures and the mean values of only the active areas in the subsets chosen in all the data analysed.

	FT	Finger tapping-SPM2	Finger tapping-SPM99	Finger tapping-AIR	visual100	Rvisual 100_SPM2	Rvisual 100_SPM99	Rvisual 100_AIR	visual10	Rvisual 10_SPM2	Rvisual 10_SPM99	Rvisual 10_AIR
	0.76	0.70	0.54	0.76	0.53	0.97	0.19	0.19	1	0.15	0.73	0.49
	0.89	0.91	0.97	0.78	0.06	1.00	0.73	0.32	0.73	0.23	0.85	0.62
	0.94	0.92	0.33	0.01	0.38	1.00	0.78	0.38	0.94	0.51	0.47	0.72
	0.99	0.61	0.97		0.46	0.55	0.35	0.09	0.77	0.96	0.61	0.17

	0.995	0.74	0.67		0.76	0.99	0.99	0.51	0.45	0.57	0.12	0.003
	0.79	0.84	0.72			0.99	0.66	0.17	0.86	0.99	0.33	0.09
	0.99	0.93				0.88	0.99	0.46	0.98	0.60	0.98	0.27
	0.96					0.37	0.96	0.28	0.09	0.96		
						0.27	0.61	0.19		0.50		
							0.84			0.56		
							0.88					
mean normality measure	0.91	0.81	0.70	0.52	0.44	0.78	0.73	0.29	0.73	0.60	0.58	0.34
	0.80	0.82	0.82	0.79	0.80	0.85	0.85	0.80	0.71	0.69	0.69	0.71
	0.85	0.84	0.82	0.76	0.86	0.84	0.84	0.77	0.76	0.81	0.81	0.74
	0.90	0.90	0.85	0.80	0.90	0.91	0.91	0.86	0.85	0.85	0.85	0.65
	0.91	0.90	0.90	0.00	0.81	0.80	0.78	0.74	0.68	0.81	0.81	0.60
					0.70	0.77	0.77	0.58	0.54	0.57	0.00	0.00
mean similarity measure at maximum activation	0.87	0.86	0.84	0.59	0.81	0.83	0.83	0.75	0.71	0.75	0.63	0.54

Summary of the above tables:

Finger Tapping:

- In all cases the signal distribution of the active areas was more normal than the signal distribution in the potentially active area (visual cortex).
- Signal distribution in the background (out of brain) areas was less normal than signal distribution in the active areas.
- White Matter:
  1. Week 16: s.d. of WM was more normal than s.d. of active area in all 4 cases.
  2. Week 17: s.d. of WM was more normal than s.d. of active area in 2 cases out of 4.
  3. Week 33: s.d. of WM was more normal than s.d. of active area in 2 cases out of 4.
  4. Week42: s.d. of WM was more normal than s.d. of active area in 2 cases out of 4.
- Grey Matter:
  1. Week 16: s.d. of GM was more normal than s.d. of active area in 3 cases out of 4.
  2. Week 17: s.d. of GM was more normal than s.d. of active area in 1 case out of 4.
  3. Week 33: s.d. of GM was more normal than s.d. of active area in 1 case out of 4.
  4. Week 42: s.d. of GM was more normal than s.d. of active area in 2 cases out of 4.
- Overall, s.d. in both WM and GM were more normal than background.

Visual data:

- Background:

  100% contrast:
  1. Subject1: Signal distribution in background is less normal than that in active areas.
  2. Subject2: Signal distribution in background is more normal than that in active areas.
  3. Subject3: Signal distribution in background is less normal than that in active areas.
  4. Subject4: Signal distribution in background is less normal than that in active areas.

5. Subject5: Signal distribution in background is less normal than that in active areas.

Realigned data (100%):
1. Subject1: Signal distribution in background is less normal than that in active areas.
2. Subject2: Signal distribution in background is less normal than that in active areas.
3. Subject3: Signal distribution in background is less normal than that in active areas.
4. Subject4: Signal distribution in background is less normal than that in active areas in 3 cases out of 4.
5. Subject5: Signal distribution in background is less normal than that in active areas.

10% contrast:
1. Subject1: Signal distribution in background is less normal than that in active areas.
2. Subject2: Signal distribution in background is less normal than that in active areas.
3. Subject3: Signal distribution in background is less normal than that in active areas.
4. Subject4: Signal distribution in background is less normal than that in active areas.
5. Subject5: Signal distribution in background is less normal than that in active areas in 3 cases out of 4.

Realigned data (10%):
1. Subject1: Signal distribution in background is more normal than that in active areas.
2. Subject2: Signal distribution in background is less normal than that in active areas in 3 cases out of 4.
3. Subject3: Signal distribution in background is less normal than that in active areas.
4. Subject4: Signal distribution in background is less normal than that in active areas.
5. Subject5: Signal distribution in background is less normal than that in active areas in 3 cases out of 4.

- White Matter:

100% contrast:
1. Subject1: s.d. of WM was more normal than s.d. of active area all 4 cases.

2. Subject2: s.d. of WM was more normal than s.d. of active area in all 4 cases.
3. Subject3: s.d. of WM was more normal than s.d. of active area in 3 cases out of 4.
4. Subject4: s.d. of WM was more normal than s.d. of active area in 3 cases out of 4.
5. Subject5: s.d. of WM was less normal than s.d. of active area in all 4 cases.

Realigned data (100%):

1. Subject1: s.d. of WM was less normal than s.d. of active area in all 4 cases.
2. Subject2: s.d. of WM was less normal than s.d. of active area in all 4 cases.
3. Subject3: s.d. of WM was less normal than s.d. of active area in all 4 cases.
4. Subject4: s.d. of WM was more normal than s.d. of active area in all 4 cases.
5. Subject5: s.d. of WM was less normal than s.d. of active area in all 4 cases.

10% contrast:

1. Subject1: s.d. of WM was less normal than s.d. of active area in all 4 cases.
2. Subject2: s.d. of WM was less normal than s.d. of active area in 3 cases out of 4.
3. Subject3: s.d. of WM was less normal than s.d. of active area in all 4 cases.
4. Subejct4: s.d. of WM was less normal than s.d. of active area in all 2 cases.
5. Subject5: s.d. of WM was more normal than s.d. of active area in all 4 case.

- Grey Matter:

100% contrast:

1. Subject1: s.d. of GM was less normal than s.d. of active area in 3 cases out of 4.
2. Subject2: s.d. of GM was more normal than s.d. of active area in all 4 cases.
3. Subject3: s.d. of GM was more normal than s.d. of active area in 2 cases out of 4.
4. Subject4: s.d. of GM was more normal than s.d. of active area in 3 cases out of 4.
5. Subject5: s.d. of GM was more normal than s.d. of active area in all 4 cases.

Realigned data (100%):

6. Subject1: s.d. of GM was less normal than s.d. of active area in all 4 cases.
7. Subject2: s.d. of GM was less normal than s.d. of active area in all 4 cases.
8. Subject3: s.d. of GM was less normal than s.d. of active area in all 4 cases.
9. Subject4: s.d. of GM was more normal than s.d. of active area in 3 cases out of 4.
10. Subject5: s.d. of GM was less normal than s.d. of active area in all 4 cases.

10% contrast:

6. Subject1: s.d. of GM was less normal than s.d. of active area in all 4 cases.
7. Subject2: s.d. of GM was less normal than s.d. of active area in all 4 cases.
8. Subject3: s.d. of GM was less normal than s.d. of active area in all 4 cases.
9. Subejct4: s.d. of GM was less normal than s.d. of active area in all 2 cases.
10. Subject5: s.d. of GM was less normal than s.d. of active area in 1 case out of 4.

Phantom: Signal distribution of background is less normal than that of inside phantom.

Overall: signal distribution in background is less normal than that in active areas.

Comparison of moco and nomoco (filtered):

1. Active area: s.d. of active area in nomoco is more normal than that in moco.
2. Potential visual active: s.d. in nomoco is less normal than that in moco.
3. Background: s.d. in nomoco is less normal than that in moco.

Comparison of 100% contrast raw data and realigned data:

1. Active area: s.d. of active area in realigned data is more normal than that in raw data.

2. Background area: s.d. in realigned data is more normal in 17 cases out of 20 compared to raw data.
3. White matter: s.d. in realigned data is more normal in 14 cases out of 20 compared to raw data.
4. Grey matter: s.d. in realigned data is more normal in 10 cases out of 20 compared to raw data.

Comparison of 10% contrast raw data and realigned data:

1. Active area: s.d. of active area in realigned data is more normal than that in raw data in 2 cases out of 5.
2. Background area: s.d. in realigned data is more normal in 13 cases out of 20 compared to raw data.
3. White matter: s.d. in realigned data is more normal in 12 cases out of 18 compared to raw data.
4. Grey matter: s.d. in realigned data is more normal in 11 cases out of 18 compared to raw data.

Comparison of 100% contrast to 10% contrast:

1. Active area: s.d. of active area in 10% contrast data is more normal than that in 100% contrast data in 4 out of 5 cases.
2. Background area: s.d. in 10% contrast data is more normal in 14 cases out of 20 compared to 100% contrast data.
3. White matter: s.d. in 10% contrast data is more normal in 11 cases out of 18 compared to 100% contrast data.
4. Grey matter: s.d. in 10% contrast data is less normal in 12 cases out of 18 compared to 100% contrast data.

Mean value of similarity measure at active areas in:

- Finger tapping (16,17,33,42) = 0.86
- Visual (100% contrast) = 0.81
- Realigned visual (100% contrast) = 0.83
- Visual (10% contrast) = 0.71
- Realigned visual (10% contrast) = 0.75

Mean value of s.d. normality at active areas:

- Finger tapping (16,17,33,42) = 0.81

- Visual (100% contrast) = 0.44
- Realigned visual (100% contrast) = 0.78
- Visual (10% contrast) = 0.73
- Realigned visual (10% contrast) = 0.60

From above results we can conclude that the realignment process has the effect of increasing the similarity measure and the cluster size. We can also conclude, that the reduction in contrast (100% to 10%) has the effect of decreasing similarity measure the cluster size.

Appendix C

SPM parameters

Realignment:

SPM99	SPM2
Number of subjects:	Num subjects:
Num sessions for subject:	Num sessions, subj 1:
Scans for subj 1, sess 1:	Images, subj 1, sess 1:
Which option? Coregister and Reslice	Which option? Coregister & Reslice
Reslice interpolation method? Sinc interpolation	Create what? All Images + Mean Image
Create what? All Images + Mean Image	
Adjust sampling errors? no	

Smoothing:

SPM99	SPM2
Smoothing {FWHM in mm}: 4	Smoothing {FWHM in mm}: 4
Select scans:	Select scans:

Normalize:

SPM99	SPM2
Which Option? Determine Parameters & Write Normalised	Which Option? Determine Parameters & Write Normalised
# Subjects: 1	Template Image(s)
Subj 1 – Image to determine parameters:	Source mage, subj 1:
Subj 1 - Images to write normalised:	Images to write, subj 1
Template image(s):	
Interpolation method? Bilinear Interpolation	

Specifying a model:

SPM99	SPM2
fMRI models: What would you like to do? specify a model	fMRI stats model setup: specify design or data: design
interscan interval: 6	interscan interval: 6
scans per session: 30	scans per session: 30
number of conditions/trials: 1	specify design in: scans
name of condition/trial: trial 1	select basis set: hrf
stochastic design: no	model interactions (Volterra): no
SOA: Fixed	number of conditions/trials: 1
SOA (scans) for trial 1: 10	name of condition/trial: trial 1
Time to 1st trial (scans): 5	vector of onsets – trial 1: 5 15 25
parametric modulation: none	duration(s): 5
are these trials : epochs	parametric modulation: none
select type of response: Fixed response (Box-car)	user specified: 0
convolve with hrf: yes	
add temporal derivatives: no	
epoch length (scans) for trial 1:	
interactions among trials (Volterra): no	
user specified regressors: 0	

Estimate a specified model:

fMRI models: What would you like to do? Estimate a specified model.	specify design or data: data
select SPM fMRIDesMtx.mat	select SPM.mat
select scans for session 1	select scans for session 1
remove global effects: none	remove global effects: none
High-pass filter? Specify	High-pass filter? Specify
cutoff period (secs): 120	cutoff period (secs): 128
low-pass filter: hrf	Correct for serial correlations? AR(1)
Model intrinsic correlations? AR(1)	Estimate: Select

Setup trial-specific F-contrasts: no	
estimate: now	

Results:

Results: select SPM.mat	Results: select SPM.mat
Select contrasts	Select contrasts
Mask with other contrast(s): no	Mask with other contrast(s): no
Title for comparison: active	Title for comparison: active
Correct height threshold: no	P value adjustment to control: none
Threshold (T or p value): 0.001	Threshold (T or p value): 0.001
& extent threshold (voxels): 0	& extent threshold (voxels): 0

Bibliography

[1] T. Nichols, "**Data Modeling General Linear Model & Statistical Inference**," 2002.

[2] M. S. Cohen, "**Real-Time Functional Magnetic Resonance Imaging**," *Methods*, vol. 25, pp. 201-220, 2001.

[3] A. L. Baert, K. Sartor, and J. E. Youker, ***Functional MRI*** **Springer-Verlag**, 2000.

[4] B. A. Ardekani, A. H. Bachman, and J. A. Helpern, "**A quantitative comparison of motion detection algorithms in fMRI**," *Magnetic Resonance Imaging*, vol. 19, pp. 959-963, 2001.

[5] A. M. Howseman and R. W. Bowtell, "**Functional magnetic resonance imaging: imaging techniques and contrast mechanisms**," *Phil Trans R Soc Lond B*, vol. 354, pp. 1179-1194, 1999.

[6] N. K. Logothetis and B. A. Wandell, "**Interpreting the BOLD Signal**," *Annual Review of Physiology*, vol. 66, pp. 735-769, 2004.

[7] P. M. Matthews and P. Jezzard, "**Functional magnetic resonance imaging**," *Journal of Neurology Neurosurgery and Psychiatry*, vol. 75, no. 1, pp. 6-12, 2004.

[8] D. W. McRobbie, E. A. Moore, M. J. Graves, and M. R. Prince, ***MRI From Picture to Proton.*** Cambridge: **Cambridge University Press**, 2003.

[9] R. Turner, A. Howseman, G. E. Rees, O. Josephs, and K. Friston, "**Functional magnetic resonance imaging of the human brain: data acquisition and analysis**," *Experimental Brain Research*, vol. 123, no. 1-2, pp. 5-12, 1998.

[10] S. Ogawa, T. M. Lee, A. R. Kay, and D. W. Tank, "**Brain magnetic resonance imaging with contrast dependent on blood**

oxygenation," *Proceedings of National Academy of Sciences*, vol. 87, pp. 9868-9872, 1990.

[11] N. A. Thacker, E. Burton, A. J. Lacey, and A. Jackson, "**The Effects of Motion on Parametric fMRI Analysis Techniques,**" *Physiological Measurement*, vol. 20, no. 3 1999.

[12] J. Ashburner and K. J. Friston, "**The role of registration and spatial normalisation in detecting activations in functional imaging,**" *Clinical MRI/Developments in MR*, vol. 7, no. 1, pp. 26-28, 1997.

[13] D. J. Heeger and D. Ress, "**WHAT DOES FMRI TELL US ABOUT NEURONAL ACTIVITY?,**" *Nature Reviews Neuroscienc*, vol. 3, no. 2, pp. 142-151, 2002.

[14] R. B. Buxton, K. Uludağ, D. J. Dubowitz, and T. T. Liu, "**Modeling the hemodynamic response to brain activation,**" *NeuroImage*, vol. 23, no. 1, p. S220-S233, 2004.

[15] M. S. Cohen and S. Y. Bookheimer, "**Localization of Brain Function with Magnetic Resonance Imaging,**" *Trends in Neuroscience*, vol. 17, no. 7, pp. 268-277, 1994.

[16] S. Clare, "**Functional Magnetic Resonance Imaging: Methods and Applications.**" PhD **University of Nottingham - UK**, 1997.

[17] E. R. Cohen, K. Ugurbil, and S.-G. Kim, "**Effect of Basal Conditions on the Magnitude and Dynamics of the Blood Oxygenation Level-Dependent fMRI Response,**" *Journal of Cerebral Blood Flow and Metabolism*, vol. 22, pp. 1042-1053, 2002.

[18] D.-S. Kim, I. Ronen, C. Olman, S.-G. Kim, K. Ugurbil, and L. J. Toth, "**Spatial relationship between neuronal activity and BOLD functional MRI,**" *NeuroImage*, vol. 21, no. 3, pp. 876-885, 2004.

[19] O. J. Arthurs and S. J. Boniface, "**What aspect of the fMRI BOLD signal best reflects the underlying electrophysiology in human somatosensory cortex?** " *Clinical Neurophysiology*, vol. 114, no. 7, pp. 1203-1209, 2003.

[20] R. B. Buxton, "**The Elusive Initial Dip,**" *NeuroImage*, vol. 13, no. 6, pp. 953-958, 2001.

[21] J. W. Scannell and M. P. Young, "**Neuronal population activity and functional imaging,**" *Proceedings of the Royal Society of London, B: Biological Sciences*, vol. 266, no. 1422, pp. 875-881, 1999.

[22] R. Turner, R. J. Ordidge, E. M. Haacke, and L. Zhi-Pei, "**Challenges of imaging structure and function with MRI,**" *IEEE Engineering in Medicine and Biology Magazine*, vol. 19, no. 5, pp. 42-54, 2000.

[23] P. J. Magistretti and L. Pellerin, "**Cellular mechanisms of brain energy metabolism and their relevance to functional brain imaging,**" *Philos Trans R Soc Lond B Biol Sci*, vol. 354, no. 1387, pp. 1155-1163, 1999.

[24] G. Marrelec, H. Benali, P. Ciuciu, and J.-B. Poline, "**Bayesian estimation of the hemodynamic response function in Functional MRI,**" in ***Bayesian Inference and Maximum Entropy Methods***. R. Fry, Ed. **Baltimore, MD: MaxEnt Workshops**, 2001.

[25] D. J. Heeger, A. C. Huk, W. S. Geisler, and D. G. Albrecht, "**Spikes versus BOLD: what does neuroimaging tell us about neuronal activity?,**" *Nature Neuroscience*, vol. 3, pp. 631-633, 2000.

[26] C. H. Liao, K. J. Worsley, J.-B. Poline, J. A. D. Aston, G. H. Duncan, and A. C. Evans, "**Estimating the Delay of the fMRI Response,**" *NeuroImage*, vol. 16, no. 3a, pp. 593-606, 2002.

[27] N. K. Logothetis, J. Pauls, M. Augath, T. Trinath, and A. Oeltermann, "**Neurophysiological investigation of the basis of the fMRI signal,**" *Nature*, vol. 412, pp. 150-157, 2001.

[28] M. Singh, S. Kim, and T.-S. Kim, "**Correlation between BOLD-fMRI and EEG signal changes in response to visual stimulus frequency in humans,**" *Magnetic Resonance in Medicine*, vol. 49, no. 1, pp. 108-114, 2003.

[29] J. Frahm, P. Dechent, J. Baudewig, and K. D. Merboldt, "**Advances in functional MRI of the human brain,**" *Progress in Nuclear Magnetic Resonance Spectroscopy*, vol. 44, no. 1-2, pp. 1-32, 2004.

[30] J. Neumann, G. Lohmann, S. Zysset, and D. Y. Cramon, "**Within-subject variability of BOLD response dynamics,**" *NeuroImage*, vol. 19, no. 3, pp. 784-796, 2003.

[31] G. K. Aguirre, E. Zarahn, and M. D'Esposito, "**The Variability of Human, BOLD Hemodynamic Responses**," *NeuroImage*, vol. 8, no. 4, pp. 360-369, 1998.

[32] D. A. Handwerker, J. M. Ollinger, and M. D'Esposito, "**Variation of BOLD hemodynamic responses across subjects and brain regions and their effects on statistical analyses**," *NeuroImage*, vol. 21, no. 4, pp. 1639-1651, 2004.

[33] F. M. Miezin, L. Maccotta, J. M. Ollinger, S. E. Petersen, and R. L. Buckner, "**Characterizing the Hemodynamic Response: Effects of Presentation Rate, Sampling Procedure, and the Possibility of Ordering Brain Activity Based on Relative Timing**," *NeuroImage*, vol. 11, no. 6, pp. 735-759, 2000.

[34] T. D. Wager, A. Vasquez, L. Hernandez, and D. C. Noll, "**Accounting for nonlinear BOLD effects in fMRI: parameter estimates and a model for prediction in rapid event-related studies**," *Neuroinage*, vol. 25, pp. 206-218, 2005.

[35] P. A. Bandettini, R. M. Birn, D. Kelley, and Z. S. Saad, "**Dynamic nonlinearities in BOLD contrast: neuronal or hemodynamic?**," *International Congress Series*, vol. 1235, pp. 73-85, 2002.

[36] R. M. Birn, Z. S. Saad, and P. A. Bandettini, "**Spatial Heterogeneity of the Nonlinear Dynamics in the FMRI BOLD Response**," *NeuroImage*, vol. 14, no. 4, pp. 817-826, 2001.

[37] A. L. Vazquez and D. C. Noll, "**Nonlinear Aspects of the BOLD Response in Functional MRI**," *NeuroImage*, vol. 7, no. 2, pp. 108-118, 1998.

[38] G. M. Boynton, S. A. Engel, G. H. Glover, and D. J. Heeger, "**Linear Systems Analysis of Functional Magnetic Resonance Imaging in Human V1**," *The Journal of Neuroscience*, vol. 16, pp. 4207-4221, 1996.

[39] S. A. Huettel, O. O. Obembe, A. W. Song, and M. G. Woldorff, "**The BOLD fMRI refractory effect is specific to stimulus attributes: evidence from a visual motion paradigm**," *NeuroImage*, vol. 23, no. 1, pp. 402-408; 2004.

[40] C. N. Guy, D. H. Ffytche, A. Brovelli, and J. Chumillas, "**fMRI and EEG Responses to Periodic Visual Stimulation,**" *NeuroImage*, vol. 10, pp. 125-148, 1999.

[41] W. van der Zwaag, K. E. Head, A. Peters, S. Francis, P. Gowland, R. W. Bowtell, and P. Morris, "**Somatosensory fMRI at 1.5, 3 and 7 T: Measuring BOLD Signal Changes,**", Proc. Intl. Soc. Mag. Reson. Med. ed 2006.

[42] A. M. Howseman, S. Grootoonk, D. A. Porter, J. Ramdeen, A. P. Holmes, and R. Turner, "**The Effect of Slice Order and Thickness on fMRI Activation Data Using Multislice Echo-Planar Imaging,**" *NeuroImage*, vol. 9, no. 4, pp. 363-376, 1999.

[43] M. S. Cohen, "**Echo-planar imaging (EPI) and functional MRI,**" in ***Functional MRI***. Bandettini and Moonen, Ed. 1998.

[44] L. Bloy, J. Hulvershorn, E. E. Gualtieri, C.-S. J. Liu, J. S. Leigh, and M. A. Elliott, "**Quantitative assessment of spin-echo and gradient-echo BOLD Sensitivity at 3 T,**" **University of Pennsylvania: Metabolic Magnetic Resonance Research and Computing Center Newsletter**, 2003.

[45] C. F. Schmidt, P. Boesiger, and A. Ishai, "**Comparison of fMRI activation as measured with gradient- and spin-echo EPI during visual perception,**" *NeuroImage*, vol. 26, no. 3, pp. 852-859, 2005.

[46] J. V. Hajnal, D. J. Bryant, L. Kasuboski, P. M. Pattany, B. De Coene, P. D. Lewis, J. M. Pennock, A. Oatridge, I. R. Young, and G. M. Bydder, "**Use of fluid attenuated IR (FLAIR) pulse sequences in MRI of the brain,**" *Journal of Computer Assisted Tomography*, vol. 16, pp. 841-844, 1992.

[47] C.-C. Chen, C. W. Tyler, and H. A. Baseler, "**Statistical properties of BOLD magnetic resonance activity in the human brain,**" *NeuroImage*, vol. 20, no. 2, pp. 1096-1109, 2003.

[48] W. F. Eddy, M. Fitzgerald, C. Genovese, N. Lazar, A. Mockus, and J. Welling, "**The Challenge of Functional Magnetic Resonance Imaging,**" *Journal of Computational and Graphical Statistics*, vol. 8, no. 3, pp. 545-558, 1999.

[49] L. Freire, A. Roche, and J.-F. Mangin, "**What is the best similarity measure for motion correction in fMRI time series?**," *IEEE Transactions on Medical Imaging*, vol. 21, no. 5, pp. 470-484, 2002.

[50] K. J. Friston, S. Williams, R. Howard, R. S. J. Frackowiak, and R. Turner, "**Movement-related effects in fMRI time-series**," *Magnetic Resonance in Medicine*, vol. 35, pp. 346-355, 1996.

[51] V. Della-Maggiore, W. Chau, P. R. Peres-Neto, and A. R. McIntosh, "**An Empirical Comparison of SPM Preprocessing Parameters to the Analysis of fMRI Data**," *NeuroImage*, vol. 17, no. 1, pp. 19-28, 2002.

[52] S. Groontoonk, C. Hutton, J. Ashburner, A. M. Howseman, O. Josephs, G. Rees, K. J. Friston, and R. Turner, "**Characterization and Correction of Interpolation Effects in the Realignment of fMRI Time Series**," *NeuroImage*, vol. 11, pp. 49-57, 2000.

[53] K. J. Friston, A. P. Holmes, J.-B. Poline, P. J. Grasby, S. C. R. Williams, R. S. J. Frackowiak, and R. Turner, "**Analysis of fMRI Time-Series Revisited**," *NeuroImage*, vol. 2, no. 1, pp. 45-53, 1995.

[54] M. Singh, L. Al-Dayeh, P. Patel, T. Kim, C. Guclu, and O. Nalcioglu, "**Correction for head movements in multi-slice EPI functional MRI**," *IEEE Transactions on Nuclear Science*, vol. 45, no. 4(2), pp. 2162-2167, 1998.

[55] S. C. Bushong, ***Magnetic Resonance Imaging: Physical and Biological Principles***, second ed Mosby, 1996.

[56] A. M. Howseman, O. Josephs, G. Rees , and K. J. Friston, "**Special Issues in Functional Magnetic Resonance Imaging**," in ***Human Brain Function*, 2nd edition** ed. R. S. J. Frackowiak, K. J. Friston, C. Frith, R. Dolan, C. J. Price, S. Zeki, J. Ashburner, and W. D. Penny, Eds. **Academic Press**, 2003.

[57] V. Kiviniemi, J. Ruohonen, and O. Tervonen, "**Separation of physiological very low frequency fluctuation from aliasing by switched sampling interval fMRI scans**," *Magnetic Resonance Imaging*, vol. 23, no. 1, pp. 41-46, 2005.

[58] L. R. Frank, R. B. Buxton, and E. C. Wong, "**Estimation of respiration-induced noise fluctuations from undersampled**

multislice fMRI data," *Magnetic Resonance in Medicine*, vol. 45, no. 4, pp. 635-644, 2001.

[59] C. D. Noll, "**Technical challenges in Functional Neuroimaging**," *IEEE International Symposium on Biomedical Imaging: Macro to Nano*, vol. 2, pp. 1208-1211, 2004.

[60] J. Ashburner, "**Computational Neuroanatomy**." Ph.D. **University College London**, 2000.

[61] J. B. A. Maintz and M. A. Viergever, "**An Overview of Medical Image Registration Methods**," *Symposium of the Belgian hospital physicists association (SBPH/BVZF)*, vol. 12, no. V, pp. 1-22, 1996.

[62] P. A. Elsen, E.-J. D. Pol, and M. A. Viergever, "**Medical Image Matching – A Review with Classification**," *IEEE Engineering in Medicine and Biology*, vol. 12, no. 4, pp. 26-39, 1993.

[63] D. L. G. Hill, P. G. Batchelor, M. Holden, and D. J. Hawkes, "**Medical image registration**," *Physics in Medicine and Biology*, vol. 46, pp. 1-45, 2001.

[64] C. R. Maurer and J. M. Fitzpatrick, "**A Review of Medical Image Registration**," in ***Interactive Image-Guided Neurosurgery American Association of Neurological Surgeons***, 1993, pp. 17-44.

[65] P. Thompson and A. W. Toga, "**Elastic Image Registration and Pathology Detection**," in ***Handbook of Medical Image Processing***. I. e. al. Bankman, Ed. **Academic Press**, 2000.

[66] B. Zitova and J. Flusser, "**Image registration methods: a survey**," *Image and Vision Computing*, vol. 21, pp. 977-1000, 2003.

[67] J. B. A. Maintz and M. A. Viergever, "**A Survey of Medical Image Registration**," *Medical Image Analysis*, vol. 2, no. 1, pp. 1-36, 1998.

[68] K. Kneoaurek, M. Ivanovic, J. Machac, and D. A. Weber, "**Medical image registration**," *Europhysics News*, vol. 31, no. 4 2000.

[69] T. V. Khac, J. Fichefet, H. Meurisse, J. P. Leclercq, F. Vandermeersch, A. de Rosee, and S. Dury, "**Review and**

comparison of image co-registration methods," Namur, Belgium,1999.

[70] C. Fookes and M. Bennamoun, "**The use of mutual information for rigid medical image registration: a review**," *IEEE International Conference on Systems, Man and Cybernetics*, vol. 4, p. 6, 2002.

[71] P. R. Bannister, "**Motion Correction for Functional Magnetic Resonance Images**." University of Oxford, 2004.

[72] L. Chmielewski and D. Kozinska, "**Image Registration**,", ***Proceeding 3rd Polish Conference of Computer Pattern Recognition Systems*** ed 2003, pp. 163-168.

[73] L. G. Brown, "**A Survey of Image Registration Techniques**," *ACM Computing Surveys*, vol. 24, no. 4, pp. 325-376, 1992.

[74] P. Chalermwat, "**High Performance Automatic Image Registration for Remote Sensing.**" ***PhD Thesis*** **George Mason University**, 1999.

[75] G. K. Matsopoulos, K. K. Delibasis, and N. A. Mouravliansky, "**Medical Image Registration and Fusion Techniques: A Review**," in ***Advanced Signal Processing Handbook: Theory and Implementation for Radar, Sonar, and Medical Imaging Real Time System*** . S. Stergiopoulos, Ed. **CRC Press LLC**, 2001.

[76] J. Ashburner and K. J. Friston, "**Nonlinear Spatial Normalization Using Basis Functions**," *Human Brain Mapping*, vol. 7, pp. 254-266, 1999.

[77] T. M. Lehmann, C. Gonner, and K. Spitzer, "**Survey: Interpolation Methods in Medical Image Processing**," *IEEE Transactions on Medical Imaging*, vol. 18, no. 11, pp. 1049-1075, 1999.

[78] A. K. Jain, ***Fundamentals of Digital Image Processing***. **Englewood Cliffs, NJ: Prentice Hall**, 1989.

[79] L. Freire and J.-F. Mangin, "**Motion Correction Algorithms May Create Spurious Brain Activations in the Absence of Subject Motion**," *NeuroImage*, vol. 14, no. 3, pp. 709-722, 2001.

[80] D. H. Wu, J. S. Lewin, and J. L. Duerk, "**Inadequacy of Motion Correction Algorithms in Functional MRI: Role of Susceptibility-Induced Artifacts**," *Journal of Magnetic Resonance Imaging*, vol. 7, no. 2, pp. 365-370, 1997.

[81] K. Kuppusamy, W. Lin, and E. M. Haacke, "**Statistical assessment of crosscorrelation and variance methods and the importance of electrocardiogram gating in functional magnetic resonance imaging**," *Magnetic Resonance Imaging*, vol. 15, no. 2, pp. 168-181, 1997.

[82] R. F. Mould, ***Introductory Medical Statistics***, Third ed. **Bristol and Philadelphia: Institute of Physics Publishing**, 1998.

[83] E. Salli, A. Korvenoja, A. Visa, T. Katila, and H. J. Aronen, "**Reproducibility of fMRI: Effect of the Use of Contextual Information**," *NeuroImage*, vol. 13, no. 3, pp. 459-471, 2001.

[84] G. E. Dallal, "**The Little Handbook of Statistical Practice**," 2003.

[85] E. Salli, H. J. Aronen, S. Savolainen, A. Korvenoja, and A. Visa, "**Contextual clustering for analysis of functional MRI data**," *IEEE Transactions on Medical Imaging*, vol. 20, no. 5, pp. 403-414, 2001.

[86] C. Goutte, P. Toft, E. Rostrup, F. A. Nielsen, and L. K. Hansen, "**On Clustering fMRI Time Series**," *NeuroImage*, vol. 9, no. 3, pp. 298-310, 1999.

[87] A. P. Holmes, R. C. Blair, J. D. G. Watson, and I. Ford, "**Non-Parametric Analysis of Statistic Images From Functional Mapping Experiments**," *Journal of Cerebral Blood Flow and Metabolism*, vol. 16, pp. 7-22, 1996.

[88] T. E. Nichols and A. P. Holmes, "**Nonparametric permutation tests for functional neuroimaging: A primer with examples**," *Human Brain Mapping*, vol. 15, pp. 1-25, 2001.

[89] E. T. Bullmore, M. J. Brammer, S. C. R. Williams, S. Rabe-Hesketh, N. Janot, A. David, J. Mellers, R. Howard, and P. Sham, "**Statistical methods of estimation and inference for functional MR image analysis**," *Magnetic Resonance in Medicine*, vol. 35, pp. 261-277, 1996.

[90] B. S. Everitt and G. Dunn, ***Statistical Analysis of Medical Data: New Developments***. London: Arnold, 1998.

[91] C. R. Genovese, N. A. Lazar, and T. Nichols, "**Thresholding of Statistical Maps in Functional Neuroimaging Using the False Discovery Rate**," *NeuroImage*, vol. 15, no. 4, pp. 870-878, 2002.

[92] J. Ashburner and K. J. Friston, "**Voxel-Based Morphometry- The Methods**," *NeuroImage*, vol. 11, pp. 805-821, 2000.

[93] A. P. Holmes and K. J. Friston, "**Statistical Models and Experimental Design**," in ***SPMcourse*** 1997.

[94] W. M. K. Trochim, ***Research methods knowledge base*** 2002.

[95] K. J. Worsley, A. C. Evans, S. Marrett, and P. Neelin, "**A three-dimensional statistical analysis for CBF activation studies in human brain**," *Journal of Cerebral Blood Flow and Metabolism*, vol. 12, no. 6, pp. 900-918, 1992.

[96] F. E. Turkheimer, C. B. Smith, and K. chmidt, "**Estimation of the Number of "True" Null Hypotheses in Multivariate Analysis of Neuroimaging Data**," *NeuroImage*, vol. 13, no. 5, pp. 920-930, 2001.

[97] S. J. Kiebel, J.-B. Poline, K. J. Friston, A. P. Holmes, and K. J. Worsley, "**Robust smoothness estimation in statistical parametric maps using standardized residuals from the general linear model**," *NeuroImage*, vol. 10, pp. 756-766, 1999.

[98] K. J. Friston, K. J. Worsley, R. S. J. Frackowiak, J. C. Mazziotta, and A. C. Evans, "**Assessing the significance of focal activations using their spatial extent**," *Human Brain Mapping*, vol. 1, pp. 214-220, 1994.

[99] K. J. Friston, C. D. Frith, P. F. Liddle, and R. S. J. Frackowiak, "**Comparing functional (PET) images: the assessment of significant change**," *J. Cereb. Blood Flow Metab*, vol. 11, pp. 690-699, 1991.

[100] K. J. Friston, C. D. Frith, P. F. Liddle, R. J. Dolan, A. A. Lammertsma, and R. S. Frackowiak, "**The relationship between**

global and local changes in PET scans," *J Cereb Blood Flow Metab*, vol. 10, pp. 458-466, 1990.

[101] K. J. Friston, A. P. Holmes, K. J. Worsley, J.-B. Poline, C. D. Frith, and R. S. J. Frackowiak, **"Statistical Parametric Maps in Functional Imaging: A General Linear Approach,"** *Human Brain Mapping*, vol. 2, pp. 189-210, 1995.

[102] K. J. Friston, W. Penny, C. Phillips, S. Kiebel, G. Hinton, and J. Ashburner, **"Classical and Bayesian Inference in Neuroimaging: Theory,"** *NeuroImage*, vol. 16, no. 2, pp. 465-483, 2002.

[103] K. J. Friston, **"Bayesian Estimation of Dynamical Systems: An Application to fMRI,"** *NeuroImage*, vol. 16, no. 2, pp. 513-530, 2002.

[104] T. Nichols and S. Hayasaka, **"Controlling the familywise error rate in functional neuroimaging: a comparative review,"** *Statistical Methods in Medical Research*, vol. 12, pp. 419-446, 2003.

[105] B. R. Logan and D. B. Rowe, **"A Comparison of fMRI Activation Thresholding Methods,"** *Proc. Intl. Soc. Mag. Reson. Med.*, vol. 11, p. 1095, 2004.

[106] D. Yekutieli and Y. Benjamini, **"Resampling based FDR controlling multiple hypotheses testing,"** *JSPI*, vol. 82, pp. 171-196, 1999.

[107] Y. Benjamini and D. Yekutieli, **"The control of the false discovery rate in multiple testing under dependency,"** *Annals of Statistics*, vol. 29, no. 4, pp. 1165-1188, 2001.

[108] Y. Benjamini and Y. Hochberg, **"Controlling the False Discovery Rate: A Practical and Powerful Approach to Multiple Testing,"** *Journal of the Royal Statistical Society. Series B (Methodological)*, vol. 57, no. 1, pp. 289-300, 1995.

[109] members & collaborators of the Wellcome Department of Imaging Neuroscience, **"Statistical Parametric Mapping (SPM),"** 2005.

[110] T. D. Wager and T. E. Nichols, **"Optimization of Experimental Design in fMRI: A General Framework Using a Genetic Algorithm,"** *NeuroImage*, vol. 18, pp. 293-309, 2003.

[111] W. Penny, N. J. Trujillo-Barreto, and K. Friston, "**Bayesian fMRI time series analysis with spatial priors**," *NeuroImage*, vol. 24, no. 2, pp. 350-362, 2005.

[112] R. N. A. Henson, "**Analysis of fMRI time series**," in ***Human Brain Function*, 2nd edition** ed. R. S. J. Frackowiak, K. J. Friston, C. Frith, R. Dolan, C. J. Price, S. Zeki, J. Ashburner, and W. D. Penny, Eds. **Academic Press**, 2003.

[113] K. Specht, K. Willmes, N. J. Shah, and L. Jancke, "**Assessment of Reliability in Functional Imaging Studies**," *Journal of Magnetic Resonance Imaging*, vol. 17, pp. 463-471, 2003.

[114] B. J. Casey, J. D. Cohen, K. O'Craven, R. J. Davidson, W. Irwin, C. A. Nelson, D. C. Noll, X. Hu, M. J. Lowe, B. R. Rosen, C. L. Truwitt, and P. A. Turski, "**Reproducibility of fMRI Results across Four Institutions Using a Spatial Working Memory Task**," *NeuroImage*, vol. 8, pp. 249-261, 1998.

[115] K. H. Zou, D. N. Greve, M. Wang, S. D. Pieper, S. K. Warfield, N. S. White, M. G. Vangel, R. Kikinis, W. M. Wells, and F. Birn, "**A Prospective Multi-Institutional Study of the Reproducibility of fMRI: A Preliminary Report from the Biomedical Informatics Research Network.** " *Lecture Notes Computer Science*, vol. 3217, no. 2, pp. 769-776, 2004.

[116] C. Tegeler, S. C. Strother, J. R. Anderson, and S.-G. Kim, "**Reproducibility of BOLD-Based Functional MRI Obtained at 4 T**," *Human Brain Mapping*, vol. 7, pp. 267-283, 1999.

[117] W. C. M. Machielsen, S. A. R. B. Rombouts, F. Barkhof, P. Scheltens, and M. P. Witter, "**FMRI of Visual Encoding: Reproducibility of Activation**," *Human Brain Mapping*, vol. 9, pp. 156-164, 2000.

[118] B. W. Kernighan and D. M. Ritchie, ***The C programming Language.*, second edition** ed **Prentice Hall**, 1988.

[119] P. A. Bandettini, A. Jesmanowicz, E. C. Wong, and J. S. Hyde, "**Processing strategies for time-course data sets in functional MRI of the human brain**," *Magnetic Resonance in Medicine*, vol. 30, pp. 161-173, 1993.

[120] H. Devlin, J. T. Devlin, M. Woolrich, K. L. Miller, and P. Jezzard, "**An efficient method for obtaining subject-specific HRF estimates in event-related fMRI**,", Proc. Intl. Soc. Mag. Reson. Med. ed 2006, p. 2774.

[121] R. T. Constable, P. Skudlarski, and J. C. Gore, "**An ROC approach for evaluating functional brain MR imaging and postprocessing protocols.**," *Magn Reson Med.*, vol. 34, no. 1, pp. 57-64, 19995.

[122] F. A. Nielsen, M. S. Christensen, K. H. Madsen, T. E. Lund, and L. K. Hansen, "fMRI Neuroinformatics," *IEEE Engineering in Medicine and Biology Magazine,* vol. 25, no. 2, pp. 112-119, 2004.

[123] V. L. Morgan, D. R. Pickens, S. L. Hartmann, and R. R. Price, "Comparison of functional MRI image realignment tools using a computer-generated phantom," *Magnetic Resonance in Medicine*, vol. 46, no. 3, pp. 510-514, 2001.

[124] A. Papoulis, *Random Variables Probability, and Stochastic Processes.*, 2nd ed. New York: McGraw-Hill, 1984, p. 576.

[125] J. Wang, R. Grunfeld, M. D. Meadowcroft, X. Sun, E. Zimmermann, P. J. Eslinger, L. Ansel, M. B. Smith, and Q. X. Yang, "**Hemodynamic Response in Human Central Olfactory System**,", Proc. Intl. Soc. Mag. Reson. Med. ed 2006, p. 2772.